

**Measurement System of Cellular
Environment Using Fluorescence
Microsensor**

Hairulazwan Bin HASHIM

Measurement System of Cellular Environment Using Fluorescence Microsensor

Hairulazwan Bin HASHIM

A thesis submitted in fulfilment of the requirement for the award of the
Doctor of Philosophy

Department of Micro-Nano Mechanical Science and Engineering
Graduate School of Engineering
Nagoya University

2020

ACKNOWLEDGMENT

In the name of Allah Most Gracious Most Merciful. It is my great pleasure to acknowledge all people who concern this work.

First of all, I would like to express my sincere to Professor Fumihito Arai in the Department of Micro-Nano Mechanical Science and Engineering, Nagoya University for guiding me with great patience, support, advice, comment and encouragement throughout the study.

Special thanks to Professor Yasuhisa Hasegawa from the Department of Micro-Nano Mechanical Science and Engineering, Professor Takeo Matsumoto from the Department of Mechanical Systems Engineering, and Associate Professor Hisataka Maruyama from the Department of Micro-Nano Mechanical Science and Engineering for kind agreement with being my doctoral committee member.

I would like to personally thank Associate Professor Taisuke Masuda, Assistant Professor Shinya Sakuma, Assistant Professor Seiji Omata, Assistant Professor Yuichi Murozaki and Research Fellow Bilal Turan for their kind advice, help and supports. Many thanks to all lab members for their advice and supports.

I also would like to acknowledge the Ministry of Higher Education Malaysia and Universiti Tun Hussein Onn Malaysia to award me with the financial support. My greatest gratitude must forward to my family especially my parents, Mr. Hashim Mohd Said and Ms. Uminah Kaseran for continual love and support. Lastly and most importantly, special thanks to my beloved wife, Ms. Norasiah Md Aspan for sharing the happiness and hardship together.

ABSTRACT

Investigation of intracellular properties is very important since deemed to provide significant information that contributes to the biology applications such as drug delivery and cancer diagnosis. The purpose of this study is to realize various manipulation and injection of fluorescence sensor into a selective target cell using optical control of zeta potential and utilizing multiple wavelength lights, and development of a hydrogel fluorescence sensor for prolonged stable temperature measurements for achieving the measurement system of physiological parameters in the cellular environment.

Chapter 1 introduces the background of the research and the previous study of this thesis. After explaining the importance of manipulation, injection, and measurements of micro-nanoparticles in single cell analysis, the fluorescence-based sensors using micro-nanoparticles, and the problems of conventional manipulation and injection of micro-nanoparticles into cells for intracellular measurements were discussed. Besides, the features of optical control in manipulation and injection of micro-nanoparticles into cells for intracellular measurements also described. Finally, the purpose of the research and the outline of the thesis are described.

Chapter 2 presented a new method of manipulation and injection of fluorescence microsensors into cells using glass nanoprobe and optical control of zeta potential. As a demonstration, a single microsensor of 750 nm diameter was picked-up using a glass nanoprobe with optical control of the zeta potential. Then, the microsensor was transported and immobilized onto a target cell membrane. After that, it was injected into the cytoplasm using NIR

laser at 1064 nm wavelength. The success rate of pick-up and cell immobilization of the microsensor were compared, and the cell injection and cell survival rates were evaluated.

In Chapter 3, the author proposed the manipulation and injection of the fluorescence microsensor into cells using multiple wavelength lights. The sensor made of 1 μm diameter polystyrene particle-containing Rhodamine B and an infrared (IR: 808 nm) absorbing dye. The polystyrene particle can be manipulated with optical tweezers by 1064 nm laser to the target cell. After being transported to the cell membrane, the fluorescence microsensor is heated by 808 nm laser and injected into the cell by melting the cell membrane. The manipulation and injection of the microsensor to the MDCK cell by 1064 nm and 808 nm laser were demonstrated. The result showed a high success rate (70%), low invasive and rapid injection within 10 s. From these results, the effectiveness of the proposed cell injection of fluorescence microsensor using multiple wavelength lights were confirmed.

In Chapter 4, the author presented a hydrogel fluorescence microsensor for prolonged stable temperature measurements. In this work, a photobleaching compensation method based on the diffusion of fluorescent dye inside a hydrogel microsensor is proposed. The factors that influence compensation in the hydrogel microsensor system are the interval time between measurements, material, the concentration of photo initiator, and the composition of the fluorescence microsensor. These factors were evaluated by comparing a polystyrene fluorescence microsensor and a hydrogel fluorescence microsensor, both with diameters of 20 μm . The effect of microsensor size on the stability of the fluorescence intensity was also evaluated. The hydrogel fluorescence microsensors, with sizes greater than the measurement area determined by the axial resolution of the confocal

microscope, showed a small decrease in fluorescence intensity, within 3%, after 900 measurement repetitions. The temperature of deionized water in a microchamber was measured for 5,400 s using both a thermopile and the hydrogel fluorescence microsensor. The results showed that the maximum error and standard deviation of error between these two sensors were 0.5 °C and 0.3 °C, respectively, confirming the effectiveness of the proposed method.

Chapter 5 gives the conclusions of this study and the future works were discussed.

In conclusion, the proposed methods allow the manipulation and cell injection of a single microsensor to be used as a carrier for intracellular and extracellular measurement, especially in biological and biomedical applications such as drug delivery and cancer diagnosis.

CONTENTS

Acknowledgment	i
Abstract	iii
Contents	vii
List of Figures	xiii
List of Tables	xvii
Chapter 1 Introduction	1
1.1 Single Cell Analysis	1
1.2 The Importance of Manipulation, Injection, and Measurements of Micro-Nanoparticles in Single Cell Analysis	4
1.3 Fluorescence-based Sensors using Micro-Nanoparticles in Single Cell Analysis	6
1.3.1 Polymeric micro-nanoparticles	7
1.3.2 Liposome micro-nano particles	8
1.3.3 Gel micro-nanobeads	10
1.3.4 Silica micro-nanoparticles	12
1.3.5 Magnetic micro-nanoparticles	14
1.3.6 Gold micro-nanoparticles	15
1.3.7 Summary	18
1.4 Conventional Manipulation and Injection of Micro-nanoparticles into Cells for Intracellular Measurements	18
1.4.1 Endocytosis	19
1.4.2 Lipofection	22

1.4.3	Micro-nano injection	22
1.4.4	Electroporation	25
1.4.5	Sonoporation	26
1.4.6	Optoporation	27
1.4.7	Summary	29
1.5	Optical Control in Manipulation and Injection of Micro-nanoparticles into Cells for Intracellular Measurements	30
1.5.1	Manipulation of nanoparticles by optical control of zeta potential	30
1.5.2	Manipulation of micro-nanoparticles by optical tweezers	32
1.5.3	Injection of nanoparticles into living cells by optical tweezers	35
1.5.4	Injection of nanoparticles into living cells by femtosecond laser	38
1.6	Thesis Overview	39
1.6.1	Research objectives	39
1.6.2	Outline of the thesis	39
Chapter 2 Manipulation and Immobilization of a Single Fluorescence Microsensor for Selective Injection Into Cells		43
2.1	Introduction	43
2.2	Materials and Methods	46
2.2.1	Principle of manipulation and cell injection of the microsensor using optical control of the zeta potential	46
2.2.2	Experimental system setup	48

2.2.3	Optical control of zeta potential using photochromic material	49
2.2.4	Fabrication of the microsensor with a photochromic lipid layer	50
2.2.5	Fabrication of the glass nanoprobe	52
2.2.6	Cell culture	52
2.3	Results and Discussion	53
2.3.1	Temperature calibration of the microsensor	53
2.3.2	Manipulation and immobilization of the microsensor using zeta potential control	54
2.3.3	Injection of the microsensor by local laser heating	56
2.4	Summary	58
Chapter 3 Injection of a Fluorescence Microsensor into a Specific Cell by Laser Manipulation and Heating with Multiple Wavelengths of Lights		61
3.1	Introduction	61
3.2	Materials and Methods	65
3.2.1	Principle of optical injection of single fluorescence microsensor to a specific cell by optical manipulation and heating with multiple wavelength lights	65
3.2.2	Experimental setup	68
3.2.3	The fabrication process of the fluorescence microsensor	69
3.2.4	Cell culture	71
3.3	Results and Discussion	72
3.3.1	Size evaluation of fluorescence microsensor	72
3.3.2	Temperature calibration of fluorescence microsensor	73

3.3.3	Heat evaluation of fluorescence microsensor using 1064 nm and 808 nm lasers	74
3.4	Manipulation and injection of the fluorescence microsensor into MDCK cell	75
3.5	Summary	78
Chapter 4 Hydrogel Fluorescence Microsensor with Fluorescence Recovery for Prolonged Stable Temperature Measurements		81
4.1	Introduction	81
4.2	Materials and Methods	84
4.2.1	Principle of photobleaching compensation for the hydrogel fluorescence microsensor	84
4.2.2	Experimental system	87
4.2.3	Fabrication of the hydrogel fluorescence microsensor	88
4.3	Results	92
4.3.1	Comparison of photobleaching compensation for different sensor materials	92
4.3.2	Effect of measurement interval time on photobleaching compensation	93
4.3.3	Effect of photo initiator concentration on photobleaching compensation	94
4.3.4	Effect of sensor size on fluorescence intensity recovery	95
4.3.5	Temperature measurement using hydrogel fluorescence microsensors	97
4.4	Discussion	99
4.5	Summary	102
Chapter 5 Conclusions and Future Works		105

5.1	Conclusions	105
5.2	Future Works	107
5.2.1	Microsensor manipulation in the cell cytoplasm	108
5.2.2	Microsensor application in intracellular measurement	108
5.2.3	Multi-fluorescence microsensor for intracellular measurement	108
	Bibliography	111
	Accomplishments	139

LIST OF FIGURES

1.1	Applications of single-cell analysis in various fields [12–16].	3
1.2	Properties of nanothermometer.	8
1.3	Schematic of three different methods to engineer liposome-nanoparticle hybrids.	9
1.4	Schematic of the encapsulation of the sensor into the liposome [68].	10
1.5	Wide range of pH measurement with fabricated gel-microbeads impregnated with different pH indicators.	11
1.6	Schematic diagrams of three different types of hybrid micro-nanogel optical probes.	12
1.7	Representative scanning electron micrographs of core-shell fluorescent silica nanoparticles of different diameters [78].	13
1.8	Schematic diagram of the surface functionalization of silica nanoparticles with, for example, peptides, antibodies, aptamers, enzymes, deoxyribonucleic acid (DNA)-fragments and different functional moieties [80].	14
1.9	Magnetic nanoparticles (MNPs).	15
1.10	Gold nanoparticles (AuNPs).	17
1.11	Schematic of endocytosis and exocytosis patterns of nanoparticles [111].	19
1.12	Images from time-lapse microscopy of cells after incubation [119].	21
1.13	Schematic of lipofection mechanism [68].	22

1.14	Micro-nanorobotic manipulation system for single-cell injection.	23
1.15	Fabrication of an on-chip nanorobot integrating functional nanomaterials for single-cell punctures [135].	25
1.16	Schematic of electroporation in biotechnology applications [136].	26
1.17	Schematic of sonoporation to enhances liposome accumulation and penetration in tumors [140].	27
1.18	Morphological changes in HEK cells.	28
1.19	Schematic of a selective injection of encapsulated fluorescent microsensor into a cell.	31
1.20	Schematic of a selective injection of encapsulated fluorescent microsensor into multi-lamellar liposome into a cell.	31
1.21	Schematic of the optical tweezers system.	33
1.22	Schematic of the optical tweezers system.	35
1.23	Plasmon resonance assisted optical injection of signaling molecules.	36
1.24	Schematic diagram of selective adhesion and rapid injection of a fluorescent sensor into a target cell using local mechanical stimulus applied by optical tweezers [68].	37
1.25	Injection of single microsensor into living cells using optical tweezers.	38
1.26	Outline of the dissertation.	41
2.1	Schematic diagram of manipulation and cell injection of a single microsensor using optical control of the zeta potential.	47
2.2	Schematic diagram of the experimental system.	49
2.3	Schematic diagram of optical control of zeta potential.	50

2.4	Fabrication process of the microsensor.	51
2.5	Optical and fluorescence image of the microsensor.	52
2.6	Measurement of fluorescence intensity vs. temperature to construct a calibration curve. The error bars represent the standard deviation of average fluorescence intensity from nine stained microsensors.	54
2.7	Pick-up and immobilization of the microsensor using a micromanipulator and optical control of the zeta potential.	55
2.8	Injection of the immobilized sensor by local laser heating.	57
3.1	Classification of injection of the microsensor into a specific cell.	66
3.2	A schematic diagram of optical manipulation of fluorescence microsensor to a specific cell by local heating using multiple wavelength lights.	68
3.3	Experimental setup.	69
3.4	A schematic image of fluorescence microsensor.	70
3.5	Fabrication process of fluorescence microsensor.	71
3.6	Bright field and fluorescence image of fluorescence microsensor.	71
3.7	Size distribution of fluorescence microsensor.	72
3.8	Calibration result of relative fluorescence intensity of the fluorescence microsensor with temperature.	73
3.9	Comparison of absorption rate of IR absorbing dye between 808 nm and 1064 nm (Thickness of microchannel 150 μm).	75
3.10	Measurement of temperature increase of fluorescence microsensor by irradiating 808 nm laser.	75

3.11	Manipulation and injection of fluorescence microsensor to MDCK cell.	76
3.12	Fluorescence image of injected fluorescence microsensor.	77
4.1	Schematic diagram of fluorescence recovery after photobleaching in a hydrogel fluorescence microsensor.	86
4.2	Experimental system.	88
4.3	Fabrication processes for fluorescence microsensors.	89
4.4	Fluorescence images of fabricated microsensors.	91
4.5	Comparison of the fluorescence intensity recovery for the different sensor materials.	93
4.6	Relationship between the variation of fluorescence intensity of the hydrogel fluorescence microsensor (9% PEGDA 575) and the interval time between exposures.	94
4.7	Evaluation of the effect of photo initiator concentration on photobleaching compensation.	95
4.8	Relationship between the recovery of relative fluorescence intensity and microsensor size.	96
4.9	Calibration of the relative fluorescence intensity with temperature.	98
4.10	Comparison of the temperatures measured by the hydrogel fluorescence microsensor with photobleaching compensation and a thermopile.	99
4.11	Photobleaching compensation of hydrogel fluorescence microsensors containing FITC and $(\text{Ru}(\text{bpy})_2\text{Cl}_2)$.	101

LIST OF TABLES

1.1	Conventional methods for sensor injection into a cell.	29
2.1	Success rate of pick-up of the microsensor by the glass nanoprobe without/with UV irradiation.	56
3.1	Comparison of injection time and success rate of injection by presented method and previous work.	78

Chapter 1

Introduction

1.1 Single Cell Analysis

Cells play a significant role in our daily life. The interactions of cells, the cellular responses of organelles to molecules, and their intracellular behavior are important, especially in biological and biomedical research. Many biological experiments are performed on groups of cells with the assumption that all particular cells are identical. However, the latest evidence shows that heterogeneity exists within small cell populations [1,2]. Individual cells can differ in terms of size, protein levels, and ribonucleic acid (RNA). For example, research concerning the differentiation behaviors of stem cells or the metastatic processes of tumor initiation requires detailed information [3–5]. Understanding genomic sequence information at a single cell level can

stimulate an understanding of how individual parts of a cell are integrated into time and space to form dynamic cellular processes [6–8]. The connection between cellular heterogeneity and signaling pathway regulation may affect an understanding of disease states that can potentially drive therapeutic interventions. Therefore, single cell analysis has been emerging as the essential method of investigating exciting new insights into genes, transcripts, proteins, metabolites, lipids, and interactions [9].

The single cell is the basic unit of living organisms that is structural, functional and biological. Cell study is a natural step in reducing the way organisms are studied [2]. Many review articles have been reported to discuss the problems and trends of single-cell analysis from the biological and biomedical perspectives [6,7,9,10]. Individual cells within the same population may differ dramatically, and these differences may have important consequences for the function of the entire population. The single-cell study would provide an objective interpretation of the cell's behavior as one cell is being analyzed at a time. Experimental approaches to single-cell analysis are required to address significant differences and ultimately improve the detection and treatment of diseases. These variations can be caused by genetic alterations and micro-environmental differences in individual cells [11].

Single cell analysis is used in various applications such as single-cell isolation, mechanical performance, micro-nano environment, and biological properties, as shown in Figure 1.1 [12–16]. For example, direct and quantitative single-cell analysis of Type 1 human immunodeficiency virus reactivation from latency was studied and showed that the following stimulation with pro-inflammatory cytokines could be uncoupled with cell activation and virus reactivation [17]. In addition, the smart-sequence approach was used to profile full-length messenger RNA (mRNA) from single cells by examining

circulating tumor cells (CTCs) from melanomas and recognizing distinct signatures of gene expression as well as alternative disease-specific splicing events [18]. Recently, single-cell research focused on the microfluidic chip equipped with high-performance and high-precision automation systems have been extensively studied [19,20]. Single cell analysis is therefore essential in order to systematically characterize a cell's state, identify natural cell-to-cell variability, measure the impact of environmental stimuli, understand cellular responses in tissues and complex environments, and resolve limitations in measurement approaches.

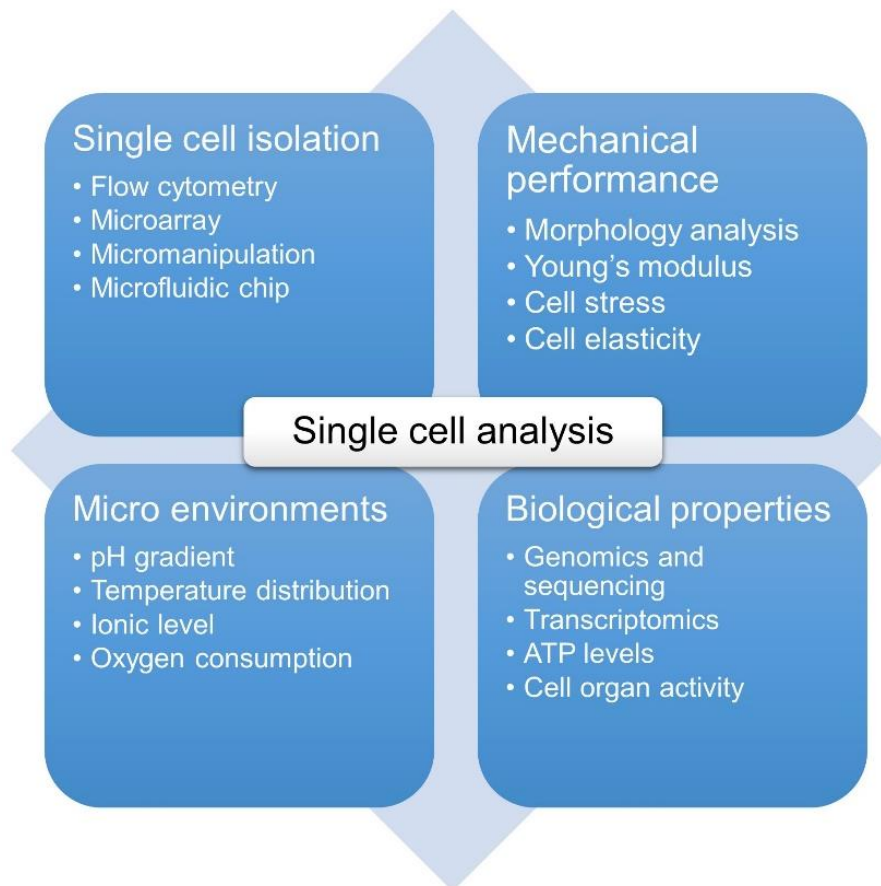


Figure 1.1 : Applications of single-cell analysis in various fields [12–16].
ATP: Adenosine triphosphate.

1.2 The Importance of Manipulation, Injection, and Measurements of Micro-Nanoparticles in Single Cell Analysis

The cellular analysis brings critical knowledge to modern biological and biomedical sciences. The conventional cellular analysis only probes the average response from the whole cell group. This potentially produces misleading readouts from a cell group with diverse outputs across the same type of cell heterogeneity [20]. Moreover, a specific cell type can have a few subsets. For example, T-cells are categorized into few subsets according to their distinct functions such as cytotoxic cells, helper cells, and regulatory cells [21]. To address the above problems, single-cell analysis techniques have been developed to analyze various cellular functions in a large cell population at an individual cell level.

Recently, manipulation and low-invasive cell injection of a single nanosensor have received extensive attention due to the significant influence on biological and biomedical applications [22]. For example, the measurement of the environment properties of the virus-infected cell is one of the most important issues to investigate virus proliferation mechanism [23] and develop new medicines and diagnosis such as diagnostic tools in ocular allergy [24], point of care testing (POCT) [25], and microbiome in cancer [26]. In particular, investigation of intracellular properties is deemed to provide significant information [27,28].

The intracellular chemical environment such as temperature [29,30], pH [31] and concentration of oxygen [32] fundamentally regulates cell events including cell division, gene expression, enzyme reaction and metabolism. Research has shown that temperature plays a major role in many cell events and correlates with cell state and cellular functions [27]. Similarly, the

intracellular pH modulates the function of many organelles and plays a key role in many environments and pathological processes [33,34]. Even a very small change in temperature or pH values may cause a difference in cell reactions. For example, the presence of specific strains of microorganisms in the tumors could provide us with a vital clue that connects spontaneous regression with microorganisms [35]. The micro-nano scale thermometers have been developed for thermal sensing and imaging of living cells and biological tissues [36]. The intracellular pH of MDCK cells dropped by 0.3 to 0.4 between 3 and 5 hours after influenza virus infection [23]. Highly reliable identification, imaging and control of reactive oxygen species (ROS) in subcellular organelles are critical to understanding the biological functions of ROS and discovering the pathogenesis of certain diseases [37]. Besides, evaluation and correction the impact of photobleaching to improve the accuracy of pharmacokinetic parameter estimates in drug delivery application [38]. Therefore, measurements of the intracellular environment such as temperature, pH and oxygen can provide critical information on cell activities.

On the other hand, a fluorescence indicator is widely used to stain either whole or part of a cell for intracellular measurement [39,40]. Fluorescence measurement enables spatiotemporal measurement of various properties such as temperature, pH, ion concentration depending on the fluorescence intensity and lifetime [41,42]. However, there are some disadvantages such as the difficulty of concentration control of fluorescence indicator and photobleaching of fluorescence intensity. Encapsulation of fluorescence indicator into micro-nanoparticles achieves the concentration control [43]. Fluorescence micro-nanoparticles sensor can be designed based on its size, shape, measurement parameters according to the purpose. However, manipulation and injection of the arbitrary fluorescence sensor to a

particular cell are difficult tasks [43]. Therefore, the key issues for accurate intracellular measurement are manipulation and injection of the specific nanoparticles with high-throughput and low invasively [44]. In this study, the measurement system includes the manipulation and injection of a fluorescence nanoparticle by optical control will be discussed and demonstrated. Relevant information will be briefly explained in the following sub-topic in this chapter whereas a detailed explanation of the application will be discussed in the following chapter.

1.3 Fluorescence-based Sensors using Micro-Nanoparticles in Single Cell Analysis

Fluorescence microscopic imaging is a commonly used approach to visualize cells and organelles and to study intracellular interactions. There a wide range of available organic fluorophores and fluorescent proteins can be selectively inserted into cell or marker, and so-called optical sensor [45,46]. Many types of sensors were developed for an instant for single-cell study, including electrical, mechanical, electrochemical, magnetic, and fluorescence. Fluorescence-based optical sensors are suitable for single-cell measurement compared to these sensors because they do not need interconnection for data acquisition [47–49].

The fluorescence-based sensor transmits this information when the temperature of the luminescent material changes resulting in fluorescence intensity changes, excitation range, lifetime, or fluorescence wavelength [50–52]. For example, intracellular and low-invasive measurement using micro-nano particles impregnated with fluorescence indicators [53–56]. While small molecule indicators have several problems, such as rapid leakage, lack of

membrane permeability and low photo-stability or sensitivity to ionic strength [57], in their practical applications these problems have been limited. Therefore, fluorescence-based micro-nano particles have great potential as sensors carriers in medicine and biotechnology since multiple indicators can be attached to a single particle [57]. Moreover, a variety of organic (*i.e* polymer, liposome, gel) and inorganic (*i.e* silica, magnetic, metallic) types of micro-nanoparticles can be fabricated as a sensing element in intracellular measurement and cell targeting [58,59].

1.3.1 Polymeric micro-nanoparticles

Polymeric nanoparticles are important carriers for anticancer drug delivery and extensively investigated due to their advantages in long circulation, passive targeting, and diversity [60]. For example, fluorescent polymeric has been used in various situations to immobilize molecular probes and sensor nanoparticles for temperature [50]. In particular, Bradley *et al.* demonstrated that amino-functionalized polystyrene microspheres filled with fluorescein are used in live cells for real-time pH measurement. [61]. The use of these sensors immobilized covalently onto polymeric particles allows the analysis of intracellular activities over a long period of time.

Oyama *et al.* fabricated fluorescent nanoparticles so-called walking nanothermometers for spatio-temporal temperature quantity of transported acidic organelles in single cells. Fluorescent nanoparticles have been fabricated by impregnating poly(methylmethacrylate) (PMMA) network with temperature-sensitive peroxide, as shown in Figure 1.2. The fluorescence nanoparticles internalized into HeLa cells via endocytosis, then enclosed in acidic organelles before transported along microtubules, can observe temperature changes to pH values and ionic strength [62]. Recently, Takei *et*

al. Here, developed a ratiometric nanothermometer (RNT) for intracellular temperature measurement in real-time. Both the thermos-sensitive fluorophore and the thermo-insensitive fluorophore which was used as a self-reference, are embedded in a polymeric particle that shields the fluorophores from intracellular conditions [12].

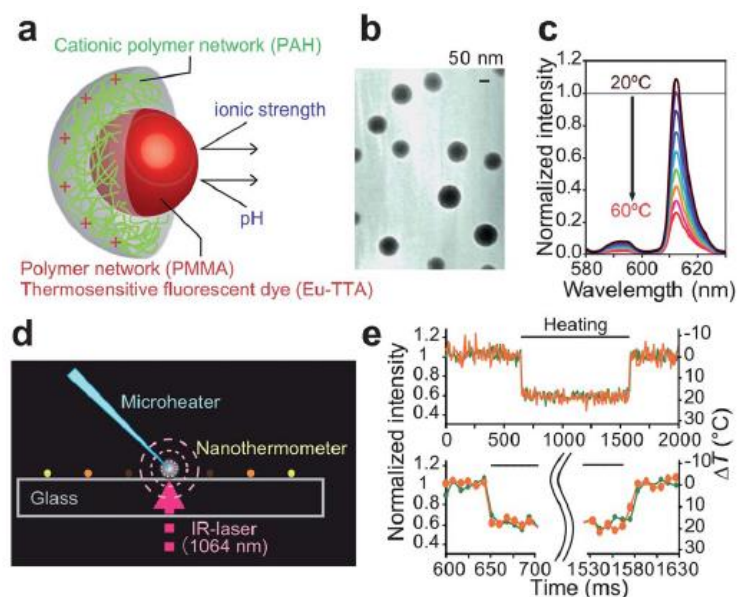


Figure 1.2 : Properties of nanothermometer.

(a) Schematic of the fluorescent nanothermometer; (b) The core of nanothermometers observed by the transmission electron microscopy; (c) Fluorescence spectrum of the nanothermometers dispersed in PBS (pH 7.4) at various temperatures. Fluorescence intensity was measured at excitation 341 nm and emission 613 nm; (d) Schematic of the micro heating system for the measurement of the response speed of the nanothermometers on the glass slide. IR-laser beam focused on a microheater, the aggregation of aluminum particles (grey sphere) at the tip of a glass micro-needle (blue), generates local temperature gradients. The bright (yellow) and dark (brown) nanothermometers illustrate high and low fluorescence intensities, respectively; (e) Time course of the fluorescence intensity responding to the abrupt temperature increase and decrease induced by the microheater. Bottom, enlarged view at the time indicated [62].

1.3.2 Liposome micro-nano particles

Liposomes are the best clinically well-known nanoscale delivery systems that are used to convey cytotoxic and anti-fungal drugs, genes, vaccines and imaging agents [63,64]. Liposome micro-nanoparticles hybrids are structurally diverse nanosystems offering a wide variety of opportunities

for engineering to achieve specific biological functions. Figure 1.3 shows an illustration of three different methods to engineer liposome micro-nanoparticle hybrids. Hydrophobic nanoparticles can be embedded in the lipid bilayer (left), encapsulated in the aqueous core (right), and nanoparticles chemically conjugated or physically adsorbed to the liposome surface (bottom) [64].

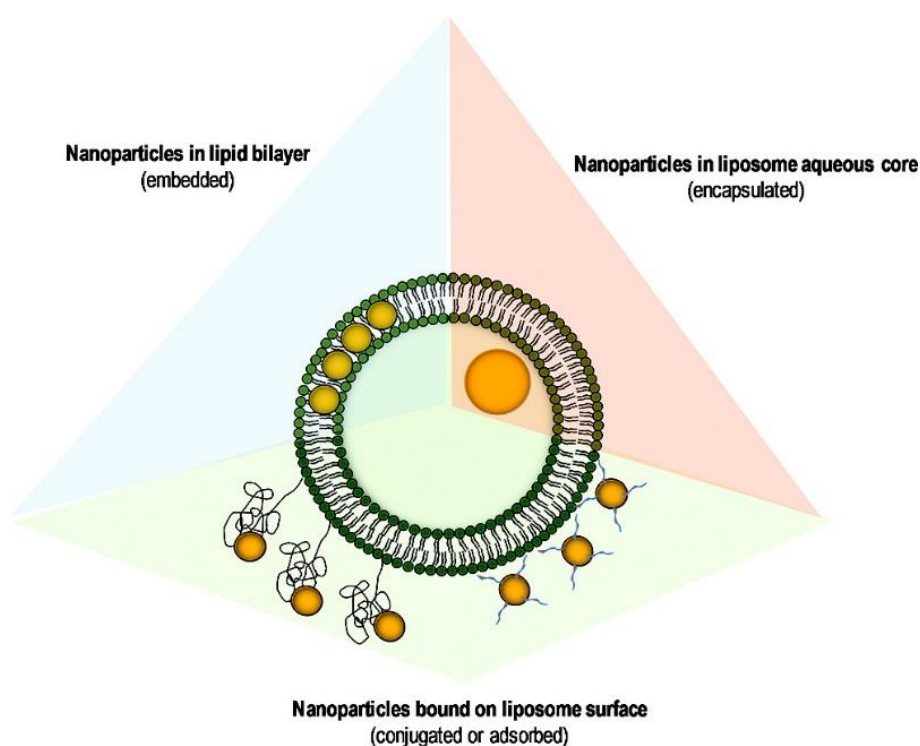


Figure 1.3 : Schematic of three different methods to engineer liposome-nanoparticle hybrids. Hydrophobic nanoparticles embedded in the lipid bilayer (left); hydrophilic nanoparticles encapsulated in the aqueous core (right); and nanoparticles chemically conjugated or physically adsorbed to the liposome surface (bottom) [64].

For example, Troutman *et al.* introduced a new method for light-induced content release from gold-coated liposomes [63]. Fluorescein was encapsulated in the temperature-sensitive liposomes at self-quenching concentrations. McNamara *et al.* demonstrated the pH-sensing capability and application of micrometric phospholipid-coated polystyrene particles in murine macrophages for intracellular pH measurements. [65]. For single

macrophages, the fluorescent lipobeads are used to test the pH. The synthesis of the pH sensing lipobeads is realized, and the dynamic range of the sensing particles is between pH 5.5 and 7.0 with a sensitivity of 0.1 pH unit. In previous studies performed in Arai Lab, through incorporating liposome membrane fusion and optical tweezers for cell temperature measurement, Masuda *et al.* demonstrated a single fluorescence microsensor injection into a specific cell. [66]. Maruyama *et al.* later developed a fluorescence sensor encapsulation in the liposome containing photochromic material for selective and rapid injection into a living cell. [67]. Recently, Liu *et al.* used polystyrene microbeads encapsulated in the liposome layer in the optical injection of a single sensor into the target cell as shown in Figure 1.4 [68].

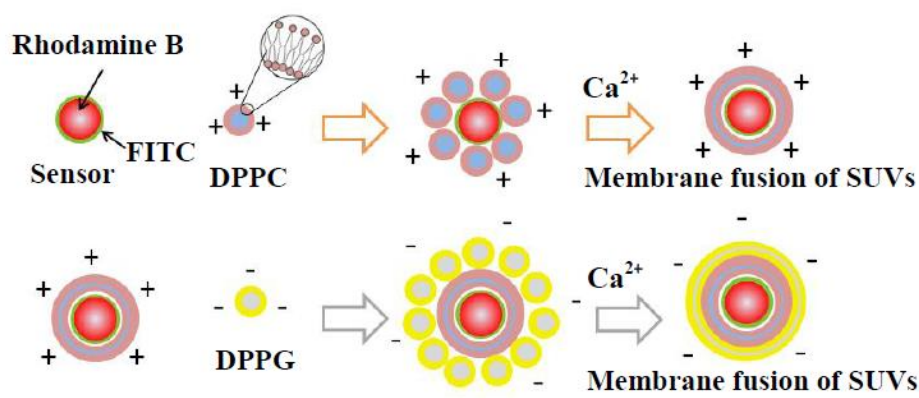


Figure 1.4 : Schematic of the encapsulation of the sensor into the liposome [68].
 FITC: Fluorescein isothiocyanate; DPPC: 1,2-dipalmitoyl-sn-glycero-3-phosphatidylcholine;
 DPPG: 1,2-dipalmitoyl-sn-glycero-3-phosphatidylglycerol; SUVs: Small unilamellar vesicles.

1.3.3 Gel micro-nanobeads

Biopolymers material have been widely used to prepare responsive hydrogels for biomedical application due to their biocompatibility, low toxicity, and high content of functional groups [69–72]. In previous research performed in Arai Laboratory, Maruyama *et al.* developed pH-sensing gel-microbead impregnated with a pH indicator for on-chip measurement [73]. Gel-microbead is made from hydrophilic photo-cross-connectable resin

salting and then handled with optical tweezers. Gel-microbead is polymerized by ultraviolet (UV) lighting and attached under an electrolyte solution to other gel-microbeads as shown in Figure 1.5. The pH value was determined in the gel-microbead by observing the color of the pH indicator [74].

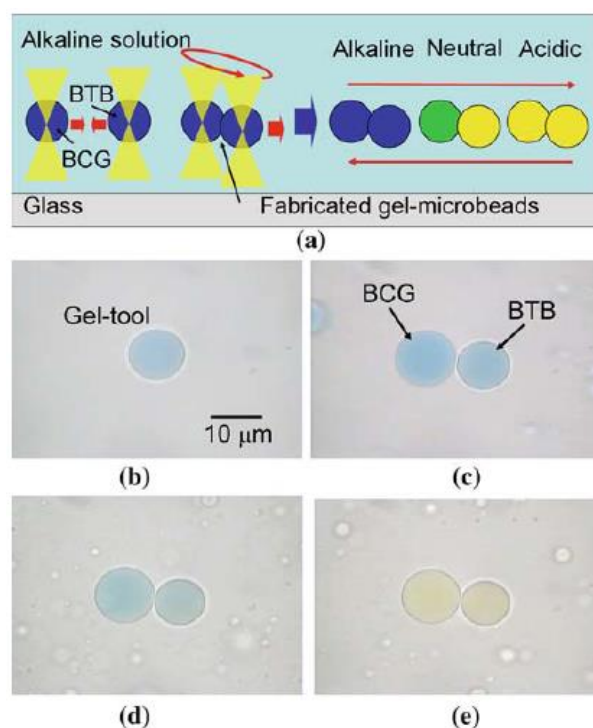


Figure 1.5 : Wide range of pH measurement with fabricated gel-microbeads impregnated with different pH indicators.

(a) Schematics diagram; (b) Gel-microbead impregnated with BTB; (c) Fabrication of gel-microbead impregnated with BTB to gel-microbead impregnated with BCG in pH 9 solution; (d) pH was changed to pH 8.1; (e) pH was changed to pH 4.6 [74]. BTB: Bromothymol blue; BCG: Bromocresol green.

Recently, Wu *et al.* reviewed the latest developments and challenges of intracellular imaging applications for hybrid micro-nano gels in optical sensing such as pH, temperature, glucose, ions and other species [75]. Hybrid micro-nano gel probes can be categorized into three types as shown in Figure 1.6. In Type 1, the specific antibodies are covalently linked to the hybrid micro-nano gels. The optical moiety acts as the chemical or biochemical signal receiver in Type 2, whereas the stimulus-responsive polymer gel network

chains serve as Type 3 chemical or biochemical signal receiver. Later, Wu *et al.* reported a new class of chitosan-based hybrid nanogels by *in-situ* immobilization of Cadmium Selenide (CdSe) quantum dots (QDs) for the incorporation of optical pH detection, tumor cell imaging and drug delivery [76]. Therefore, the polymer microgels are ideal candidates for biomaterial applications because they can respond to various environmental stimuli such as pH, temperature, ionic strength or magnetic fields [77].

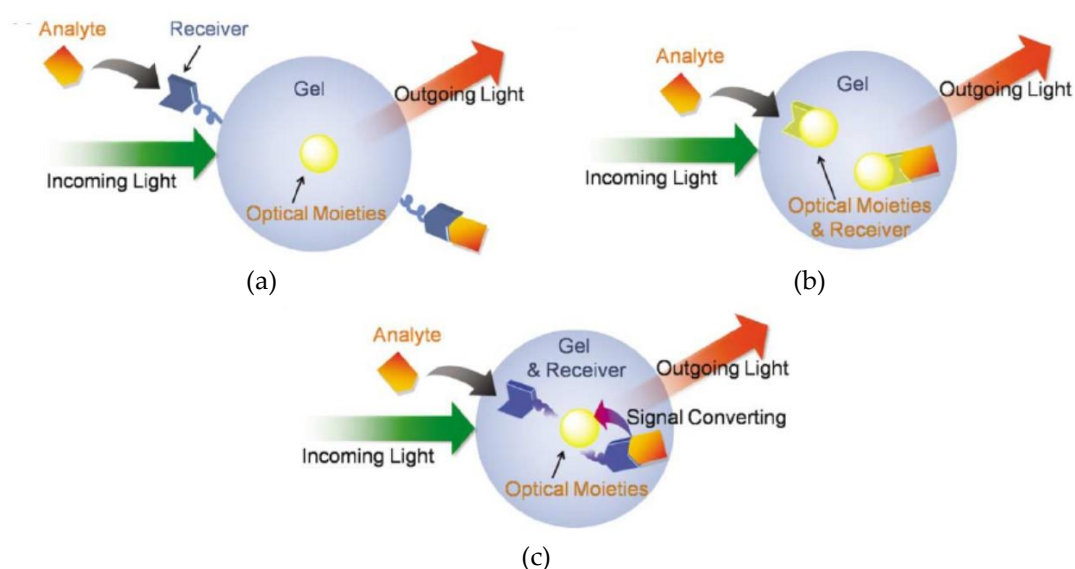


Figure 1.6 : Schematic diagrams of three different types of hybrid micro-nanogel optical probes.

- (a) Type 1, the antibody or specific targeting ligand acts as a chemical/biochemical signal receiver; (b) Type 2, an optical moiety acts directly as the chemical/biochemical signal receiver; (c) Type 3, a responsive polymer gel network chain acts as the chemical/biochemical signal receiver. [75]

1.3.4 Silica micro-nanoparticles

For quantitative chemical sensing in live cells, fluorescent colors encapsulated in silica nanoparticles were developed. The fluorescein encapsulated in these particles tends to be brighter and more photostable in solution than the corresponding free colors [78,79]. For applications ranging

from biology to photonics, it is desirable to tailor particle size throughout the nanometer to micron-scale as shown in Figure 1.7.

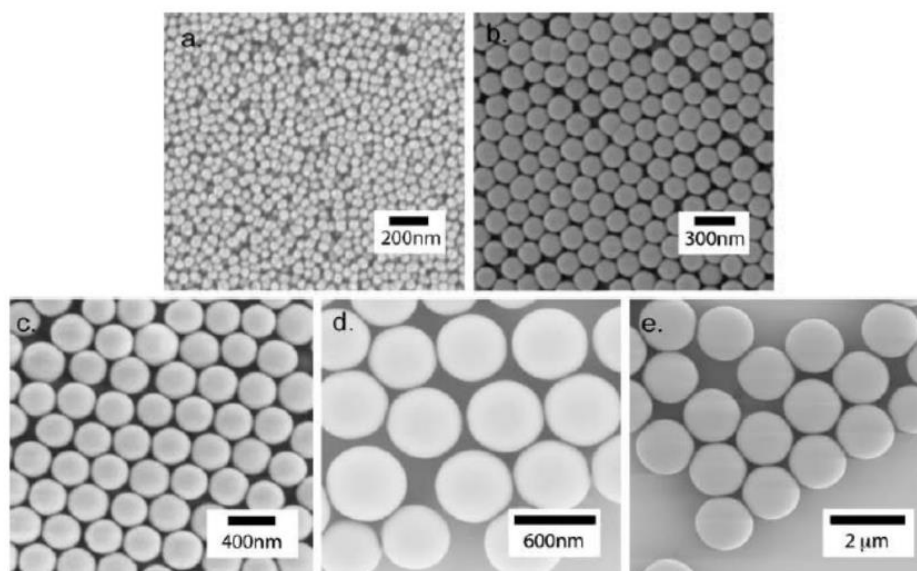


Figure 1.7 : Representative scanning electron micrographs of core-shell fluorescent silica nanoparticles of different diameters [78].
(a) 50 nm; (b) 150 nm; (c) 250 nm; (d) 500 nm; (e) 1500 nm.

Anja Schulz and Colette McDonagh documented the encapsulation of fluorophores into silica nanoparticles and their use as optical sensors for intracellular sensing [80]. Studies have shown that these nanoparticles of silica have great potential for real clinical and biomedical applications. In addition, surface functionalization can also be used to build one or more shells around a nucleus of nanoparticles, as shown in Figure 1.8.

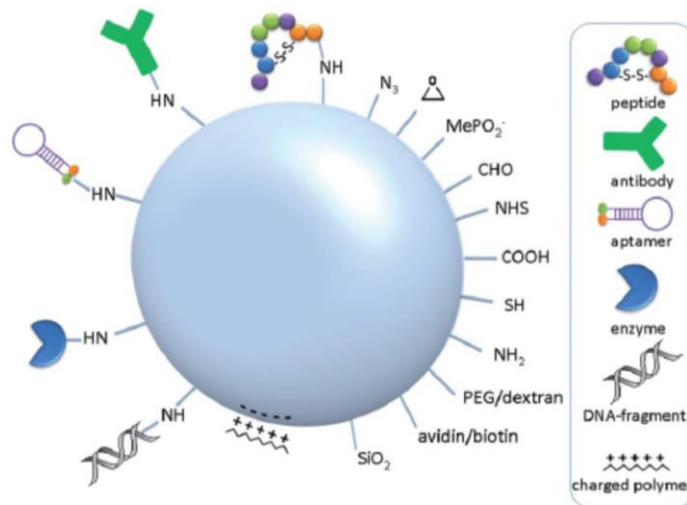


Figure 1.8 : Schematic diagram of the surface functionalization of silica nanoparticles with, for example, peptides, antibodies, aptamers, enzymes, deoxyribonucleic acid (DNA)-fragments and different functional moieties [80].

1.3.5 Magnetic micro-nanoparticles

Magnetic nanoparticles (MNPs) which commonly consist of two components, a magnetic material, often iron, nickel and cobalt, and a chemical component are a class of nanoparticle that can be manipulated using magnetic fields. Magnetic nanomaterials have now been used extensively in biological, biomedical and industrial applications [81–88]. For example, as a hydroquinone biosensor [89], magnetic-based nanomaterials such as core-shell ($\text{Fe}_3\text{O}_4\text{-SiO}_2$) nanoparticles and iron oxide (Fe_3O_4) nanoparticles were used to improve sensor sensitivity [90] and catalyst recycling or activity [85]. Likewise, superparamagnetic iron oxide nanoparticles were used for the delivery of drugs and cancer hyperthermia [91,92]. In addition, magnetic nanoparticles have contributed significantly to cell sorting and isolation [91,93], waste-water treatment [94] and biological cell manipulation [95]. Several strategies have been explored to yield a water-soluble biocompatible with chemically reactive function using magnetic nanoparticle, as shown in Figure 1.9(a). In the previous study, Zhong *et al.*

used a magnetic polystyrene nanobead with an amine group surface which comprised of polystyrene bead (core) and iron oxide nanoparticles (shell) in cell injection experiment as shown in Figure 1.9(b) [96,97]. The 1064 nm continuous wave laser irradiated magnetic nanobeads adhered to cell membranes and subsequently inserted into living cells.

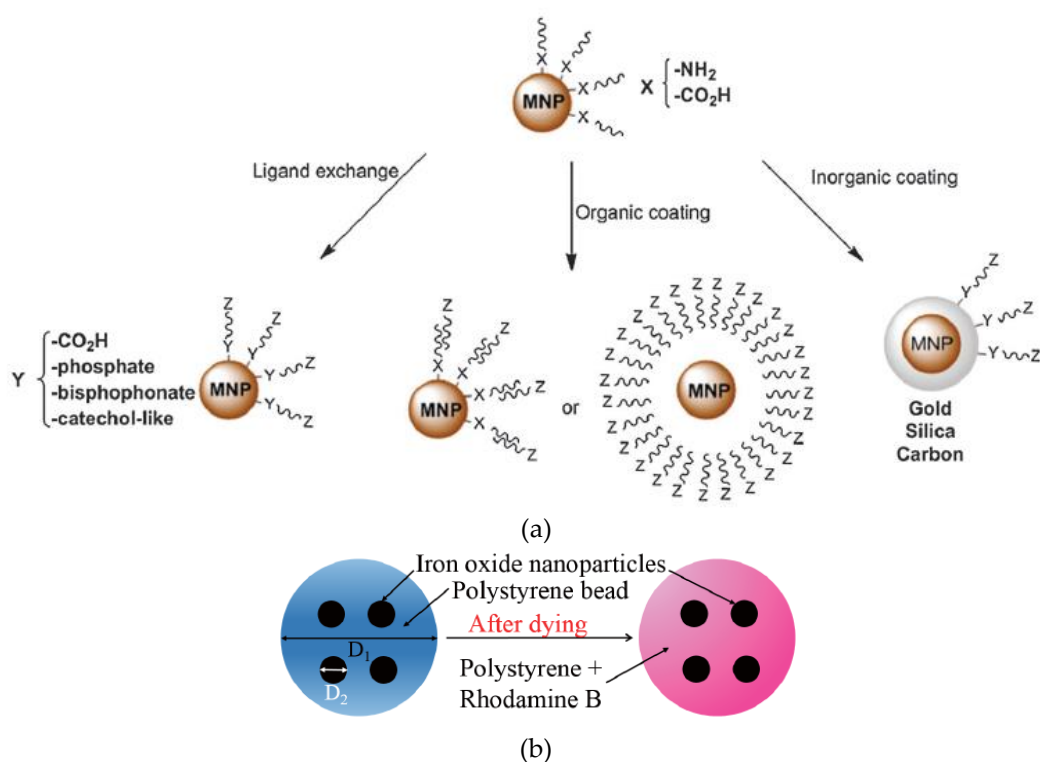


Figure 1.9 : Magnetic nanoparticles (MNPs).

(a) Schematic representation of the different strategies available to obtain water-soluble and chemically active nanoparticles. The final ligands on the nanoparticles can be either small molecules or polymers [81]; (b) Schematic of dyeing magnetic polystyrene nanobeads with Rhodamine B [96].

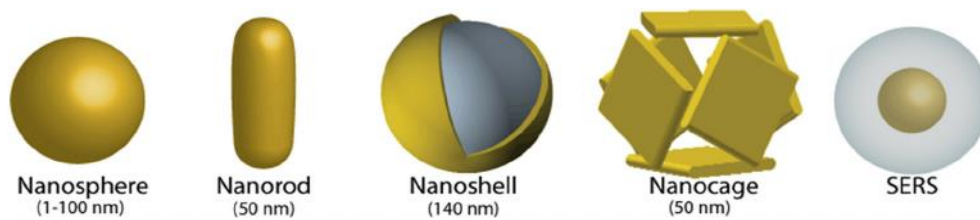
1.3.6 Gold micro-nanoparticles

Among metallic nanoparticles, gold nanoparticles (AuNPs) have been significantly used in a wide range of applications starting from catalysis to biomedicines [98,99]. The optical properties of AuNPs greatly depend on its morphological and physiological characteristics such as size, shape, and aggregation state, which can be fine-tuned by choosing the appropriate

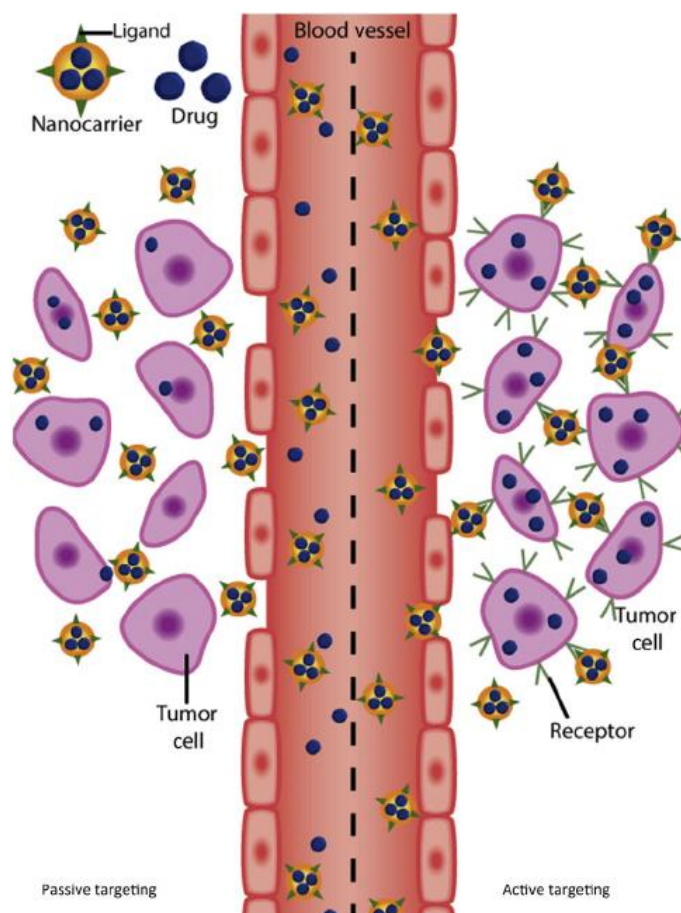
synthesis and stabilization agent gold nanoparticles are incorporated into biosensors to enhance its stability, sensitivity, and selectivity [100]. A key property of AuNPs is their plasmon absorption in the visible (VIS) or near-infrared (NIR) region. The surface plasmon resonance (SPR) stems from the free electrons at the metal surface, collectively resonating with the incident photons [101].

The fluorescence-based AuNP recognition strategy relies on the fluorescence change on the target due to the surface-modified fluorescence (SMF) or the fluorescence resonance energy transfer (FRET). The SMF is the variation of fluorescence by an electromagnetic environment, whereas the FRET is based on the resonant energy transfer occurring between an excited donor fluorophore and an acceptor fluorophore via induced dipole-dipole interactions.

AuNPs have recently been used extensively in biological and biomedical applications [101–103]. Figure 1.10(a) shows the different types of AuNPs which commonly used in the anti-cancer diagnosis and therapeutic applications. Graphical illustration of the accumulation of AuNPs delivering a drug into the tumor sites is illustrated in Figure 1.10(b). AuNP carriers reach the tumor site selectively through the leaky vasculature in a tumor. After nanocarriers penetrate the tumor, targeted nanocarriers can bind or enter the cell via receptor-mediated endocytosis [104].



(a)



(b)

Figure 1.10 : Gold nanoparticles (AuNPs).

(a) Different types of AuNPs commonly used in the anticancer diagnosis and therapeutic applications; (b) Schematic of the accumulation of AuNPs delivering a drug into the tumor sites by passive or active targeting. AuNP carriers reach the tumor site selectively through the leaky vasculature in a tumor. After nanocarriers penetrate the tumor, targeted nanocarriers can bind or enter the cell via receptor-mediated endocytosis [104]. SERS: surface-enhanced raman spectroscopy

Orsinger *et al.* demonstrated that AuNPs coated with liposomes were heated under continuous-wave laser irradiation at 1064 nm wavelength for injection of biosensor into single cells [105]. Furthermore, individual AuNPs were printed on the cell membrane and injected into the mammalian cell by using optical forces and plasmonic heating [106]. On the other hand, femtosecond pulses laser also has been used with strongly focused and high energy to heat the AuNPs and hence generates a transient hole in the cell membrane [107]. A femtosecond laser is an ideal choice for imaging living tissue in an optical window within the range of 600 to 1100 wavelength [108,109] while limiting the potential damage.

1.3.7 Summary

Nanoparticles of fluorescence contain fluorescent polymers, a green fluorescent protein (GFP) and other color markers such as Rhodamine B and QDs. They are ideal for intracellular injection and measurements as they can move through the membrane of the cell and stain the entire cell. At the same time, the cell would receive an extra stimulus from the big, fluorescent dyes that passed through the cell membrane. Therefore, the fluorescence sensors based on micro-nano particles show great potential in single-cell analysis. In this study polystyrene nanobead containing magnetic nanoparticles will be used as a sensor carrier to achieve rapid injection into the target cell. A detailed explanation will be discussed in the following chapter.

1.4 Conventional Manipulation and Injection of Micro-nanoparticles into Cells for Intracellular Measurements

In biological investigations, the cell membrane naturally impermeable external molecules such as drugs, organic, and nanoparticle to penetrate cell

cytoplasm and nucleus [110]. Therefore, several approaches have been developed to pass through this natural barrier either by means of introducing chemical substances such as endocytosis [111] and lipofection [112] or implementing physical approaches including micro-nano injection [113], electroporation [114,115], sonoporation [116], and optoporation [117] to achieve cell injection. Therefore, the principle of these techniques will be briefly discussed.

1.4.1 Endocytosis

Endocytosis is a process of active transport in which a cell brings substances into the cell. Exocytosis is the reverse process of endocytosis. This process results in the discharge of nanoparticles from vesicles at the cell surface to the outside of the cell. Figure 1.11 shows a schematic of endocytosis and exocytosis patterns of nanoparticles [111].

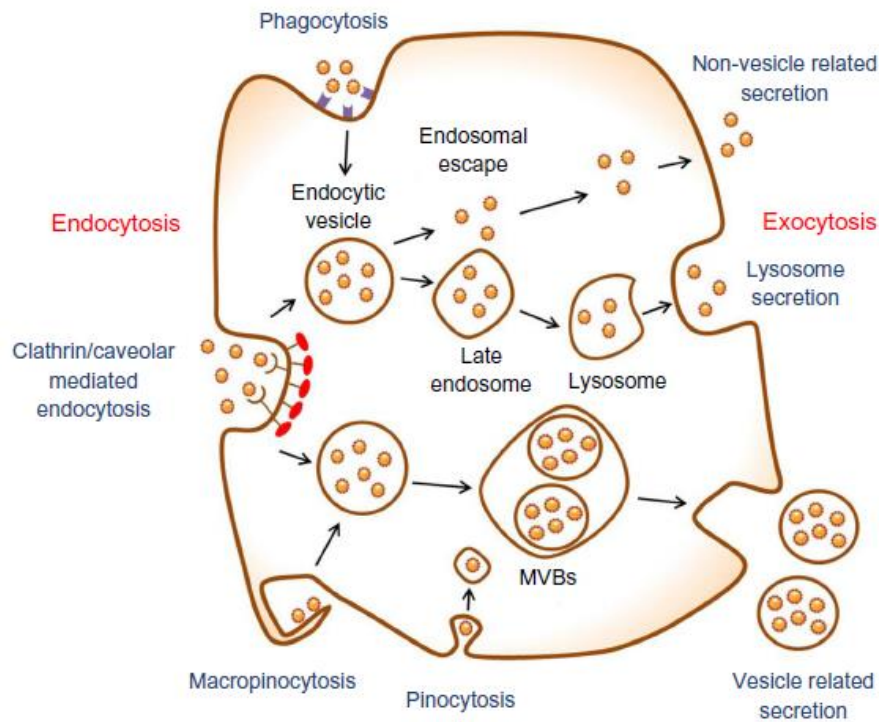


Figure 1.11 : Schematic of endocytosis and exocytosis patterns of nanoparticles [111].

In one hand, nanoparticles enter the cell via four types of the pathway which are clathrin- and caveolar-mediated endocytosis, phagocytosis, macropinocytosis, and pinocytosis. On the other hand, nanoparticles exit the cell via three types of pathway named lysosome secretion, vesicle-related secretion, and non-vesicle-related secretion.

Truschel *et al.* has demonstrated that stretch modulates mucosal surface area by coordinating both exocytosis and endocytosis on the surface membrane of umbrella cells [118]. In addition to activating exocytosis, mechanical stimuli also induce endocytosis, and the balance of these events governs the size of the umbrella cell membrane. Kurtz-Chalot *et al.* were developed as a pH-sensitive double fluorescent particle for biological endocytosis investigations [119]. Figure 1.12 shows a proof-of-concept that was validated in cellular conditions. The upper images show a single cell (pointed square) was selected and followed over time while the middle pictures show a selected cell enlargement. The lower image illustrates an automatic measurement of the Fluorescein isothiocyanate (FITC)/pHrodo ratio changes for 20 hours by software. Recently, Boulant *et al.* have discussed the early stage of virus-host cell interactions including virus adheres on the cell surface, interaction with receptor and internalization [120].

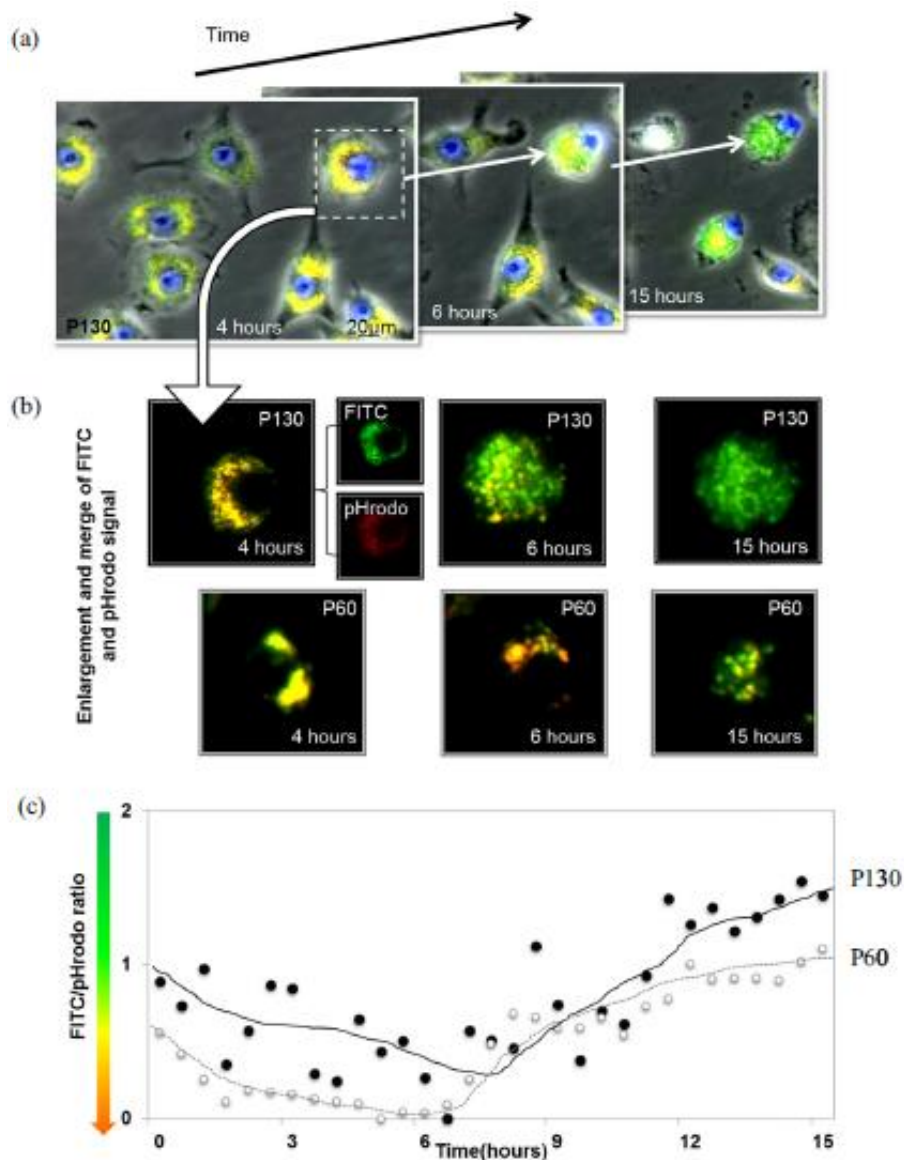


Figure 1.12 : Images from time-lapse microscopy of cells after incubation [119].
 (a) Images from time-lapse microscopy of RAW 264.7 cells after incubation with 300 µg/mL P130. A single cell was selected (dotted square) and followed over time, (b) Enlargement of the previously selected cell (the same thing was done with P60). Only the merge image of FITC and pHrodo signals allowed distinguishing endocytosed particles (that appeared yellow due to the merge of green and red fluorescences). It also allowed detecting the particle release outside the cells (green due to the lack of red pHrodo signal) during the cell death as it was accompanied by loss of membrane integrity, (c) Automated measurement of the FITC/pHrodo ratio changes during 20 h by software.

1.4.2 Lipofection

Lipofection is a process used to inject biological particles into a liposome-based cell that can quickly combine with the cell membrane as they are both made of a bilayer of phospholipids. Lipid bilayers have been used for encapsulation and control delivery in the drug delivery system [64,121] and nanoparticle injection into living cells for liposome transfection. In previous research performed in Arai Lab, the fluorescence sensor was encapsulated into a liposome layer in cell injection applications [66–68,122–125]. As shown in Figure 1.13, lipofection could deliver the sensor encapsulated in the liposome to the cytoplasm [68].

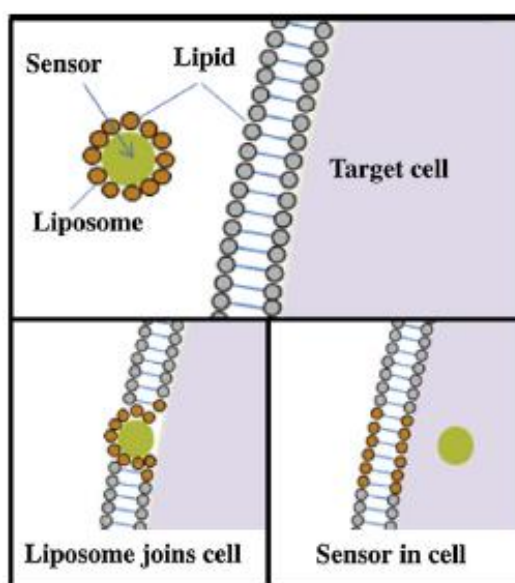


Figure 1.13 : Schematic of lipofection mechanism [68].

1.4.3 Micro-nano injection

Micro-nano injection is normally performed with a micromanipulator, which usually involves the usage of a glass micropipette either to push-in or pull-out substances from a living cell [126–128]. There are two main key procedures in the process which are how to manipulate the pipette precisely and how to penetrate the cell membrane safely. These important procedures

directly determine the success rate of injection and cell viability. As such, it is inefficient and ineffective to perform the injection process by hand manually, especially in the micro-nano scale. Therefore, two types of injection system based on the micro-nano robotic manipulation system is widely used as shown in Figure 1.14.

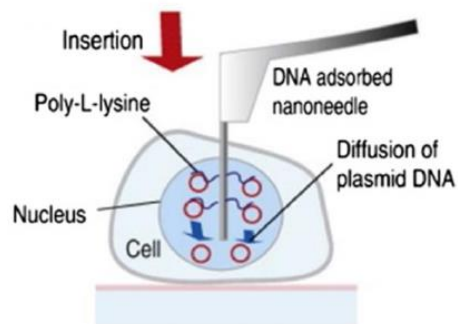
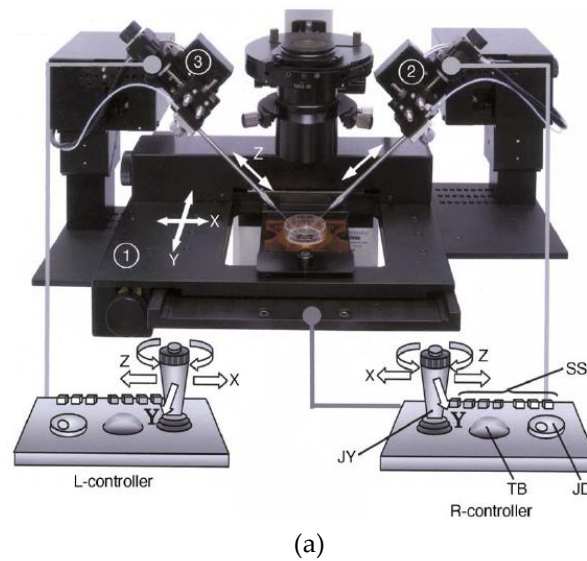


Figure 1.14 : Micro-nanorobotic manipulation system for single-cell injection. (a) Micro-nano manipulation using micromanipulator [127]; (b) Schematic of atomic force microscopy (AFM) cantilever-based nano injection [129].

The glass pipette has become an essential tool for biological studies such as intracellular microelectrode and drug delivery [129,130]. In the micro-nano robotic manipulator, the glass micropipette is attached to the micro-nanoinjector. The movement of the micropipette can be controlled precisely

by using a 3-degrees of freedom (DOF) micromanipulator [131]. However, this process is done manually in conventional methods. Therefore, the automatic injection system is developed based on the robotic control technique in recent years to improve accuracy and injection time [129]. These include a hybrid visual servo control scheme [126], supporting robot [127], force sensor feedback [131], position and force control [132], and piezo-controlled [133,134].

Micro-nano injection is a simple process in which a needle penetrates the cell membrane. The micro-nano robotic manipulation system provides an effective platform for the injection process. Comparing with manual injection, a robotic manipulation system has the advantages of high quality, productivity, and repeatability. For example, Hayakawa *et al.* demonstrated a single-cell puncture by utilizing the high thermal characteristic of the fabricated hybrid nanorobot with the carbon nanotube (CNT) [135]. Femtosecond laser exposure was generated on-chip nanorobots as shown in Figure 1.15(a, b). They integrated CNTs with the nanorobot and used a new nanorobot function, such as nanoparticles being injected into a single cell. A single-cell puncture was performed with this nanorobot by irradiating the CNTs with an infrared laser and local laser heating. Figure 1.15(c) shows that optical nanorobot manipulation and nanobead injection was performed with high accuracy of positioning and high flexibility in space. This method enables a new approach for manipulation and injection of micro-nano particles. In this study, a commercially available 3-DOF micromanipulator was utilized to manipulate a single microsensor by glass nanoprobe using zeta potential control to achieve non-invasive cell injection with local laser heating.

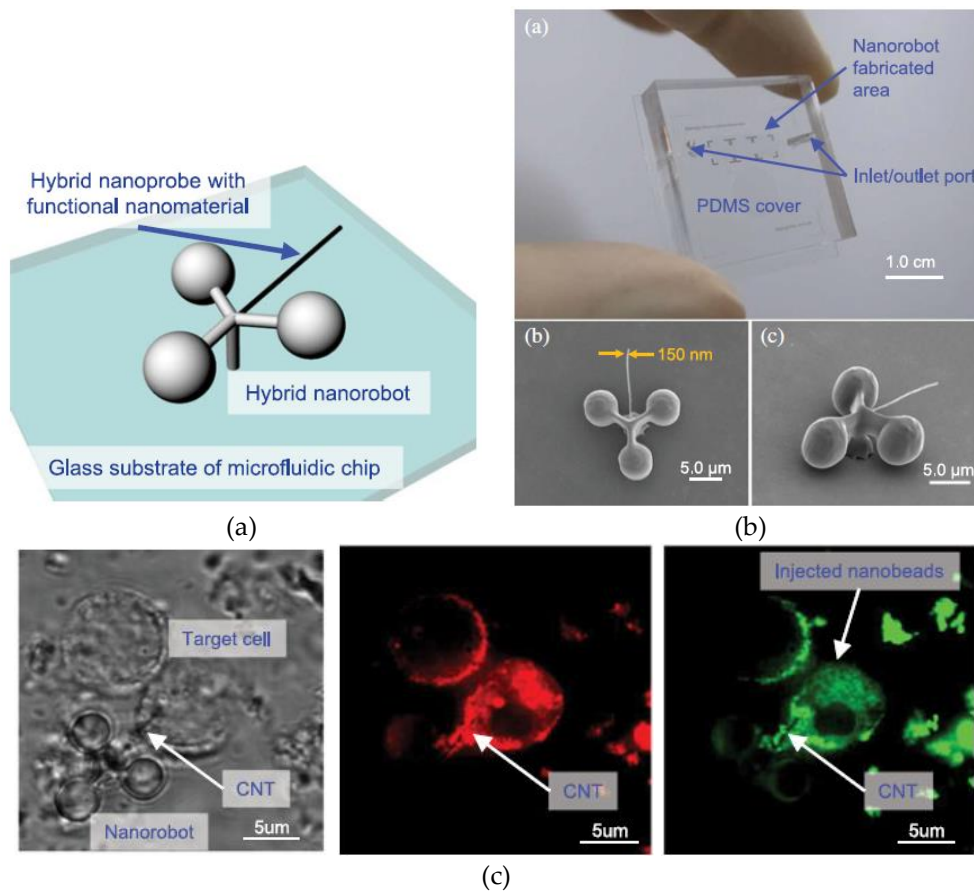


Figure 1.15 : Fabrication of an on-chip nanorobot integrating functional nanomaterials for single-cell punctures [135].

(a) Concept of the hybrid nanorobot with a functional nanomaterial; (b) Images of fabricated hybrid nanorobot; (c) Result of cell puncture by the hybrid nanorobot. CNT: Carbon nanotube.

1.4.4 Electroporation

Electroporation is a physical method of cell transfection. It uses electricity to get plasmids, drugs, proteins or nanoparticles inject into cells. The transient increase in the permeability of the cell membrane is achieved when the cells are exposed to short pulses of an intense electric field. As shown in Figure 1.16, this method allows nanoparticles to be introduced into cells and to be extracted from within the cells [136]. In particular, electroporation has been utilized in single-cell transfection including multifunctional pipette [114], nano fountain probe [115], and microdevices [137]. Since this method is non-

viral, non-toxic and safe in all cell types, it can be used in all forms *in vitro* or *in vivo* applications. However, electroporation requires complicated pulse generators to produce short high-voltage pulses and expertise is needed for equipment handling. Electroporation also can be used to introduce foreign molecules such as DNA and proteins into cells by temporarily disrupting the cell membrane by a voltage shock [138].

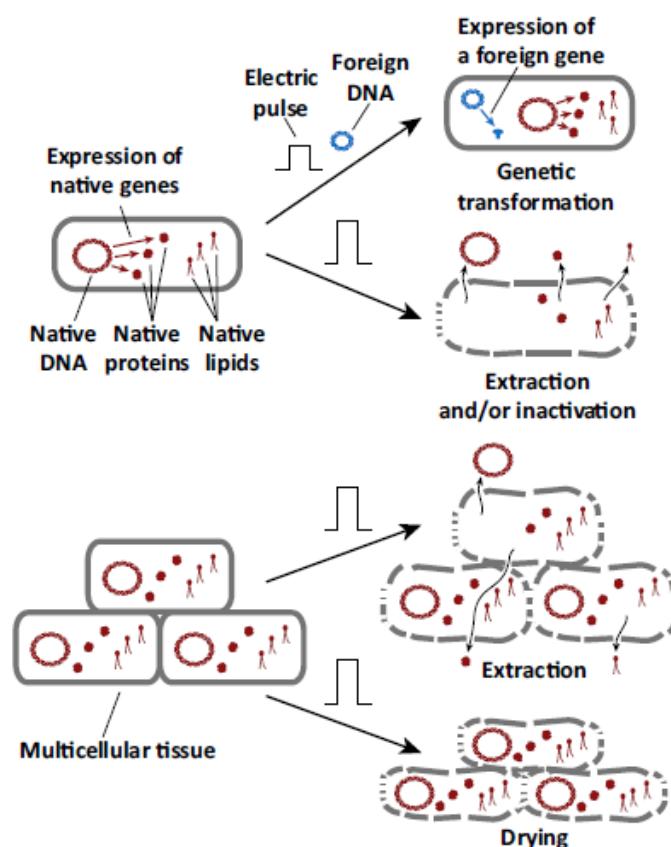


Figure 1.16 : Schematic of electroporation in biotechnology applications [136].

1.4.5 Sonoporation

High amplitude acoustic wave cavitation is considered the main mechanism of sonoporation for intracellular delivery. Sonoporation is an approach to facilitate intracellular delivery by applying ultrasound. Ultrasound is shown to be promising for cancer and tumor treatment. For example, Lin *et al.* reported enhanced tumor deposition of lipid-coated CdSe

QDs with the aid of ultrasound and ultrasound contrast agents (microbubbles) [139]. Similarly, sonoporation can be used to enhance liposome nanocarriers in tumors with low levels of enhanced permeability and retention as shown in Figure 1.17 [140]. Instead of using microbubbles as a cavitation generation medium, Yang *et al.* demonstrated the use of Fe_3O_4 nanoparticle for controlled release to tumor cells through sonoporation. In this approach, the nanoparticles can be effectively delivered into tumor cells noninvasively, and the delivery rate can be controlled by acoustic intensity [116].

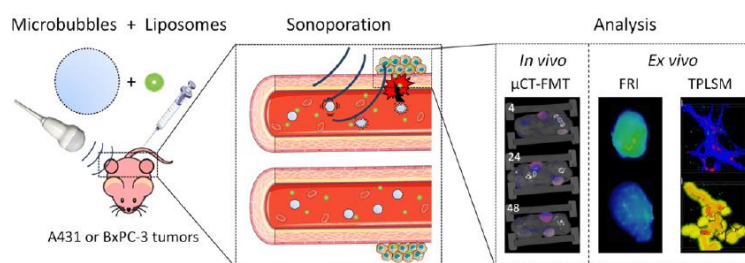


Figure 1.17 : Schematic of sonoporation to enhance liposome accumulation and penetration in tumors [140].

1.4.6 Optoporation

Optoporation is a method where a tiny hole is transiently generated in the plasma membrane of a cell using a highly focused laser for optical injection. Optical techniques provide exquisite control of both the location and magnitude of power applied to a target cell, permitting a single cell and even subcellular experiments to be conducted routinely [117]. This technique also referred with a different name such as optical injection [106,141], optical transfection [142], optoinjection [143], phototransfection [144], photoporation [145,146], laser heating [147], optical heating [96,148] and laser-assisted [97,145,149] in which makes reviewing the literature very difficult [142]. The injection of nanoparticles by laser irradiation has many names, but the term ‘optical injection’ is preferred in this dissertation.

This approach was first reported by Tsukakoshi *et al.* who used a diode-pumped Neodymium Yttrium Aluminium Garnet (Nd: YAG) to generate stable and transient transfection of normal rat kidney cells [150]. Since then, the optical injection has been demonstrated using a variety of laser sources including continuous wave and pulsed wave. For example, the femtosecond laser-focused was commonly used to create a small transient hole on the cell membrane to inject an impermeable color molecule into targeted living cells. [107,149,151,152]. Figure 1.18 indicates that an optical injection created a temporary hole on the cell membrane and thus enables molecules to be injected into a cell.

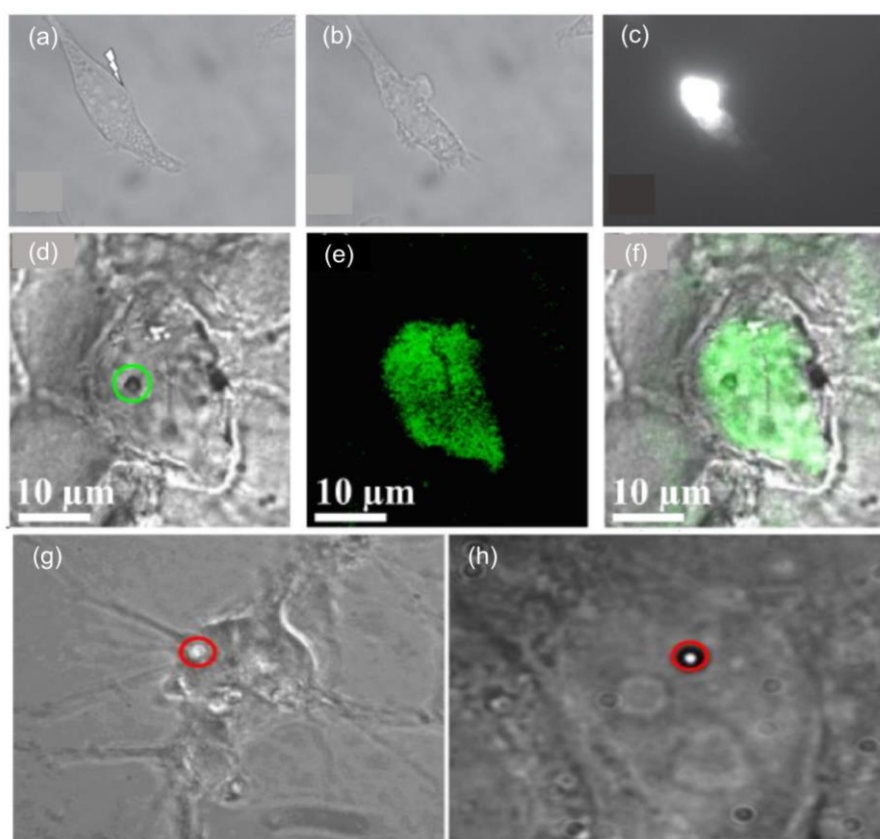


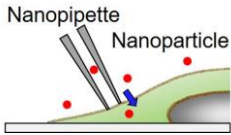
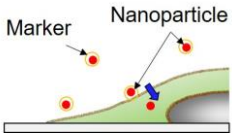
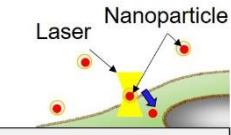
Figure 1.18 : Morphological changes in HEK cells.

(a) 0 min; (b) 10 min; and (c) 20 min after laser treatment [149]. Confocal laser scanning images of MCF-7 cell 96 hours after optical tweezing the plasmid coated 1 μm particle into the cell, (d) optical image; (e) fluorescence image; and (f) merged image [107]. (g-h) A transient hole (marked by the red circle) observed during an optical injection [152].

1.4.7 Summary

An effective injection method is needed for intracellular measurements for the sensors of fluorescence nanoparticles. Table 1.1 shows a summary of conventional approaches for sensor injection. Since the pipette is inserted into the cytoplasm, micro-nano injection with a micro-nano pipette is a simple and direct process. However, it will damage a target cell easily. On the other hand, through endocytosis and lipofection, the nanoparticles can be inserted into a cell without destroying the cell membrane. Unfortunately, it is challenging to quantitatively inject nanoparticles into an individual cell and requires a long duration of injection. Conversely, optical injection seems promising for cell injection since the quantitative injection of nanoparticles into a target cell can be realized and injection time was improved dramatically. In this thesis, the author proposes a single microsensor can be injected into target cells by optical injection method. A detailed explanation will be discussed in the following chapter.

Table 1.1 : Conventional methods for sensor injection into a cell.

Method	Micro-nano injection	Endocytosis and lipofection	Optical injection
Schematic image			
Injection of micro-nano objects	Yes	Yes	Yes
Injection volume control	Yes	No	Yes
Damage to cell	Yes	No	No
Injection of individual cell	Yes	Yes	Yes
Injection time	Short	Medium/Long	Short

1.5 Optical Control in Manipulation and Injection of Nanoparticles into Cells for Intracellular Measurements

In this study, the manipulation and injection of nanoparticles into cells were performed using optically controlled light and laser irradiation. These optical control will be briefly explained in this chapter while a further detailed explanation will be discussed in the following chapter. Additionally, emerging techniques using optical control in the manipulation of a single nanoparticle and cell injection will be highlighted.

1.5.1 Manipulation of nanoparticles by optical control of zeta potential

Effective manipulation of a specific nanoparticle and positioning of the nanoparticle at the arbitrary point on the cell membrane was challenging. In previous studies performed in Arai Lab, Maruyama *et al.* introduced liposome layers containing photochromic material, Leuco Crystal Violet (LCV) on the surface of nanotool to realize selective adhesion into a living cell and cell injection [124]. Masuda *et al.* then introduced another photochromic material, Spiropyran (SP) impregnated with fluorescent microsensor for optical adhesion control of liposome [66]. Figure 1.19 and Figure 1.20 show a schematic diagram of both approaches in optical manipulation control of nanoparticles by using different photochromic material.

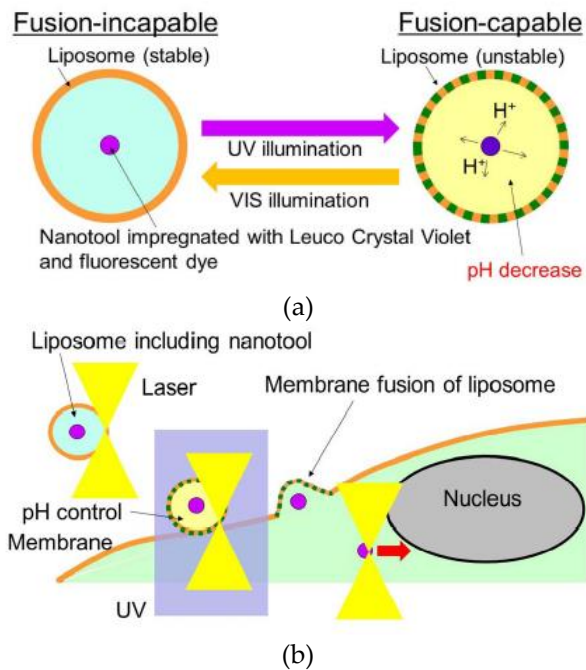


Figure 1.19 : Schematic of a selective injection of encapsulated fluorescent microsensor into a cell.

(a) Optical pH regulation in the liposome using photo-induced reaction using Leuco Crystal Violet (LCV); (b) Cell injection of nanotool by photo-induced pH control using photoresponsive chemical [124].

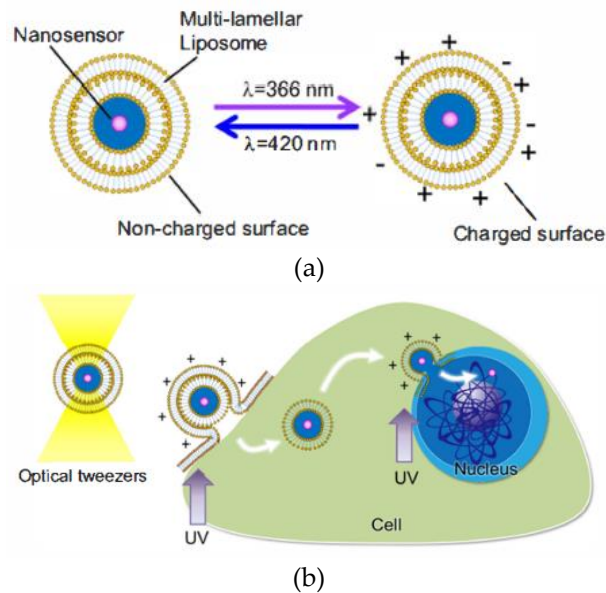


Figure 1.20 : Schematic of a selective injection of encapsulated fluorescent microsensor into multi-lamellar liposome into a cell.

(a) Optical control of the surface charge of liposome; (b) Selective injection of a sensor using optical tweezers [66].

Photochromism is simply defined as the reversible transformation of chemical properties in response to photo-illumination. Photochromic materials change their color due to light absorption and can be reversed to the original properties, either thermally or photo irradiation with a specific wavelength [153,154]. For example, nanoparticle surface charge with zeta potential control is one of the important properties which could play a major role in the effectiveness of the drug delivery system [155]. Furthermore, charges modification offers the opportunity to extend the blood circulation time, increases the likelihood of cell interaction and alter the pharmaceutical properties in micro-nano system applications [155,156]. Through photo-isomerizing SP, the zeta potential of the liposome layers can alternatively be modified between positive and negative. Maruyama and his group then managed to precisely control the adhesion of a single nanoparticle on the cell membrane by zeta potential of the fabricated microsensor to achieve rapid cell injection [122,125,157]. In this study, manipulation and cell immobilization of a single microsensor using optical control of zeta potential will be implemented. A detailed explanation will be discussed in Chapter 2.

1.5.2 Manipulation of micro-nanoparticles by optical tweezers

Optical trapping and manipulation of nanoparticles are rapidly growing the field and its relevance beyond physics towards biology and chemistry applications. One of the most common tools for micro-nanoparticles manipulation is optical tweezers. Optical tweezers are the most versatile technique as a non-contact manipulation tool in biological and biomedical applications [158]. It was generally known that before the advent of a laser, light induces optical strain. The detection of optical scattering and gradient forces on micro-sized particles was first reported by Arthur Ashkin in 1970

[159]. These findings are then referred to as optical tweezers in which a tightly focused beam of light is capable of holding and manipulating microscopic particles in three dimensional [160]. Figure 1.21 shows a schematic of an optical tweezers system.

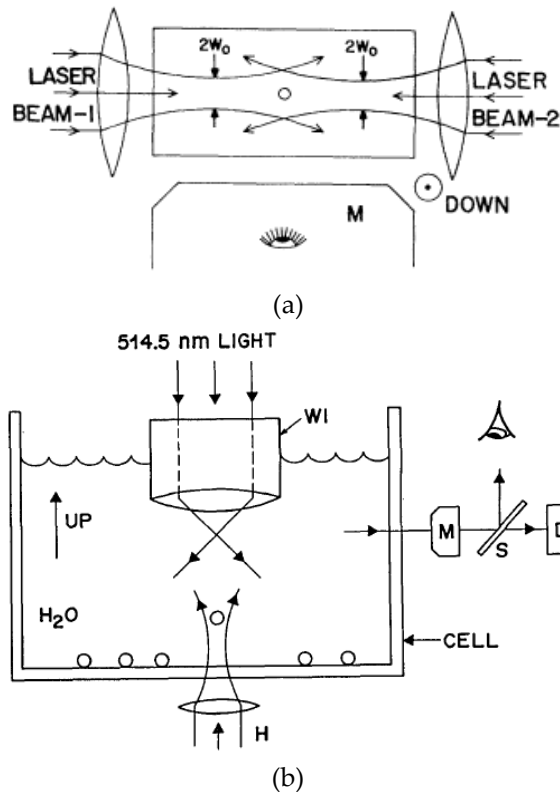


Figure 1.21 : Schematic of the optical tweezers system.

(a) The trapping of a high-index particle in a stable optical well [159]; (b) Optical trapping of particles in water utilizing a single-beam gradient force radiation-pressure trap [160].

Trapping was observed using an opposite direction dual laser configuration as shown in Figure 1.21(a) while this technique can trap a nanoparticle with single-beam are shown in Figure 1.21(b). The single-beam gradient force trap [160,161] is capable of trapping micro-nano particles *in vitro* [162,163] or organelles within cells [164–166] with non-contact force by photon linear momentum transfer. The capability of rapid, accurate positioning and non-invasive of optical tweezers are widely used in trapping and

manipulation [167–169], single-cell analysis [170,171], nanoparticles sorting [172], cell transportation [173], cell palpation [174] and cell injection [123].

As a major work, Ashkin and Dziedzic used optical tweezers to trap and manipulate the viruses and bacteria [165]. In aqueous solution, individual tobacco mosaic viruses (TMV) were stuck. However, the laser irradiation of 514 nm damaged to bacteria cells. Therefore, Ashkin *et al.* proposed an infrared laser beam for trapping and manipulation of a single cell. Consequently, this approach avoided optical damage [175]. Optical tweezers can provide an optical pressure and force of trapping pointing at the middle of the beam. In previous research performed in Arai Lab, Arai *et al.* established a time-shared scanning (TSS) approach which, by changing the discrete laser scanning pattern, uses synchronized laser manipulation for multiple targets independently. [176]. Later, Onda *et al.* realized the holographic optical tweezers (HOT) system [177]. This method utilizes computer-generated hologram (CGH) calculated by a graphical processor unit (GPU) to accelerate the calculation speed of hologram and enable high-speed manipulation of multiple targets.

Several measurements were also carried out with the use of optical tweezers. For example, Zhong *et al.* demonstrated the usage of optical tweezers to trap red blood cells in living animals [168]. Figure 1.22 shows the optical tweezers system which is capable of manipulating microparticles by exerting small forces via a highly focused laser beam. In this study, optical tweezer was used in two ways (i) trapping and manipulation of a single microsensor, and (ii) injection of a single microsensor into target cells. The trapping and manipulation of a single microsensor will be discussed in Chapter 2 while microsensor injection into target cells using optical tweezers will be highlighted in Chapter 3.

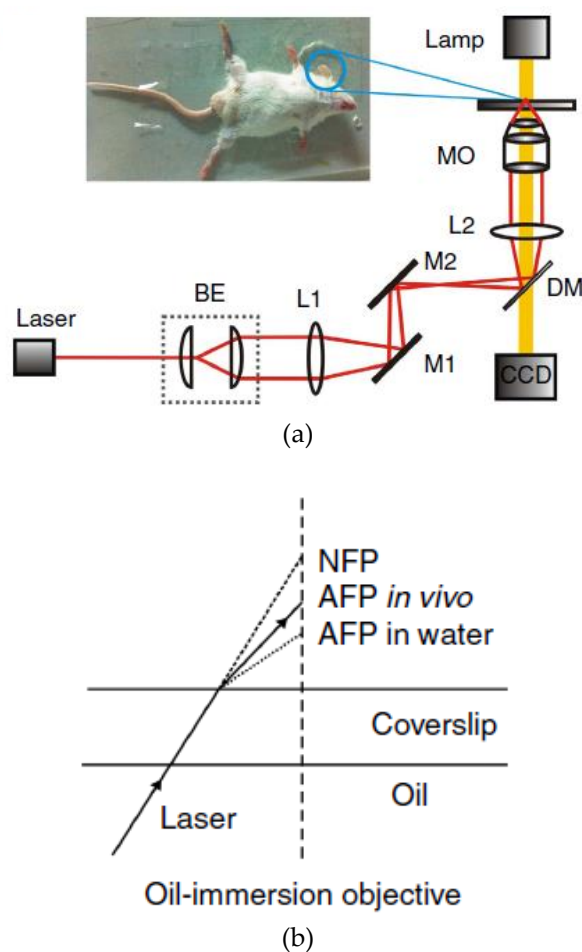


Figure 1.22 : Schematic of the optical tweezers system.

(a) Optical paths for 1064 nm trapping laser (red) and halogen lamp for bright-field imaging (yellow); (b) The geometric optics representation of the refraction of a light beam focused *in vivo* and water. NFP: Nominal focal position; AFP: Actual focal position [168].

1.5.3 Injection of nanoparticles into living cells by optical tweezers

The optical injection has increasingly attracted attention due to its non-contact and non-invasive advantages. It is based on the temporary increase in the permeability of a cell membrane caused by a laser beam, which enables the diffusion of nanoparticles on a micro-nano scale through a cell membrane. Usually, extremely high laser peak power in the optical injection mechanism [141] and therefore has the potential to damage the cell [178]. In this regard, there is a high demand for less harmful approaches to optically guided membrane injection of nanoparticles.

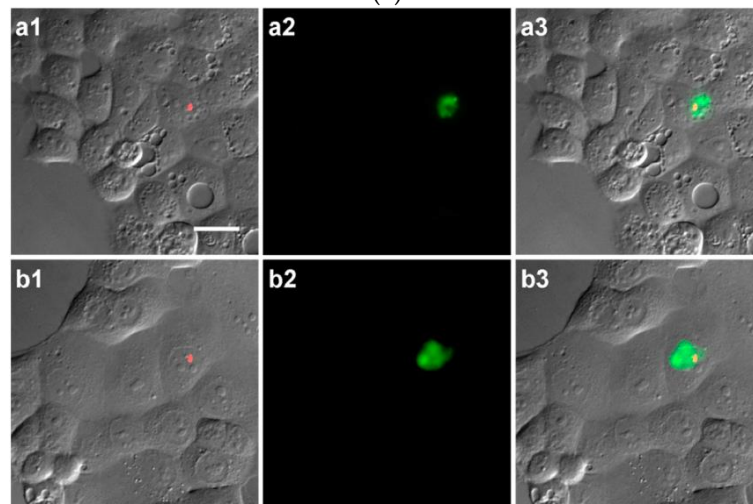
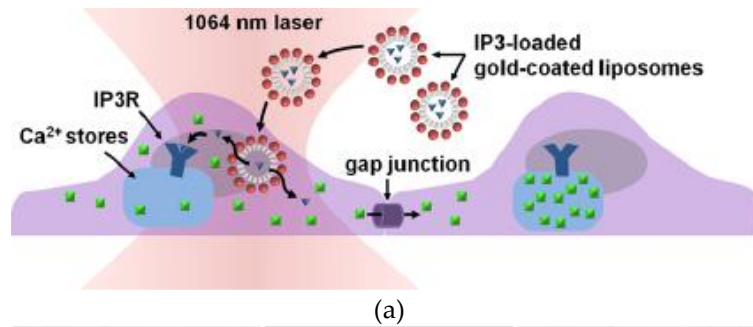


Figure 1.23 : Plasmon resonance assisted optical injection of signaling molecules. (a) Freely diffusing gold-coated liposome encapsulating inositol trisphosphate (IP3); (b) Optical injection of a fluorescently tagged gold-coated liposome. Column 1 is the experimental field of view with the location of the optical injecting laser overlaid in red. Column 2 shows the resulting fluorescence signal after 60 or 120 s of optical injection. Column 3 is merged image [105].

Urban *et al.* developed a novel optical injection strategy based on the combination of optical powers of optical tweezers and plasmonic heating of laser-exposed gold-coated liposomes [179]. Likewise, Orsinger et al. applied optical tweezers to the cell allowing the free diffusion of gold-coated liposomes that are pushed to the cell under the optical forces of optical tweezers as shown in Figure 1.23(a) [105]. The liposomes can be injected into cell cytoplasm in combination with the plasmonic heating effect of gold-coated liposomes with a quick average injection time of 5.7s for one liposome. Figure 1.23(b) shows the effects of the optical injection of Rhodamine B fluorescently

labeled gold-coated liposomes. By using optical stimulation on gold-coated liposomes, they demonstrated quantitative focal activation of the individual cells.

In previous research performed in Arai Lab, cell injection was performed by optical tweezers utilizing continuous-wave laser irradiation at 1064 nm. Specifically, Liu *et al.* synthesized a multi-fluorescent microsensor which can respond to both temperature and pH change for intracellular measurement [43]. Liu *et al.* subsequently demonstrated an injection of fluorescence sensors into target cells by using optical tweezers to apply local vibration stimulus [68]. Figure 1.24 shows the principle of a selective adhesion and rapid injection of a single sensor into a target cell using optical tweezers. Optical tweezers successfully manipulated a single sensor, and the injection time is approximately 30 min. By using this process, the injection rate was also increased to 80% compared to the lipofection method [122]. Recently, Zhong *et al.* achieved the injection of fluorescence polystyrene nanobeads containing iron oxide nanoparticles by local laser heating (Figure 1.25) [96,97]. The injection times of the fluorescence polystyrene nanobeads and survival rates of the injected cells are a few seconds and approximately 100%, respectively.

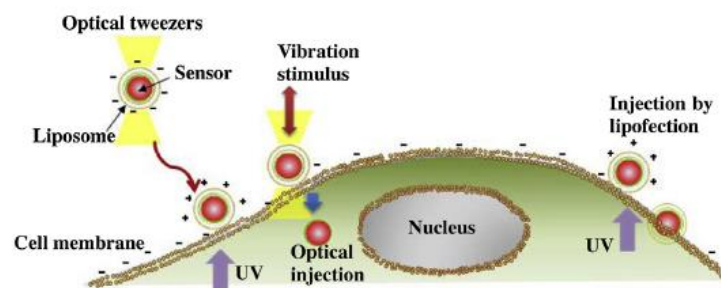


Figure 1.24 : Schematic diagram of selective adhesion and rapid injection of a fluorescent sensor into a target cell using local mechanical stimulus applied by optical tweezers [68].

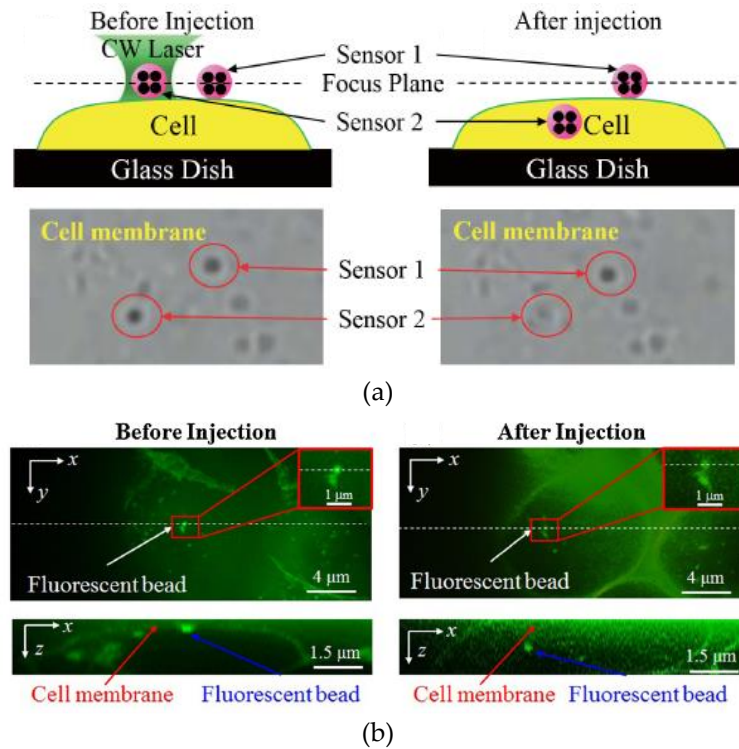


Figure 1.25 : Injection of single microsensors into living cells using optical tweezers. (a) Continuous-wave laser irradiation with the power of 6 mW for injecting sensor into a living cell before and after injection [96]; (b) Fluorescence images of z-scanning used to confirm the successful injection of 750 nm diameter magnetic nanobeads into living cells [97].

1.5.4 Injection of nanoparticles into living cells by femtosecond laser

The optical injection has been demonstrated using a variety of laser sources and the interaction differs depending on the laser source used. The mechanism is probably based on localized heating when continuous-wave lasers were used. With pulsed sources, the irradiated nanoparticles or cell depends strongly on the pulse duration usually either in a very short pulse (femtosecond) or longer pulse duration (nanosecond). To date, the focused femtosecond laser has been used extensively to create a small transient hole on the cell membrane or to irradiate target nanoparticles in optical injection [107,149,151,152].

In this thesis, both types of laser sources will be demonstrated in order to achieve rapid and non-invasive cell injection. First, a continuous-wave laser

at 1064 nm wavelength will be used to inject a single microsensor into a living cell. Second, a single microsensor will be irradiated by a femtosecond laser at 808 nm wavelength for cell injection. A detailed explanation will be discussed in Chapter 3.

1.6 Thesis Overview

1.6.1 Research objectives

The key points in single-cell micro-nano environmental analysis are the manipulation of selective microsensors and the effective injection of a single microsensor into a target cell with a high injection rate, low invasive and high survival rate. Therefore, the research aim is as follows: (1) to manipulate fluorescence microsensor by pick-up and immobilized on the cell membrane, (2) to inject a single microsensor into the target cell without destroying the cell, and (3) to prepare a stable fluorescence microsensor for measurement of temperature in intracellular environment.

1.6.2 Outline of the thesis

This thesis consists of five chapters, as illustrated in Figure 1.26. Chapter 1 provides the background of the research and describes the research objective.

Chapter 2 demonstrated the manipulation and immobilization of a single fluorescence microsensor for selective injection into cells. In this chapter, the temperature with the relative fluorescence intensity of the fabricated microsensor was first calibrated. Then, pick-up and cell immobilization of the microsensor by optical control of the zeta potential was performed, and the success rates without and with zeta potential control were compared. Finally,

injection of the immobilized microsensor by local heating was performed, and the success rates of injection and viability of the injected cells were evaluated.

Chapter 3 demonstrated the rapid and low-invasive injection of a single fluorescence microsensor into a specific cell using optical methods with multiple wavelengths. Multiple tasks include trapping, cell immobilization and injection were performed by utilizing the irradiation of the laser at a different wavelength. In particular, a new approach of manipulating a fluorescence microsensor by optical tweezers (1064 nm) and then injecting that particular sensor into living cells by a continuous wave laser (808 nm) was presented. Experimental results of manipulation and the injection of fluorescence microsensor into target cells were demonstrated. Additionally, the success rates of injection cell survival were evaluated.

Chapter 4 proved a photobleaching compensation method based on the diffusion of fluorescent dye inside a hydrogel microsensor for prolonged stable temperature measurements. The factors that influence compensation in the hydrogel microsensor system are the interval time between measurements, material, the concentration of photo initiator, and the composition of the fluorescence microsensor. These factors were evaluated by comparing a polystyrene fluorescence microsensor and a hydrogel fluorescence microsensor, both with diameters of 20 μm . The effect of microsensor size on the stability of the fluorescence intensity was also evaluated.

Chapter 5 summarized the research that has been performed and the future works are discussed.

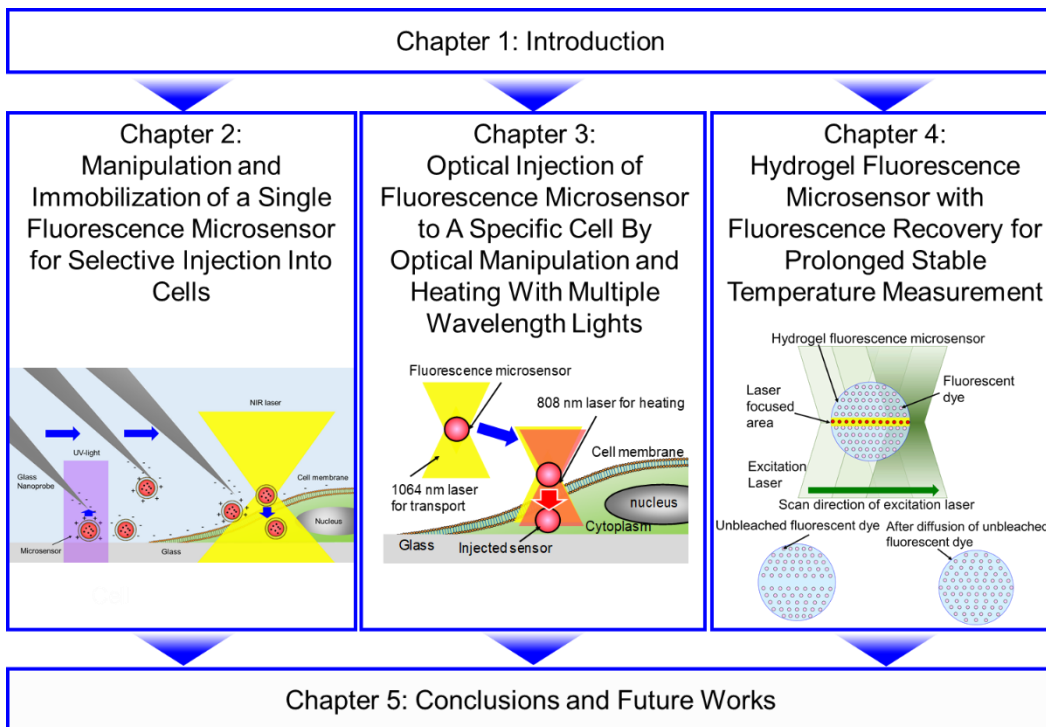


Figure 1.26 : Outline of the dissertation.

Chapter 2

Manipulation and Immobilization of a Single Fluorescence Microsensor for Selective Injection Into Cells

2.1 Introduction

Recently, the manipulation and injection of single microsensors into cells with minimal invasiveness has received attention due to its potential biological and biomedical applications [22]. For example, measuring the environment properties of a virus-infected cell is a useful means to investigate the mechanism of viral proliferation to develop new medicines and diagnostic tools [23]. In particular, the investigation of intracellular properties provides useful information [27]. Conventionally, staining whole or part of a cell by

fluorescence indicators has been used for intracellular measurement of environment properties such as temperature, pH, or ion concentrations [39–42]. Fluorescence measurements are performed by detecting variations in fluorescence intensity and lifetime due to environmental conditions. However, fluorescence measurements have some disadvantages, such as difficulty in controlling the concentration of the indicator and diffusion of the indicator inside cells. Encapsulation of fluorescence indicators into artificial nanobeads allows control over the indicator concentration [43].

Intracellular measurements require selective manipulation and injection of specific microsensors with minimal invasiveness [44,110]. Several injection methods such as micro-nano injection [180], endocytosis [118], lipofection [112], electroporation [115], and local heating [68,106] have been developed to inject a particular nanobead into a target cell. In particular, Zhong *et al.* achieved the injection of fluorescence polystyrene nanobeads containing iron oxide nanoparticles by local laser heating [96,97]. The injection times of the fluorescence polystyrene nanobeads are on the order of a few seconds, and survival rates of the injected cells are approximately 100%. However, selective injection with manipulation and cell immobilization of a specific fluorescence polystyrene nanobead has still not been achieved, as the manipulation of a single nanobead in solution is difficult.

Fluorescence polystyrene nanobeads containing iron oxide nanoparticles cannot be manipulated by optical tweezers, since focused laser irradiation onto iron oxide nanoparticles leads to a temperature increase and bubble formation [181]. Electromagnetic tweezers require high current input to the electromagnets to manipulate individual fluorescent polystyrene nanobeads [182,183]. Mechanical manipulation using a glass nanoprobe is suitable for manipulation without environmental fluctuation. However, the

success rate for the manipulation of individual fluorescent polystyrene nanobeads using glass nanoprobe with Van der Waals forces is quite low for an unskilled operator.

In this study, the author proposes the manipulation and immobilization of a single microsensor using optical control of the zeta potential. The Coulomb force was used for manipulation and immobilization of the microsensor since the zeta potential of the microsensor can be controlled using 1,3,3-trimethylindolino-6'-nitrobenzopyrylospiran, which is a photochromic material [184]. The microsensor is fabricated by staining a polystyrene nanobead containing iron oxide nanoparticles with a temperature-sensitive fluorescence indicator and encapsulating the nanobead into a lipid layer with SP. The zeta potential of the microsensor, glass, and cell membrane are negative. The zeta potential of the microsensor becomes positive upon UV irradiation due to the photo-isomerization of SP. A positively-charged microsensor can be picked-up, transported, and immobilized on the cell membrane using the negatively-charged glass nanoprobe. As a demonstration, selective pick-up, transportation, and immobilization on Madin–Darby Canine Kidney (MDCK) cells using optical control of the zeta potential were performed to confirm the effectiveness of the proposed method. Additionally, the cell injection rate and viability of injected cells were evaluated by a fluorescence viability test.

2.2 Materials and Methods

2.2.1 Principle of manipulation and cell injection of the microsensor using optical control of the zeta potential

Figure 2.1 shows the principle of the manipulation and cell injection of a single microsensor to a target cell using optical control of the zeta potential. The microsensor is made up of a polystyrene nanobead containing iron oxide nanoparticles, Rhodamine B, a lipid layer, and SP. Rhodamine B is a temperature-sensitive fluorescence indicator. The lipid layer is composed of the neutral lipid dioleoylphosphocholine (DOPC). SP, purchased from Tokyo Chemical Industry Co. Ltd. (Tokyo, Japan), is used for zeta potential control. The microsensor is fabricated by staining the nanobead with Rhodamine B and encapsulating the stained nanobead by the lipid layer with SP. Zeta potentials of the glass nanoprobe and polystyrene nanobead in water are approximately -50 mV and -30 mV, respectively [185]. DOPC is electrically neutral. The molecular conformation of SP changes from the *cis*-type to *trans*-type by UV irradiation and is recovered by VIS light irradiation. The zeta potential of the microsensor switches from negative to positive by UV irradiation, since the zeta potential of *trans*-type SP is higher than that of *cis*-type SP. Therefore, the positively-charged microsensor adheres to the glass nanoprobe and cell membrane.

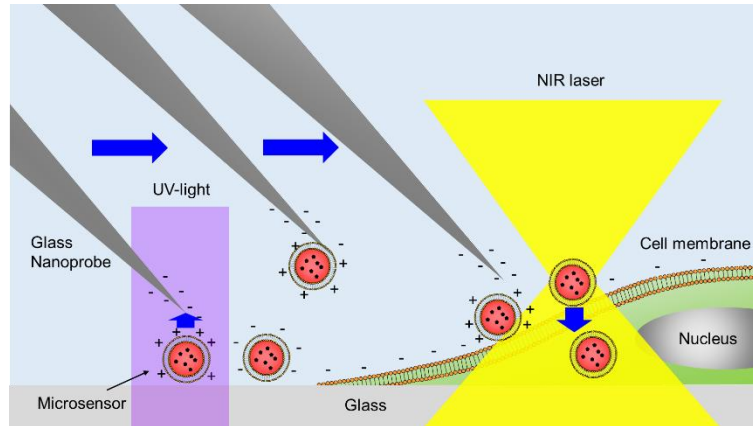


Figure 2.1 : Schematic diagram of manipulation and cell injection of a single microsensor using optical control of the zeta potential.

UV: Ultraviolet; NIR: Near-infrared.

First, the selected microsensor is irradiated with UV light to switch the zeta potential from negative to positive. Then, the positively-charged microsensor is picked-up and transported to the target cell using the glass nanoprobe due to the attractive Coulomb force. Negatively-charged microsensors do not adhere to the glass nanoprobe because of the repulsive force. The transported microsensor is immobilized on a cell membrane. For example, the zeta potential of an MDCK cell is approximately -40 mV [186]. The positively-charged microsensor can immobilize on the cell membrane and detach from the glass nanoprobe by pushing the cell membrane with the microsensor to increase the contact area. The zeta potentials of the glass nanoprobe and MDCK cells are similar. Therefore, an increase in the contact area between the microsensor and cell is needed to detach the microsensor from the glass. The flexibility of the glass nanoprobe is also useful for manipulating the microsensor on the cell membrane without damage to the cell.

After cell immobilization, the microsensor is injected into the cell cytoplasm by local laser heating. In this study, cell activities such as

endocytosis and lipofection were not used for injection because the injection of large nanoparticles by either method takes a long time. The injection of the microsensor made up of a 750 nm diameter polystyrene nanobead containing iron oxide nanoparticles into cells using laser heating (wavelength: 1064 nm, power: 28 mW) was achieved within a few seconds [97]. The iron oxide absorbs the 1064 nm light and generates heat locally. The author used the same polystyrene nanobeads as material for the microsensors and the same laser wavelength and power for cell injection in the present study.

2.2.2 Experimental system setup

Figure 2.2 shows a schematic diagram of the experimental setup consisting of optical and fluorescence microscopy systems. An inverted optical microscope (IX71, Olympus, Tokyo, Japan) having an epi-fluorescence observation system and laser confocal system was used to observe the microsensor and cell. A 3-DOF micromanipulator (SMX, Sensapex, Oulu, Finland) was used for manipulation of the microsensor. The range of motion for all three dimensions was 20 mm, and the step resolution was 30 nm. To observe the manipulation process, a digital charge-coupled device (CCD) camera (Grasshopper, Point Gray, Richmond, BC, Canada) was used. A confocal laser scanning system (CSU-X1, Yokogawa Electric Co., Tokyo, Japan) with an excitation laser of 488 nm and 561 nm, and electron multiplying-CCD (EM-CCD) camera (DU-897, iXon, Andor Technology Ltd., Belfast, UK) was used to acquire fluorescence images. The movement of the piezoelectric z-stage (E-665, Physik Instrumente GmbH & Co. KG, Karlsruhe, Germany) that coupled to the high magnification objective lens (UPlanSApo 100×/1.40, Olympus, Tokyo, Japan) was used to acquire 3D fluorescence images. A mercury lamp was used for photo-isomerization of SP by UV

irradiation. A 1064 nm NIR laser with a maximum power of 10 W was used for local heating [177]. The beam diameter at the focus was 1.4 μm . In this study, the power of the NIR laser was adjusted to 28 mW [97].

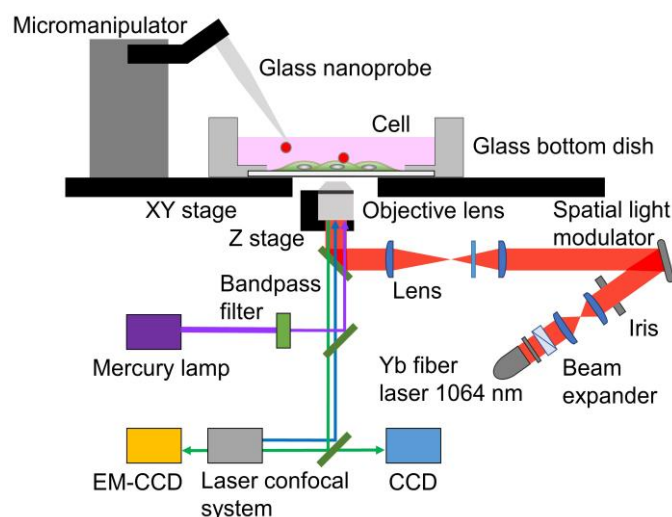


Figure 2.2 : Schematic diagram of the experimental system.
 CCD: Charge-coupled device; EM-CCD: Electron multiplying-CCD.

2.2.3 Optical control of zeta potential using photochromic material

Figure 2.3 shows a schematic diagram of the optical control of the zeta potential of the microsensor using SP. The molecular structure of SP changes from *cis*-type (left side) to *trans*-type (right side) by UV irradiation. The zeta potential of the *trans*-type structure is higher than that of the *cis*-type structure [187]. This photo-isomerization is reversible and repeatable by UV/VIS irradiation. A schematic diagram of the microsensor is shown in Figure 2.3(b). The polystyrene bead containing iron oxide nanoparticles is encapsulated by a lipid layer with SP. The zeta potential of the microsensor changes from negative to positive upon UV irradiation. The positively charged microsensor adheres to the negatively charged glass nanoprobe and cell membrane.

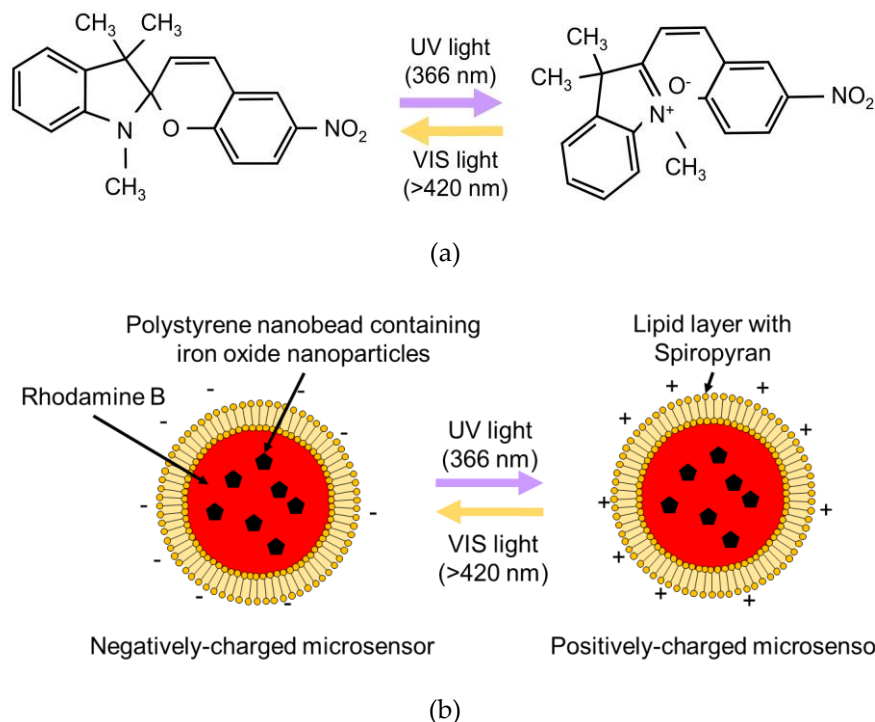
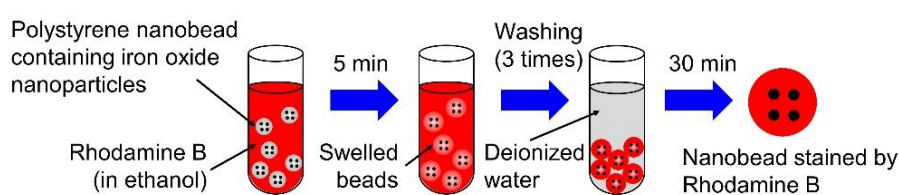


Figure 2.3 : Schematic diagram of optical control of zeta potential. (a) Changes in the molecular structure of SP by photo-isomerization; (b) Optical control of zeta potential of the microsensor.

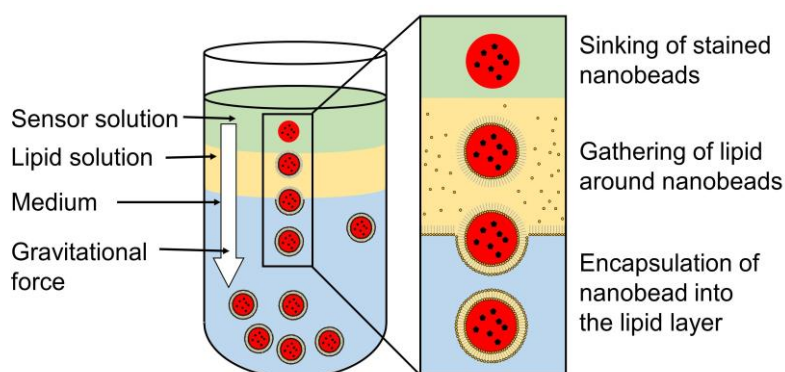
2.2.4 Fabrication of the microsensor with a photochromic lipid layer

The microsensor was made up of 750 nm diameter polystyrene nanobeads containing iron oxide nanoparticles (EPRUI Nanoparticles & Microspheres Co. Ltd., Nanjing, China), Rhodamine B, DOPC, and SP. The diameter of iron oxide nanoparticles inside the polystyrene nanobead ranges from 20 to 40 nm [97]. Figure 2.4 shows the fabrication process of the microsensor. First, polystyrene nanobeads containing iron oxide nanoparticles were stained with 6 g/L Rhodamine B in ethanol, as shown in Figure 2.4(a). Rhodamine B is a temperature-sensitive fluorescence indicator. After immersion in ethanol for 5 min, the stained polystyrene nanobeads were washed with deionized (DI) water three times. Then, the fluorescence polystyrene nanobeads were encapsulated in the lipid layer with SP by spontaneous transport [123,188], as shown in Figure 2.4(b). DOPC, a non-

charged lipid, was used to form the lipid layer. The lipid layer was prepared by mixing 10 mM of DOPC and 40 μ M of SP in mineral oil. After forming a multilayer of 0.7 mL of phosphate buffered saline (PBS) solution and 0.3 mL of lipid solution in a microtube, a 0.2 mL mixture of the fluorescence polystyrene nanobeads and mineral oil was introduced. During the sinking of the fluorescent polystyrene nanobeads by gravity, the lipids gathered and formed a layer with SP on the surface of the microsensor.



(a)



(b)

Figure 2.4 : Fabrication process of the microsensor.

(a) Stain of the polystyrene nanobead by Rhodamine B; (b) Encapsulation of the fluorescence polystyrene nanobead into the lipid layer with Spiropyran (SP).

Figure 2.5 shows the optical and fluorescence images of fabricated microsensors. The microsensors were excited by the 561 nm laser in the fluorescence image. The mean diameter of the microsensors was 1089 nm, which was evaluated by a tunable resistive pulse sensing (TRPS) nanoparticle analyzer (qNano, Izon Science Ltd., Christchurch, New Zealand). The thickness of the lipid layer was also measured to be approximately 170 nm.

The concentration of the microsensor after fabrication was 1.4×10^{10} particles/mL. The microsensor was diluted to a suitable concentration in the experiments.

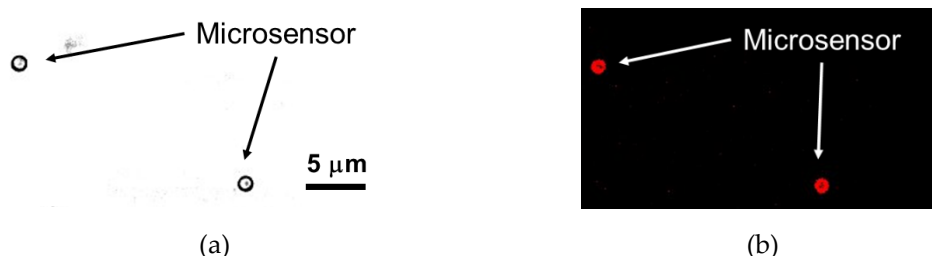


Figure 2.5 : Optical and fluorescence image of the microsensor.
(a) Optical image; (b) Fluorescence image.

2.2.5 Fabrication of the glass nanoprobe

A glass nanoprobe was used for manipulation of the microsensor and was controlled by a 3-DOF micromanipulator. The nanoprobe was fabricated by a borosilicate glass rod (G-1000, Narishige Scientific Instrument Lab., Tokyo, Japan) and then pulled using a magnetic glass microelectrode horizontal puller (PN-31, Narishige Scientific Instrument Lab., Tokyo, Japan). The tip diameter of the glass nanoprobe was less than 1 μm .

2.2.6 Cell culture

MDCK cells were used for the experiments in this study. MDCK cells were cultured in a glass-bottom dish (27 mm diameter) with 2.7 mL of Dulbecco's Modified Eagle Medium (DMEM) and 0.3 mL of fetal bovine serum (FBS). The culture conditions were an atmosphere of 5% CO_2 and 95% air at 37 $^\circ\text{C}$ temperature. MDCK cells were cultured for 8 h before the experiments. The cells were stained after the injection with Calcein-AM to test for cell viability. To dye the cell cytoplasm, the cells were washed twice using PBS, then 10 μL of 0.5 mg/mL Calcein-AM solution was mixed with 5 mL of PBS to produce the dye solution. Then, 1 mL of culture medium in the dish was

replaced with the dye solution. After 30 min of incubation at 37 °C, the stained MDCK cells were used for the experiments.

2.3 Results and Discussion

In this study, the temperature with relative fluorescence intensity of the microsensor was first calibrated. Then, pick-up and cell immobilization of the microsensor by optical control of the zeta potential was performed, and the success rates without and with zeta potential control were compared. Finally, injection of the immobilized microsensor by local heating was performed, and the success rates of injection and viability of the injected cells were evaluated.

2.3.1 Temperature calibration of the microsensor

In this study, microsensors for temperature measurements was fabricated. The principle of the temperature measurement is a measurement of the variation in fluorescence intensity of a microsensor due to changes in temperature. The fluorescence intensity of Rhodamine B decreases according to the temperature increase [43]. Figure 2.6 shows a calibration curve of the relative fluorescence intensity vs. temperature based on 24 °C. The environmental temperature was controlled by a cell culture chamber (ZILCS, Tokai Hit. Co. Ltd., Shizuoka, Japan) with an accuracy of 0.3 °C. The calibration temperature ranged from 24 °C to 40 °C. From this calibration curve, the sensitivity of the microsensor was determined to be $-2.4 \text{ \%}/^{\circ}\text{C}$.

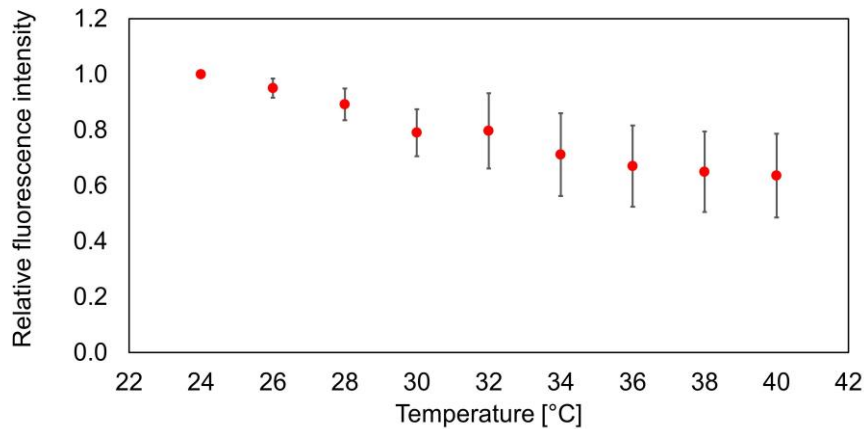


Figure 2.6 : Measurement of fluorescence intensity vs. temperature to construct a calibration curve. The error bars represent the standard deviation of average fluorescence intensity from nine stained microsensors.

2.3.2 Manipulation and immobilization of the microsensor using zeta potential control

Figure 2.7 shows experimental results of pick-up and immobilization of the microsensor using a micromanipulator and zeta potential control. The final concentration of the microsensor in the glass bottom dish was 9.3×10^7 particles/mL. A single microsensor could be picked-up within a few minutes at this concentration. At first, UV light from the mercury lamp (λ : 330–380 nm) was used to irradiate the target microsensor. The UV and VIS power densities were about 3.5 mW/cm^2 and 5.4 mW/cm^2 , respectively. The zeta potential of the UV-irradiated microsensor switched to positive. The microsensor was picked up using a glass nanoprobe by the Coulomb force, as shown in Figure 2.7(b). The microsensor was kept on the glass nanoprobe at least 5 min under VIS light irradiation. Table 2.1 shows the success rate of the pick-up of the single microsensor with and without UV irradiation in a different solution. The effect of the solution was evaluated using PBS and DMEM+FBS. Over ten microsensors were evaluated under each condition. In PBS, the success rate of the pick-up of the microsensor without UV irradiation was only 10%. On the

other hand, the success rate was increased to 75% with UV irradiation. In DMEM+FBS, the success rate of pick-up with and without UV irradiation were 43% and 5%, respectively. Based on these results, the PBS is suitable for the pick-up of the microsensor using optical control of the zeta potential.

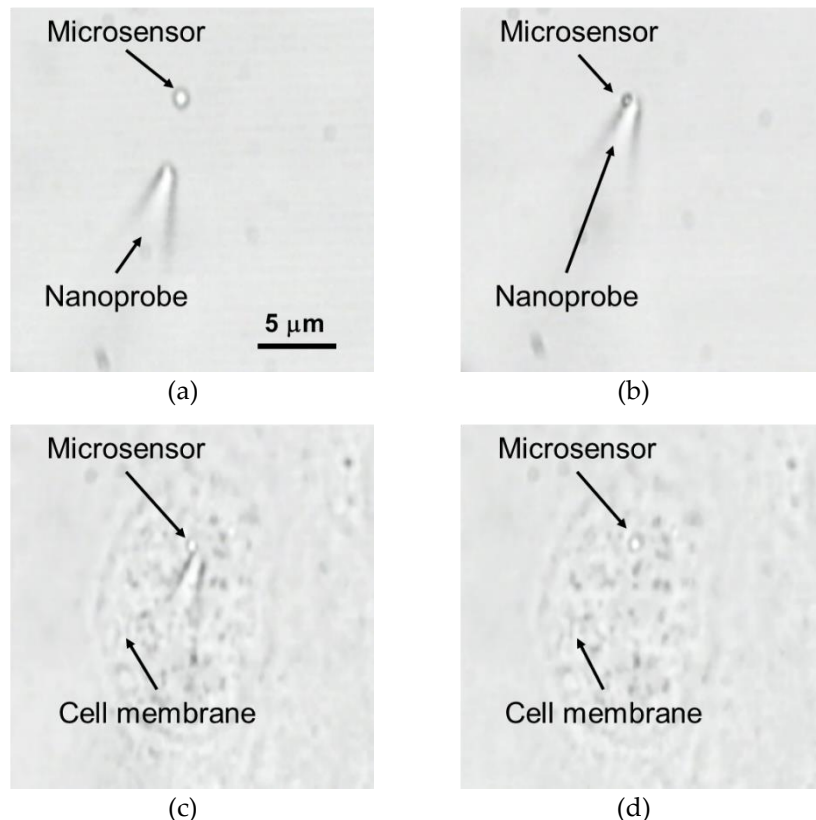


Figure 2.7 : Pick-up and immobilization of the microsensor using a micromanipulator and optical control of the zeta potential.

(a) The approach of the glass nanoprobe under UV irradiation; (b) Pick-up of the microsensor; (c) Contact of the microsensor to the membrane of a Madin-Darby Canine Kidney (MDCK) cell; (d) After immobilization of the microsensor.

Figure 2.7(c, d) shows immobilization of the microsensor to an MDCK cell. The positively-charged microsensor on the glass nanoprobe contacted the cell membrane and was immobilized on it by the Coulomb force since the zeta potential of the cell was negative. The success rate of cell immobilization with UV irradiation was 64%. The success rate of cell immobilization was lower than that of pick-up. The reason is likely the effect of the position of the microsensor on the glass nanoprobe. When the microsensor was on the tip of

the glass nanoprobe, the success rate of cell immobilization was high, since the contact of the microsensor with the cell membrane is easy. On the other hand, when the microsensor was at the upper side of the glass nanoprobe, the success rate was low, since contact with the cell membrane is difficult. This problem will be addressed by adding a rotating mechanism to the micromanipulator for attitude control of the microsensor.

Table 2.1 : Success rate of pick-up of the microsensor by the glass nanoprobe without/with UV irradiation.

Solution	Without UV	With UV
PBS	10%	75%
DMEM+FBS	5%	43%

DMEM: Dulbecco's Modified Eagle Medium; FBS: Fetal bovine serum; PBS: Phosphate-buffered saline.

2.3.3 Injection of the microsensor by local laser heating

Figure 2.8 shows the injection result of the microsensor into an MDCK cell by local laser heating. MDCK cells were stained with a cell-permeable fluorescent dye (Calcein-AM) after laser irradiation and kept in the incubation chamber for 30 min at 37 °C. To observe cell viability and position of the fluorescence microsensors after injection, 3D fluorescence images were acquired using a confocal laser scanning system approximately one hour after injection. Alive cell can be detected by observing the fluorescence of Calcein-AM, since Calcein-AM in the cytoplasm of alive cells is hydrolyzed by esterase activity and emits green fluorescence. The damaged cells were not evaluated in this study since MDCK cells are not stained using Ethidium homodimer-1 (EthD-1) as reported by Zhong *et al.* [96,97]. EthD-1 is cell-impermeant and only enters cells with damaged membranes producing red fluorescence. In this study, I considered cells are alive if they emitted green fluorescent since

Calcein-AM in the cytoplasm of alive cells is hydrolyzed by esterase activity and emits green fluorescence. Local laser heating was performed using the focused NIR laser at 28 mW, as in Zhong *et al.* [97]. The extinction coefficient of water is 14.2 m^{-1} at 1064 nm laser [189]. This value is quite small, so the temperature increase of water by laser heating can be ignored.

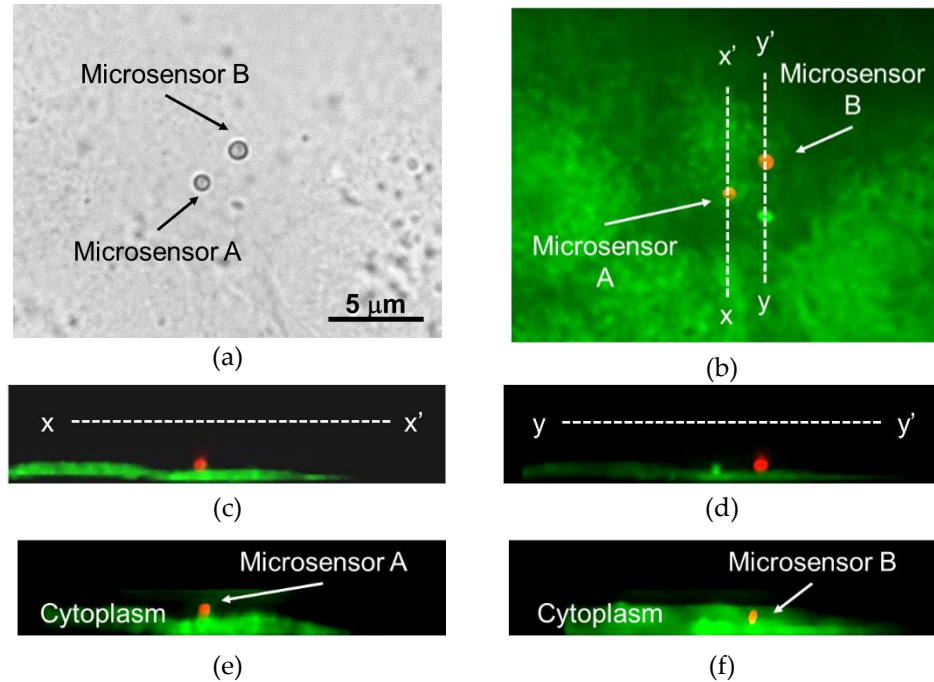


Figure 2.8 : Injection of the immobilized sensor by local laser heating.

(a) Optical image of the microsensors on an MDCK cell; (b) Fluorescence image before injection (red is the microsensor, bright green is fluorescence from the cell); (c) Cross-sectional view of microsensor A before laser irradiation ($x-x'$); (d) Cross-sectional view of microsensor B before laser irradiation ($y-y'$); (e) Cross-sectional view of microsensor A after laser irradiation; (f) Cross-sectional view of microsensor B after laser irradiation.

Figure 2.8(a) shows the optical image of two microsensors on an MDCK cell. Positions of microsensors A and B were confirmed by cross-sectional fluorescence imaging, as shown in Figure 2.8(c, d). In these images, both microsensors are red, and the MDCK cell is green. Therefore, both sensors were located on the cell membrane. The distance between these microsensors was approximately $3 \mu\text{m}$. After irradiation with the NIR laser to microsensor B for one second, it was injected into the MDCK cell. The positions of these

microsensors are shown in Figure 2.8(e, f). While microsensor B was inside the MDCK cell, microsensor A was still on the cell membrane. This result indicates that author succeeded in the local injection of an arbitrary microsensor on the cell membrane by local laser heating. Moreover, the MDCK cell injected the microsensor still emitted green fluorescence. Among five attempts to inject a microsensor using local laser heating, four were successfully injected, and all four cells were alive after injection. Therefore, the success rate of injection and cell viability were 80% and 100%, respectively. The effect of the microsensor size was not examined in this study. Zhong *et al.* reported the injection of polystyrene nanobeads containing iron oxide nanoparticles by local laser heating [96,97]. The diameters of the polystyrene nanobeads were 300 nm and 750 nm. As in that study, the polystyrene nanobeads used here had a diameter of 750 nm. Applying the current method to other bead sized will be the topic of a future study.

2.4 Summary

In this chapter, a new approach for the manipulation and injection of a single microsensor into a cell using a glass nanoprobe with optical control of the zeta potential and local laser heating was presented. This method was suitable for selective manipulation of a fluorescence microsensor since the tip was safe for contact with cell membranes, and transparency of the glass allowed for observation of the microsensor. This approach was also suitable for improving immobilization of the microsensor to the cell membrane. The microsensor was stained with Rhodamine B, and could be used for temperature measurement. Photo-isomerization of SP achieved a switch of the zeta potential of the microsensor from negative to positive. The positively-

charged microsensor made the pick-up and transport by the negatively-charged glass nanoprobe and immobilization on a cell membrane much easier rather than without UV irradiation. Success rate of the pick-up and cell immobilization of the microsensor were improved to 75% and 64%, respectively. Moreover, the immobilized microsensor was injected into the cell cytoplasm by NIR laser irradiation within one second. The injection rate and viability of the injected cells were 80% and 100%, respectively.

Liu *et al.* achieved pH measurement of an influenza virus-infected cell on the cell membrane using a fluorescence microsensor [190]. However, intracellular measurement was not achieved since rapid injection of the selected microsensor into a specific cell was still too difficult. The current proposed method allowing injection of a fluorescence microsensor will be a break-through for single cell analyses such as pH and temperature measurements inside virus-infected cells.

Chapter 3

Injection of a Fluorescence Microsensor into a Specific Cell by Laser Manipulation and Heating with Multiple Wavelengths of Lights

3.1 Introduction

Recent advances in micromanipulation and micro-sensing techniques have enabled the analysis of intracellular mechanical and environment parameters and activity changes due to external stimuli through manipulation and measurement within specific cells [191]. For example, in the cell infection of an influenza virus, the growth of the virus in the cell nucleus leads to (1) an increase in temperature with the consumption of ATP [192], and (2) a decrease

intracellular pH [190]. Techniques to directly measure intracellular biochemical parameters are needed to analyze in detail the changes in the activity of these cells [22]. These techniques develop potential therapeutic approaches by decoding cell function, inducing cell fate, and reprogramming cell behavior. However, the measurement of environment parameters inside cells has not been well studied compared with the measurement of environment parameters around cells or at the cell surface.

Direct measurement of intracellular environment parameters requires the injection of microsensors into a specific cell and the measurement of environment parameters [193]. Intracellular environment measurements using microsensors can be classified into tethered and non-tethered approaches. A tethered approach involves inserting sharp micropipettes or cantilevers into cells that have electrode or optode probe integrated at the tips of a few micrometers [194]. However, tethered approaches need to maintain intracellular and extracellular connections of the microsensor and, therefore, not suitable for long-term and multi-point measurements [195]. Moreover, these approaches have a risk of cell damage by microsensor insertion.

On the other hand, non-tethered approaches include the injection of the microsensors capable of measuring environment parameters in a non-contact method, such as magnetic and optical techniques. As a magnetic microsensor, an oxygen concentration sensor has been developed by electron paramagnetic resonance method using microparticles of Lithium phthalocyanine [196]. Although low invasive measurements can be realized by using magnetic particles with low cytotoxicity, there are issues such as the need for several tens of seconds for a single measurement and the influence of other environment parameters to be measured.

As an optical microsensor, a method has been developed for producing microparticles doped with an environment-sensitive fluorescent dye and measuring changes in environment parameters such as temperature, pH, oxygen concentration, and ion concentration from the change of fluorescence intensity [43]. Fluorescent dyes have been developed that are sensitive to a wide variety of environments and doping the dye into microparticles of low cytotoxic polymers and hydrogels allows measurement of multiple parameters. The change in fluorescence intensity of the microsensor can be measured by CCD from microscopic images, and the time required for a single measurement is from several hundred milliseconds to a few seconds. Researchers in Arai lab have studied the measurement of environment parameters of cells using fluorescent microsensors and discovered that the cell infected with influenza virus increased temperature by 4.2 °C and decreased pH by 0.6 at 4 hours after infection on the surface using 1 μm fluorescence microsensor [190,192].

Intracellular measurements with fluorescent microsensors using a non-tethered approach require manipulation and cell injection of a single fluorescent microsensor. Micromanipulators [126,197], micropipette aspiration [198,199], dielectrophoretic (DEP) tweezers [200], magnetic tweezers [201,202], and optical tweezers [159,167,168,173] have been developed as manipulation techniques for single microsensor. While micromanipulator has promising advantages such as high power, multi-dimensional, and high-resolution manipulation, manipulation of the order of 1 μm requires advanced skill. Manipulation of a single fluorescence microsensor by fixing to the tip of the micropipette by aspiration also have the difficulty of manipulating a single microsensor of 1 μm. A microsensor made of dielectric materials is captured and manipulated with DEP tweezers, but

the capture force is as low as 50 pN [200]. Magnetic tweezers achieve precise three-dimensional manipulation of single microsensors. However, the complex magnetic field circuit is needed to be constructed around the sample on the microscope [202]. Optical tweezers are capable of three-dimensional manipulation of single microsensors in water to achieve a strong operating force of 100 pN or more. Liu *et al.* have applied optical tweezers with 1064 nm laser to manipulate microtools and measurement of cell environment parameters using fluorescent microsensors [68].

On the injection of microsensors into a specific cell, high success rates, low invasiveness, and short induction times are important parameters [110]. Naturally, cell membranes resist the penetration into the cytoplasm against external molecules such as drugs, organic and micro-nanoparticles. Thus, a successful injection of microsensors requires passage through this barrier using either biochemical or physical methods [68]. To date, biochemical methods such as endocytosis and lipofection and physical methods such as microinjection [203], electroporation [114,115], and laser heating [106,179] have been developed. Biochemical techniques such as endocytosis and lipofection are minimally invasive to cells, but the injection of a 1 μm object takes more than one hour. In physical techniques, a microinjection is a simple approach, but this method easily damages cells. Electroporation injects nanoparticles from holes generated by applying a pulse current to the cell membrane, but there are challenges such as difficulty in a selective injection of a single microsensors and risk of cell damage. Laser heating of metal nanoparticles is accomplished within a few seconds for rapid injection, but the method has a challenge of low viability of the injected cells. Researchers in Arai Lab have used local laser heating to demonstrate rapid and low invasive injection of magnetic fluorescence microsensors made of 1 polystyrene

microparticle containing 20 nm iron oxide nanoparticles [97,204]. However, manipulation of single fluorescence microsensor by optical tweezers could not be applied since the iron oxide nanoparticles absorb 1064 nm laser and caused the high temperature to increase during operation using optical tweezers.

This chapter presents a unique laser injection method that manipulates fluorescent microsensor by optical tweezers and injects fluorescence microsensor to the cytoplasm by laser heating to achieve intracellular environment parameter measurements using a non-tethered approach. By incorporating a dye with wavelength-selective absorption dye into a fluorescence microsensor, the two functions of manipulation and cell injection are controlled by switching the wavelength of input laser. The manipulation of the fluorescence microsensor is conducted by optical tweezers with a 1064 nm laser. Fluorescence microsensors are injected into the target cell using laser heating with 808 nm laser. Environment parameters are measured using fluorescence measurements at wavelengths from ultraviolet to visible light. Fabrication and evaluation of fluorescence microsensor were conducted and demonstration of injection of the fluorescence microsensor was performed.

3.2 Materials and Methods

3.2.1 Principle of optical injection of single fluorescence microsensor to a specific cell by optical manipulation and heating with multiple wavelength lights

Figure 3.1 shows the classification of conventional injection of fluorescence microsensor into a specific cell.

A) Micromanipulation and insertion of the fluorescence microsensor by a mechanical micromanipulator. The fluorescence microsensor is

manipulated to the target cell and inserted inside the cell by mechanical force with a micromanipulator or micropipette.

- B) Manipulation of the fluorescence microsensor by optical tweezers and injection by endocytosis and lipofection. The fluorescence microsensor is manipulated by optical tweezers and immobilized on the cell surface and injected to the cytoplasm by endocytosis and lipofection.
- C) Dispersion of the metallic fluorescence microsensor and injection by local laser heating. Metallic fluorescence microsensor is dispersed on the cell surface and immobilized microsensor is injected by laser heating.
- D) Manipulation and injection of the microsensor by multiple wavelength lights. Manipulation of fluorescence microsensor and injection of the microsensor to the cytoplasm by laser heating using multiple wavelength lights.

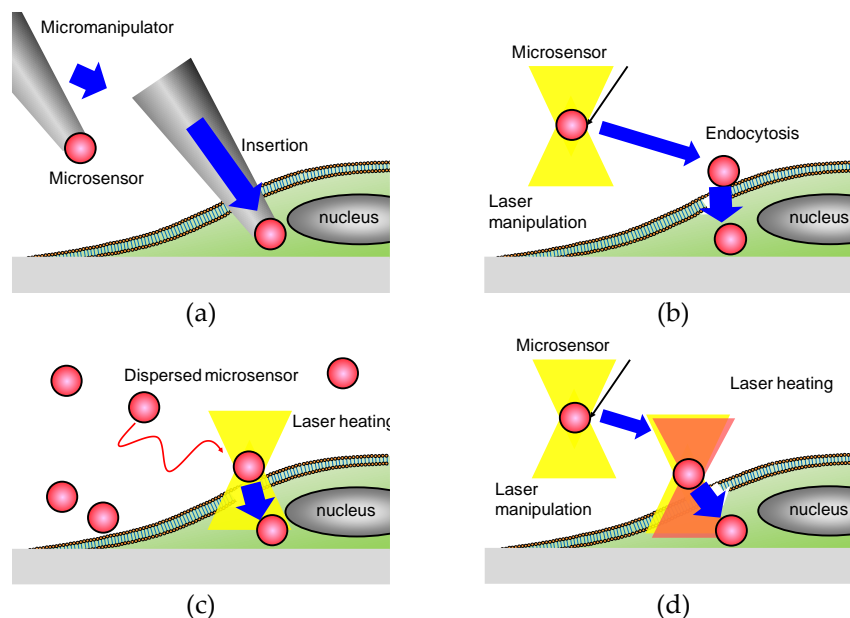


Figure 3.1 : Classification of injection of the microsensor into a specific cell.

- (a) Micromanipulation and insertion of the microsensor by mechanical micromanipulator,
- (b) Manipulation of the microsensor by optical tweezers and injection by endocytosis,
- (c) Dispersion of the microsensor and insertion by local laser heating,
- (d) Manipulation and injection of the microsensor by multiple wavelength lights.

While method (A) can achieve the fluorescence microsensor can be inserted to the target cell accurately, the mechanical injection easily damages the cell and skillful operator is required.

Method (B) manipulate the single fluorescence microsensor coated by lipid membrane by optical tweezers with 1064 nm laser and immobilized on the cell membrane. After immobilization, the microsensor is injected into the cell by endocytosis or lipofection. While this method is low-invasive to a cell, endocytosis takes a long time for injection. For example, injection of 1 μm microsensor took 3 hours. We also reduced the injection time until 30 minutes by local vibration stimulus on the cell membrane by optical tweezers. However, it still takes a long time.

Method (C) can achieve short-time injection by heating the metallic fluorescence microsensor containing metal material, for example, iron dioxide, by laser irradiation. The laser heating induces the melting cell membrane and the injection of the microsensor on the cell membrane. By adjusting the appropriate laser power, injection of 750 nm fluorescence microsensor was injected within 2 seconds with 100% injection success rate and 90% viability. However, metallic fluorescence microsensor cannot be manipulated by optical tweezers since metal material absorbs laser. Although the manipulation and cell immobilization of the metallic fluorescence microsensor using micromanipulator was also succeeded, picking the metallic fluorescence microsensor and immobilizing the microsensor to cell membrane take time.

In this study, a unique method for injecting a single fluorescence microsensor into a specific cell using optical manipulation and heating with multiple wavelengths of light was proposed, as shown in Figure 3.1(d) and Figure 3.2. The fluorescence microsensor is made of a 1 μm diameter polystyrene microparticle containing Rhodamine B and IR (808 nm) absorbing

dye. The polystyrene microparticle can be manipulated in water using a 1064 nm laser as the refractive index of the polystyrene is 1.6 (refractive index of water: 1.3). Rhodamine B is a temperature-sensitive fluorescent dye (excitation wavelength: 488 nm, emission wavelength: 560 nm). The IR absorbing dye absorbs 808 nm light but does not absorb 1064 nm laser light. Therefore, the wavelengths chosen for each function do not interfere with each other. First, a fluorescence microsensor is manipulated to the target cell membrane using 1064 nm laser optical tweezers. Then, the fluorescent microsensor is injected into the cytoplasm by heating with an 808 nm laser on the cell membrane.

This newly proposed method for the injection of a fluorescence microsensor into a specific cell using optical manipulation and heating can achieve selective, low invasive, and rapid injection of the fluorescence microsensor.

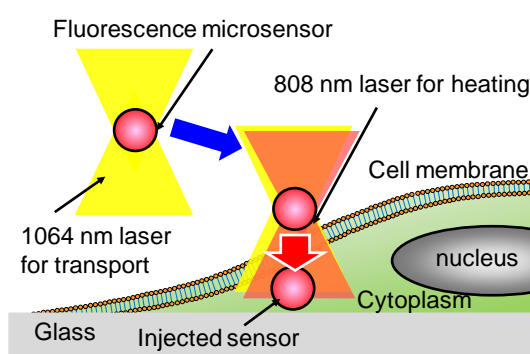


Figure 3.2 : A schematic diagram of optical manipulation of fluorescence microsensor to a specific cell by local heating using multiple wavelength lights.

3.2.2 Experimental setup

A schematic of the experimental setup consisting of optical tweezers and heating system with laser confocal fluorescent microscopy is shown in Figure 3.3. A commercialized inverted optical microscope (IX71, Olympus, Tokyo, Japan) with a fluorescence observation system was used for observing the microsensor and cell [177]. To acquire the manipulation image and

fluorescence image, EM-CCD (iXon Ultra, Andor, Canada) and confocal laser scanning system (CSU-X1, Yokogawa Co. Ltd., Japan) with excitation laser of 488 nm were used. The optical tweezers system generated by diode-pumped Nd:YAG/YVO₄ laser (IPG laser) with 1064 nm wavelength and 10 W of maximum power was used for the manipulation process of the fluorescence microsensor. The power of the 1064 nm laser was adjusted 40 mW on the objective lens. An 808 nm continuous wave laser (OBIS, Coherent) with a maximum power of 150 mW was used for local heating. The power of 808 nm laser was also adjusted 40 mW on the objective lens. The diameter of both laser circle focus point was approximately 1.4 μm. Piezoelectric z-stage (PI) with the high magnification objective lens (Plan Fluor 100×, Olympus, Japan) was used for acquiring a 3D fluorescence image. Moreover, the cell-culture chamber (ZILCOS, Tokai hit, Japan) was used for maintaining the temperature of the cell environment at 37 °C during the experiment.

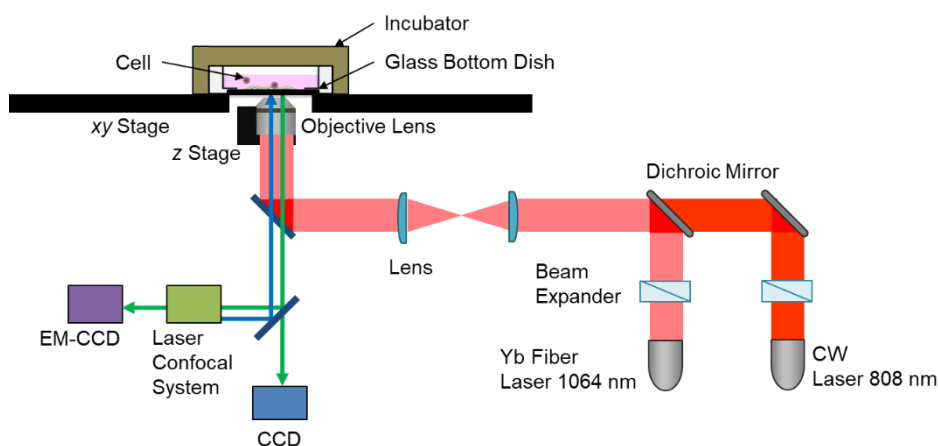


Figure 3.3 : Experimental setup.

3.2.3 The fabrication process of the fluorescence microsensor

In this paper, the fluorescence microsensor was fabricated and used to verify the proposed injection method. A schematic image of the fluorescence microsensor is shown in Figure 3.4. Figure 3.5 shows the fabrication process of

fluorescence microsensors made of 1 μm amino-coated polystyrene microparticle (Funakoshi, Japan), Rhodamine B (Wako pure chemical), which is a temperature-sensitive fluorescence dye, and IR absorbing dye FDN-002 (Yamada Chemical Industry, Japan). The excitation and emission wavelength of Rhodamine B are 488 nm and 580 nm, respectively. IR absorbing dye FDN-002 was used for heating by 808 nm laser. The absorption of the 1064 nm laser is quite low in this dye.

The fabrication process of the hydrogel fluorescence microsensor is as follows:

1. Injection of 100 μL amino-coated polystyrene microparticle in 1.5 mL microtube.
2. Preparation of staining solution containing 1 mg/L Rhodamine B and 1 mg/mL IR absorbing dye in ethanol solution.
3. A stain of the amino-coated polystyrene microparticle by staining solution for 30 minutes.
4. Centrifuging the stained microsensors at 10000 \times g for 15 minutes for washing.
5. The repeat of the washing process at five times.

Figure 3.6 shows the bright field and fluorescence images of fabricated fluorescence microsensors.

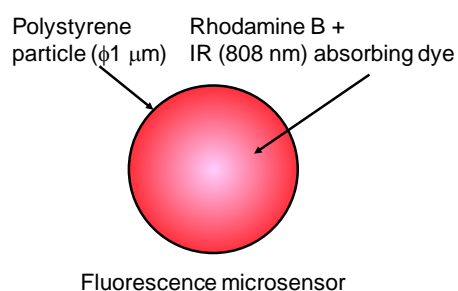


Figure 3.4 : A schematic image of fluorescence microsensor.

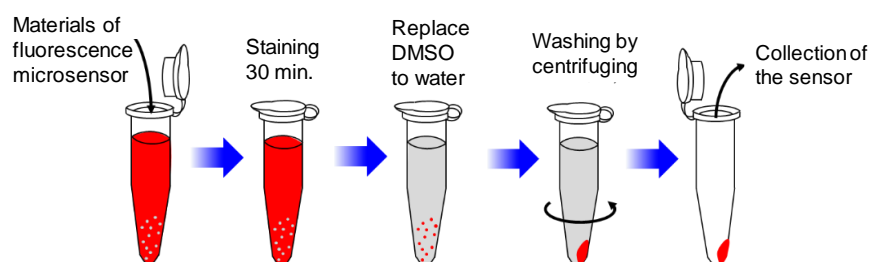


Figure 3.5 : Fabrication process of fluorescence microsensor.

(a) Mixing the materials of fluorescence microsensor, (b) Staining, (c) Replace of staining solution to water, (d) Washing by DI water, (e) Collection of the microsensor.

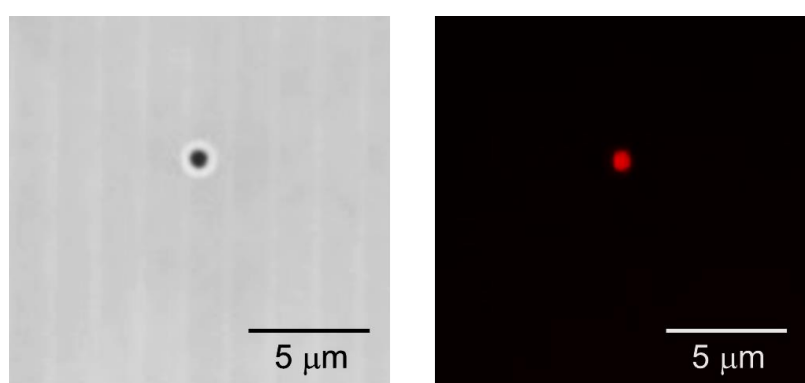


Figure 3.6 : Bright field and fluorescence image of fluorescence microsensor.

(a) fluorescence microsensor in bright field, (b) Fluorescence image.

3.2.4 Cell culture

MDCK cells were used in the injection experiment. MDCK cells were cultured in a 27 mm diameter of the glass-bottom dish containing 2.0 mL of DMEM and 0.2 mL of FBS. The culture conditions were 5% CO₂ and 95% air at 37 °C. MDCK cells were cultured for 8 h prior to the injection experiment. MDCK cells were stained after injection with Calcein-AM (excitation wavelength: 488 nm, emission wavelength: 515 nm) to investigate the cell viability. Calcein-AM in the cytoplasm of alive cells is hydrolyzed by esterase activity and emits fluorescence of Calcein-AM. A 100 μL of 0.5 mg/mL Calcein-AM solution was added to the glass-bottom dish. The stained MDCK cells were incubated at 37 °C for 30 min. Then, the fluorescence of Calcein-AM inside MDCK cell was observed approximately one hour after the injection.

3.3 Results and Discussion

3.3.1 Size evaluation of fluorescence microsensor

First, the size distribution of the fluorescence microsensor was evaluated as the staining solution containing ethanol could have dissolved the polystyrene, causing changes in the sensor size and shape. In optical tweezers, the spherical structure is suitable for stable manipulation. In fluorescence temperature measurement, relative fluorescence intensity and temperature were calibrated using fluorescent microsensors with uniform size. If the size of fluorescence microsensors varies, the fluorescence intensity of microsensors varies even at the same temperature. The mean diameter of the microsensor was evaluated using a tunable resistive pulse sensing (TRPS) nanoparticle analyzer (qNano, Izon Science Ltd., New Zealand). The mean size of the microsensor was evaluated by collecting calibration data using approximately 10000 commercial 1 μm microparticles (4010A, Thermo Scientific, USA). Figure 3.7 shows the size distribution of the fluorescence microsensor. The measured mean size of the microsensor was 0.98 μm and the standard deviation was approximately 0.1 μm . These results confirmed that the fabrication process does not have adverse effects on the sensor size distribution of the sensor.

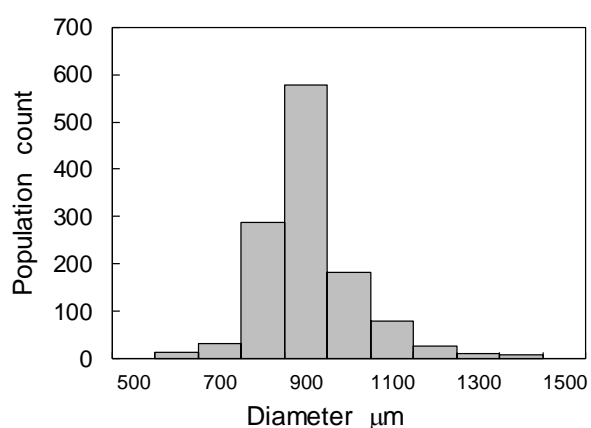


Figure 3.7 : Size distribution of fluorescence microsensor.

3.3.2 Temperature calibration of fluorescence microsensor

There is a proportional relationship between the relative fluorescence intensity of Rhodamine B and temperature ranging from 0 °C to 100 °C [205]. Therefore, the temperature range of calibration was chosen from 30 °C to 40 °C to acquire the temperature sensitivity of fluorescence microsensors. Figure 3.8 shows the calibration data for the relative fluorescence intensity as a function of temperature. The horizontal and vertical axes show the temperature measured by the thermopile in the chamber and the relative fluorescence intensity based on the fluorescence intensity at 30 °C, respectively. The fluorescence intensity of the hydrogel fluorescence microsensor decreased monotonically with increasing temperature. The fitting obtained using the least-squares method is shown in Equation 3.1.

$$\frac{I}{I_o} = -0.015 \cdot \text{Temp.} + 1.5 \quad (3.1)$$

The temperature sensitivity of the hydrogel fluorescence microsensor was calculated to be -1.5 %/°C and the precision of the temperature measurement was ± 0.5 °C.

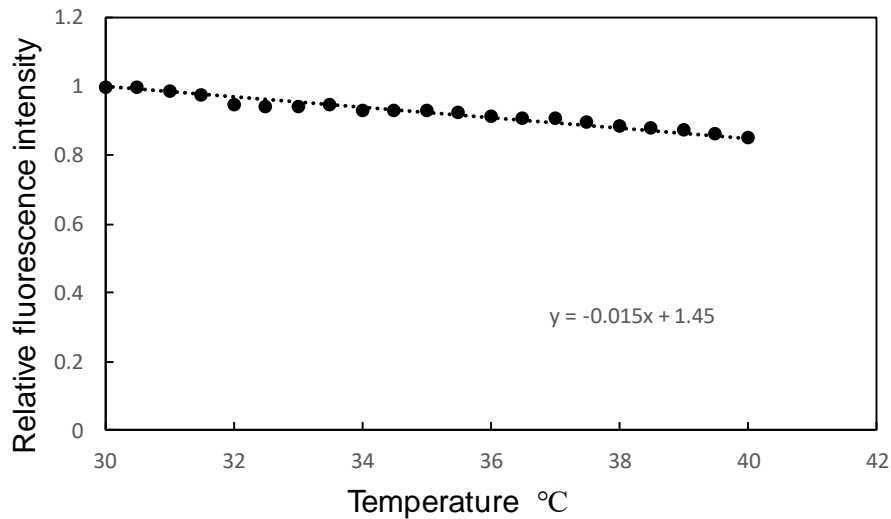


Figure 3.8 : Calibration result of relative fluorescence intensity of the fluorescence microsensor with temperature.

3.3.3 Heat evaluation of fluorescence microsensor using 1064 nm and 808 nm lasers

To confirm the wavelength-specific heating of the fluorescence microsensor, the absorbance properties of the fluorescence microsensor were evaluated as shown in Figure 3.9. First, the absorbance property of the FDN-002 was evaluated. A glass microchannel (depth: 150 μm) was fabricated and the FDN-002 ethanol solution was injected into the microchannel. 1064 nm and 808 nm lasers were applied, and the laser power was measured before and after passing through the microchannel. Figure 3.9 shows that the absorbance rates of the 1064 nm and 808 nm lasers at 1 mg/mL were 1% and 85%, respectively. This result confirmed the wavelength selectivity of the laser heating of the fluorescence microsensor.

Figure 3.10 shows the experimental results for the temperature measurement using the fluorescence microsensor during optical heating with 1064 nm and 808 nm lasers. Both laser powers were adjusted by 40 mW. The environmental temperature was maintained at 37 $^{\circ}\text{C}$ using the cell culture chamber. Temperature measurement was conducted at every 1 s. First, single fluorescence microsensors were trapped using the 1064 nm laser to avoid heat diffusion to a glass substrate. After 22 temperature measurements, the fluorescence microsensor was irradiated with the 808 nm laser. In the case of 1064 nm laser irradiation, the temperature remained almost uniform, while the temperature dramatically increased under 808 nm laser irradiation. The approximate temperature of the fluorescence microsensor increased by 15 $^{\circ}\text{C}$ for 10 s heating. In the previous study performed in Arai Lab, 50 $^{\circ}\text{C}$ was required to inject a microsensor using laser heating [97]. As the environmental temperature was maintained at 37 $^{\circ}\text{C}$, the observed heating properties were considered sufficient for the injection of the fluorescence microsensor into

cytoplasm. These results confirmed the effectiveness of selective laser heating of the microsensor using IR absorbing dye.

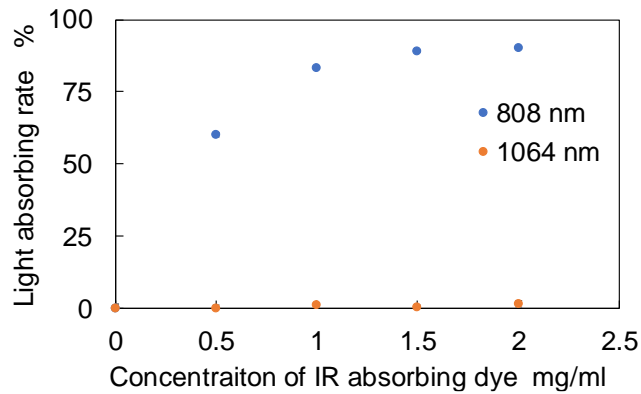


Figure 3.9 : Comparison of absorption rate of IR absorbing dye between 808 nm and 1064 nm (Thickness of microchannel 150 μm).

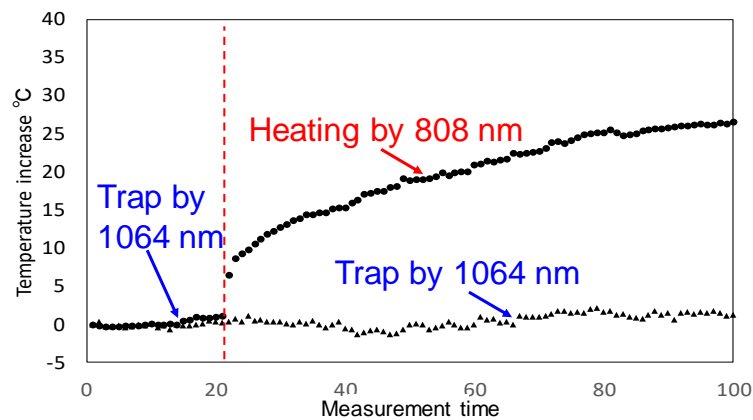


Figure 3.10 : Measurement of temperature increase of fluorescence microsensor by irradiating 808 nm laser.

3.4 Manipulation and injection of the fluorescence microsensor into MDCK cell

Figure 3.11 shows the optical injection of the fluorescence microsensor using optical manipulation with a 1064 nm laser and heating using a 808 nm laser. Both laser powers of 1064 nm and 808 nm were adjusted to 40 mW. The environmental temperature was maintained at 37 $^{\circ}\text{C}$ by a cell culture chamber. MDCK cell was used as a sample specimen. As shown in Figure 3.11(a), the

fluorescence microsensor was successfully trapped by optical tweezers with 1064 nm. After transport of the fluorescence microsensor to the target cell membrane. Then, the fluorescence microsensor was heated by 808 nm laser for 10 seconds. After laser heating, the focus plane of the fluorescence microsensor was moved to downward (inside the cytoplasm). The success rate of the injection was 70% (Total number of experiments was 10).

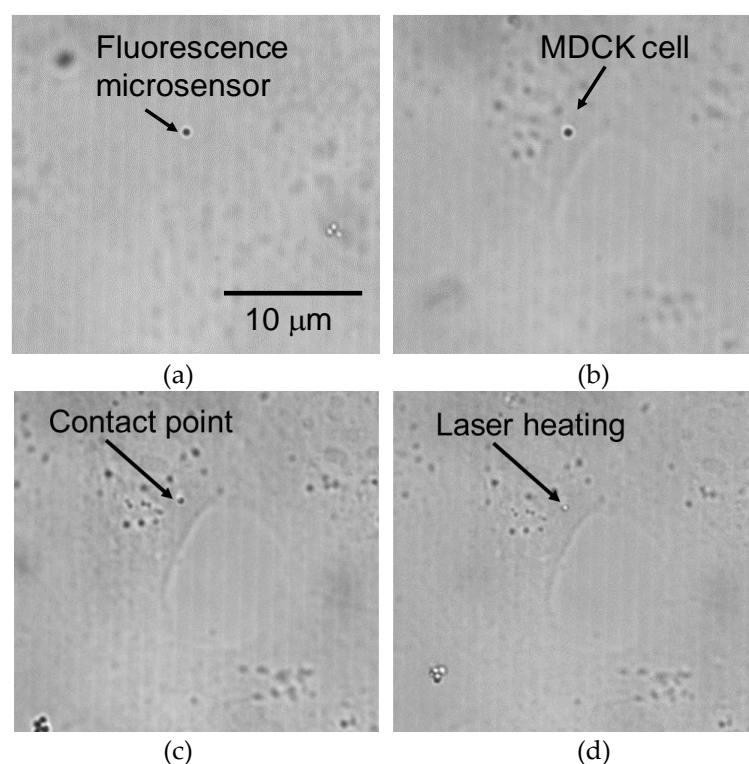


Figure 3.11 : Manipulation and injection of fluorescence microsensor to MDCK cell. (a) A trap of the microsensor, (b) Transport to MDCK cell, (c) Contact to the cell membrane, (d) 808 nm laser irradiation to the sensor.

To confirm the injection of the fluorescence microsensor into MDCK cells, laser-confocal fluorescence imaging of the MDCK cell and the injected fluorescence microsensor was acquired for the whole cell (pitch of the slice image: 0.5 μm) as shown in Figure 3.12. From Figure 3.12(b) the presence of the fluorescence microsensor inside the cytoplasm of the MDCK cell was observed. Moreover, the location of the fluorescence microsensor inside the

MDCK cell was confirmed by the cross-sectional image as shown in Figure 3.12(d).

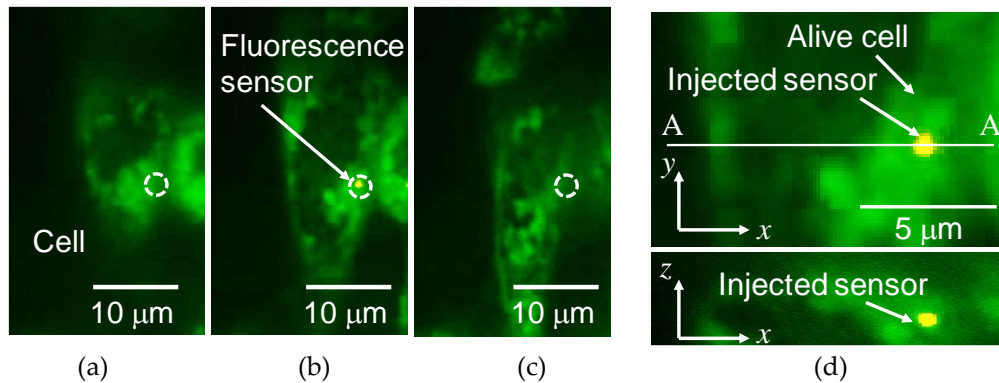


Figure 3.12 : Fluorescence image of injected fluorescence microsensor.

(a) Fluorescence image at $3\ \mu\text{m}$ upper to focus plane of the microsensor, (b) Fluorescence image at focus plane of the microsensor. (c) Fluorescence image at $3\ \mu\text{m}$ upper to focus plane of the microsensor. (d) Upper: zoom image of red rectangle at (c), lower: cross-sectional image at A-A' line. (amber: fluorescence microsensor, green: cytoplasm of alive cell).

Table 3.1 shows the comparison of the proposed method with the previous work [68,204]. The injection time was defined as the duration of laser heating or vibration-assisted endocytosis in this study. The manipulation of fluorescence microsensors by optical tweezers has an advantage in transporting to target cells relative to the manipulation of fluorescence microsensors incorporating metallic nanoparticles by a micromanipulator. Injection of fluorescence microsensor by laser heating has the advantage of short-injection time relative to vibration-assisted endocytosis. From these results, the effectiveness of the proposed method was confirmed.

Table 3.1 : Comparison of injection time and success rate of injection by the proposed method and previous work.

Method	Manipulation	Injection time	Success rate
Proposed method	Optical tweezers	< 10 s	70%
Vibration-assisted endocytosis [68]	Optical tweezers	30 min	71%
Manipulation and heating of metal containing sensor [204]	Micromanipulator	2 s	60%

3.5 Summary

In this study, the author proposed and experimentally confirmed the optical injection of a single fluorescence microsensor into a specific cell using optical manipulation and heating with multiple wavelengths of light. The fluorescence microsensors stained with Rhodamine B and IR absorbing dye were successfully fabricated. The fluorescence microsensor was not heated by the 1064 nm laser, but the 808 nm laser did induce temperature changes. Therefore, the trapping and manipulation of the fluorescence microsensor with optical tweezers using a 1064 nm laser was succeeded. In the current experimental setting, the direct measurement of light absorption property in each 1 μm microsensor was difficult. The direct evaluation of light absorption property is future work. In addition, injecting the fluorescence microsensor into a specific cell by heating with an 808 nm laser was succeeded. Furthermore, the author showed the presence of the injected fluorescence microsensor in the cell and demonstrated that the injected cell was still alive. These findings demonstrate a high success rate (70 %), low invasive, and rapid injection within 10 s. However, the measurement of time required for fluorescence microsensors to cross the cell membrane is difficult in the current

experimental system. The measurement of crossing time for fluorescence microsensor is the future work.

The presented method can control the temperature of the microsensor during the heating by measuring the temperature of the microsensor. Therefore, this method has the potential for automated injection of fluorescence microsensors to the target cells.

Chapter 4

Hydrogel Fluorescence Microsensor with Fluorescence Recovery for Prolonged Stable Temperature Measurements

4.1 Introduction

Both the measurement and control of the cellular environment with the high spatial resolution are essential for investigating cellular conditions systematically, defining normal cell-to-cell variation, quantifying the influence of environmental perturbations, and understanding cellular responses in the tissues and complex environments. For example, the local pH around octacalcium phosphate in granule form was determined using an optical

measurement method to analyze the release of inorganic phosphate ions from octacalcium phosphate upon biomolecule absorption [206]. In addition to pH measurement [190], the use of optical sensors to determine various environmental parameters—such as temperature [192,207–209] and oxygen concentration [210]—with the high spatial resolution is promising for biological investigation.

Optical sensors using fluorescent dyes have significant potential in non-contact measurement for microscale applications. Environmental parameters such as temperature [27,50], oxygen concentration [211–213], pH [214,215], and organophosphate compounds [216] can be measured by utilizing fluorescent dyes that are sensitive to these parameters. The author has developed fluorescence sensors in which fluorescent dyes are impregnated into various processable materials such as polymers, photoresists, and hydrogels [46]. Fluorescence sensors have paved the way for the investigation of cells, tissues, and the environmental conditions of culture systems, amongst other parameters.

The fluorescence of the sensor can be measured in terms of its fluorescence intensity and fluorescence lifetime [192,210,217,218]. The direct introduction of fluorescent dyes into cells carries the risk of cell damage as well as the efflux of the dyes. Therefore, the impregnation of fluorescent dyes into microparticles made of polymers and hydrogels enables low invasivity and long-term measurement. Changes in the fluorescence intensity and fluorescence lifetime of the microsensor can be measured using a microscope with an image sensor, such as a CCD. This approach is suitable for multipoint measurement [219]. In addition, positioning the microsensor at arbitrary points is possible through the manipulation of the microsensor using non-contact techniques such as optical tweezers [74,192,204].

When using fluorescent microsensors, photobleaching of the fluorescent dyes that occurs as a result of exposure to the light required for observation is one of the most critical issues [220]. When a sensor is irradiated, some of the fluorescent molecules are excited, resulting in their molecular structure being altered, while the remaining molecules do not emit fluorescence. In microscopic measurement, the effect of photobleaching must be considered because the objective lens focuses the excitation light, and high-energy radiation reaches the fluorescence microsensor. The fluorescence lifetime is used for stability measurements [218,221], however, the equipment required for fluorescence lifetime measurement is expensive and not widely used. In contrast, the equipment for fluorescence intensity measurement can be more easily implemented. In this case, the effect of photobleaching on the evaluation of fluorescence intensity is quite severe, which is related to the concentration of the fluorescent dye.

This work proposes a new method for the prolonged stable measurement of hydrogel fluorescence microsensors based on the measurement of fluorescence intensity. Fluorescence recovery after photobleaching is thought to compensate for the decrease in fluorescence intensity of the microsensor [222,223]. In the hydrogel fluorescence microsensors used in this work, the fluorescent dye is uniformly distributed. When a region of the microsensor is photobleached by the exposure to light, the unbleached fluorescent dye diffuses into the photobleached region. The concentration of fluorescent dye in the photobleached portion is recovered after an appropriate time interval, which enables stable fluorescence measurements to be made over prolonged periods. The hydrogel fluorescence microsensors were fabricated and evaluated the time interval of measurement, material, the concentration of photo initiator, and composition of the

fluorescence microsensor to investigate the effect of these parameters on photobleaching. In addition, the effect of the microsensor size on the stability of the fluorescence intensity was also evaluated. A temperature-sensitive fluorescent dye was used for temperature measurement inside a stage-top chamber, and a thermocouple was used for calibration to confirm the effectiveness of the proposed measurement method.

4.2 Materials and Methods

4.2.1 Principle of photobleaching compensation for the hydrogel fluorescence microsensor

Fluorescence intensity is represented by Equation 4.1 [224].

$$I = I_0 \Phi \epsilon C x \exp(-t/\tau) \quad (4.1)$$

where I [W] is the fluorescence intensity emitted from the fluorescent material per unit time, I_0 [W] is the excitation light flux of the fluorescent material, Φ is the fluorescence quantum yield, C [mol/L] is the concentration of the fluorescent dye, ϵ is the absorbance index [L/mol·cm], x [cm] is the diameter of the hydrogel fluorescence microsensor, t [s] is the total exposure time, and τ [s] is the decay coefficient of the fluorescence intensity. The structure of some of the fluorescent dye molecules changes to a non-fluorescent structure with every exposure to the excitation light. Therefore, the concentration of fluorescent dye and the fluorescence intensity decrease with increasing measurement repetition. This phenomenon, known as photobleaching, is one of the most serious challenges in achieving long-term stable measurement based on fluorescence intensity. The recovery of the concentration of the fluorescent dye after exposure is a promising approach for addressing this limitation.

Figure 4.1 shows a schematic diagram of fluorescence intensity recovery in the hydrogel fluorescence microsensor. The microsensor is made of photo-crosslinkable hydrogel, water, and fluorescent dye. The fluorescent dye is uniformly distributed inside the microsensor, which is made of the photo-crosslinkable hydrogel. In this method, a confocal laser scanning microscope is used to measure the fluorescence. The excitation laser is scanned inside the microsensor to measure fluorescence. All fluorescent dyes in the path of the excitation laser will photo-bleach by laser excitation. The dependency of photo-bleaching to the intensity of excitation laser has been reported previously in reference [225]. The study indicated that the higher the excitation laser intensity, the higher the photobleaching of fluorescent dye. Distribution of laser intensity is determined by the laser profile of the focused laser beam. Laser intensity of the laser focused area is considered higher than that of the other part. Therefore, based on reference [225], the effect of photo-bleaching at the laser focused area is considered higher than that at the other part of total excited area. The thickness of the laser focused area is highlighted in yellow in Figure 4.1(a). Fluorescent dye in the microsensor emits fluorescence and some of the fluorescent dye molecules are bleached. As a result, the concentration of unbleached fluorescent dye decreases as shown in Figure 4.1(b). The bleached and unbleached fluorescent dyes then diffuse inside the hydrogel fluorescence microsensor to give uniform concentrations of both dyes across the microsensor. After diffusion of the dyes is complete, the concentration of unbleached fluorescent dye at the laser focused area is recovered, as shown in Figure 4.1(c).

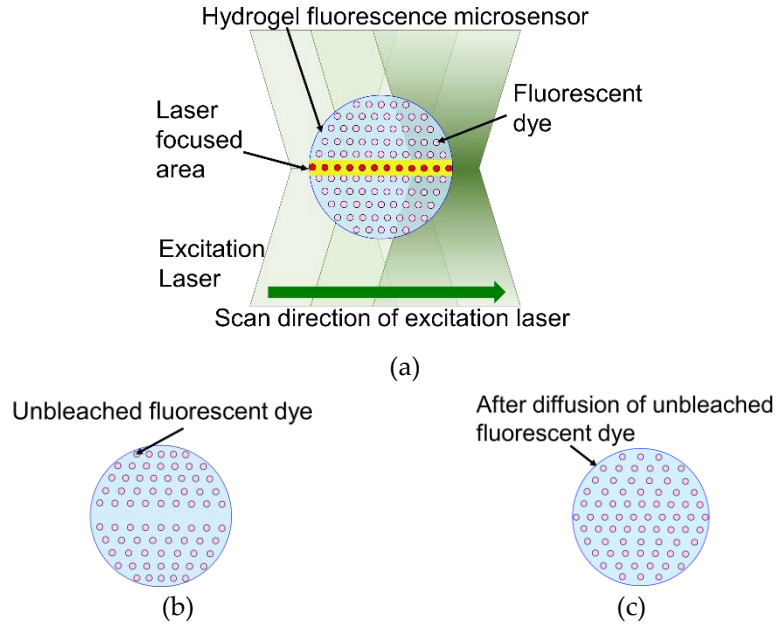


Figure 4.1 : Schematic diagram of fluorescence recovery after photobleaching in a hydrogel fluorescence microsensor.

(a) Scanning of the hydrogel fluorescence microsensor with the excitation laser for measurement, (b) Diffusion of unbleached fluorescent dye in the hydrogel fluorescence microsensor, (c) Hydrogel fluorescence microsensor with recovered unbleached fluorescent dye distribution.

The time required for the diffusion of unbleached fluorescent dye depends on the concentration of the hydrogel. The low-concentration hydrogel allowed the fluorescent dye to demonstrate high diffusivity. The relationship between the size of the hydrogel fluorescence microsensor and the thickness of the excitation area is critical for the long-term stability of the fluorescence intensity. In photobleaching compensation, unbleached fluorescent dye moves to the excitation as some of the fluorescent dye molecules in the excitation area are bleached by irradiation with the excitation light. The thickness of the excitation area D is calculated using Equation 4.2 [223].

$$D = \frac{0.67\lambda_{ex}}{n - \sqrt{n^2 - (NA)^2}} \quad (4.2)$$

where λ_{ex} is the wavelength of the excitation light, n is the refractive index of the solution, and NA is the numerical aperture. When λ_{ex} , n , and NA are 561 nm, 1.33 (water), and 0.45, respectively, D is calculated as approximately 4.7 μm . The amount of unbleached fluorescent dye is determined from the concentration of fluorescent dye and the sensor size. Therefore, author assume that a larger sensor represents a greater resistance to photobleaching.

In summary, using a hydrogel fluorescence microsensor with a size that is larger than D and an appropriate interval time that is longer than the diffusion time of the unbleached fluorescent dye, should result in long-term measurement stability.

4.2.2 Experimental system

Figure 4.2 shows a schematic diagram of the experimental system. A commercial inverted microscope (ECLIPSE Ti-E, Nikon) with confocal laser scanning unit (CSU-X1, Yokogawa Electric Co.), objective lens (CFI Apochromat 20 XC, Nikon), and electron multiplying-charge coupled device (iXon Ultra, Andor Technology Ltd.) were used to acquire the confocal fluorescence images. The diameter of the pinhole of CSU-X1 was 50 μm . The NA of the objective lens was 0.45. During the fluorescence measurement, the focus of the fluorescence image was maintained using the automatic focusing system (Perfect Focus System) of the Ti-E. An excitation laser with a wavelength of 561 nm was used to excite the fluorescent dye in the hydrogel fluorescence microsensor. A stage top incubator with a feedback temperature controller (ZILCS, Tokai Hit) was placed on the microscope stage. The accuracy of the temperature control was $\pm 0.3^\circ\text{C}$. The fluorescence microsensors were attached to the glass surface of the glass bottom dish. First, 100 μL of the solution containing the fluorescence microsensors was dropped

onto the glass surface. The fluorescence microsensors were fixed on the glass surface by the evaporation of the solution as a result of heating for 30 min at 80°C on a hot plate. After fixing the fluorescence microsensors, 2 mL of deionized water was introduced into the glass bottom dish. The dish was then placed in the stage top incubator. A thermopile was used to measure the temperature of the deionized water inside the glass bottom dish. The acquisition of fluorescence images and analysis of the fluorescence intensity were performed using NIS-Elements Ar software (Nikon).

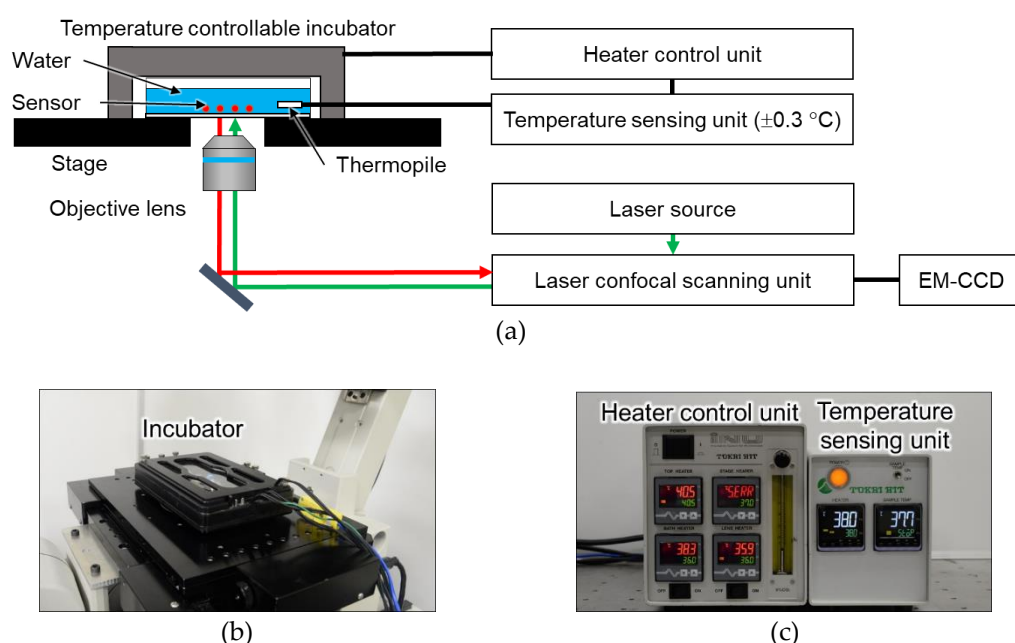


Figure 4.2 : Experimental system.

(a) Schematic diagram of the experimental system, (b) Photograph of the stage-top incubator. (c) Temperature control unit for the stage-top incubator.

4.2.3 Fabrication of the hydrogel fluorescence microsensor

Hydrogel and polystyrene fluorescence microsensors were fabricated to demonstrate the effectiveness of photobleaching compensation as a result of the diffusion of unbleached fluorescent dye inside the hydrogel fluorescence microsensor. Figure 4.3 shows the fabrication processes for the hydrogel and polystyrene fluorescence microsensors. Both fluorescence

microsensors were impregnated with Rhodamine B (Wako Pure Chemical Co., Japan), which is a temperature-sensitive fluorescent dye. The excitation and emission wavelength of Rhodamine B are 561 nm and 580 nm, respectively [43].

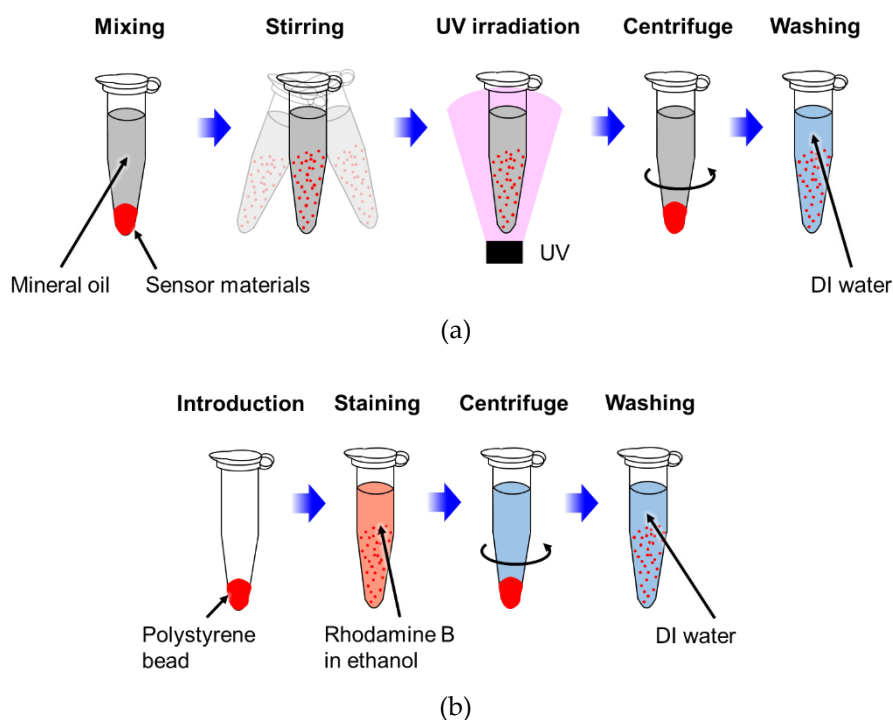


Figure 4.3 : Fabrication processes for fluorescence microsensors.
 (a) Hydrogel fluorescence microsensor, (b) Polystyrene fluorescence microsensor. (UV: ultraviolet, DI: deionized)

The hydrogel fluorescence microsensor consisted of PEGDA 575 (Sigma-Aldrich), deionized water, and Omnirad 1173 (BASF Japan Co., Ltd.), which is a photo initiator. The hydrogel fluorescence microsensor was fabricated using different concentrations of PEGDA 575 (9% and 99%) and Omnirad 1173 (0.5%, 1.0%, 1.5%, 2.0%, 2.5%, and 3.0%) to evaluate the effects of the photo-crosslinkable hydrogel and photo initiator concentrations.

The fabrication process for the hydrogel fluorescence microsensor (9% PEGDA575, 1.0% Omnirad 1173) was as follows (Figure 4.3(a)).

1. First, 100 μL PEGDA 575, 1000 μL deionized water, 100 μL Rhodamine B aqueous solution (1 g/L), and 10 μL Omnirad 1173 were mixed, and 100 μL of the mixture was introduced into 1 mL of mineral oil in a 1.5 mL microtube.
2. The hydrogel fluorescence microsensor solution was emulsified by stirring.
3. The hydrogel fluorescence microsensor emulsion was photopolymerized by ultraviolet light illumination (wavelength: 330–380 nm) for 10 min with Xcite-LED1 (Excelitas Technologies Corp.).
4. The polymerized microsensors were centrifuged at a speed of 14,000 g for 15 min to concentrate the hydrogel fluorescence microsensors at the bottom of the microtube.
5. The hydrogel fluorescence microsensors were washed by replacing the mineral oil with deionized water.

A polystyrene fluorescence microsensor was fabricated for comparison with the hydrogel fluorescence microsensor as fluorescent dye does not diffuse in polystyrene. The polystyrene fluorescence microsensor consisted of 20 μm polystyrene microparticles (Duke Scientific) and Rhodamine B. The fabrication process is described in Figure 4.3(b) [43].

1. First, 1 μL of polystyrene microparticles was stained with Rhodamine B ethanol solution (1 g/L).
2. The stained fluorescence microsensors were centrifuged at a speed of 14,000 g for 15 min.
3. The stained microsensors were washed three times using DI water.

Figure 4.4 shows the fluorescence images of the hydrogel fluorescence microsensor and polystyrene fluorescence microsensor. The size of the fabricated hydrogel fluorescence microsensors ranged from a few to 60 μm as shown in Figure 4.4(d). The evaluation of the photobleaching compensation was performed using 20 μm hydrogel fluorescence microsensors.

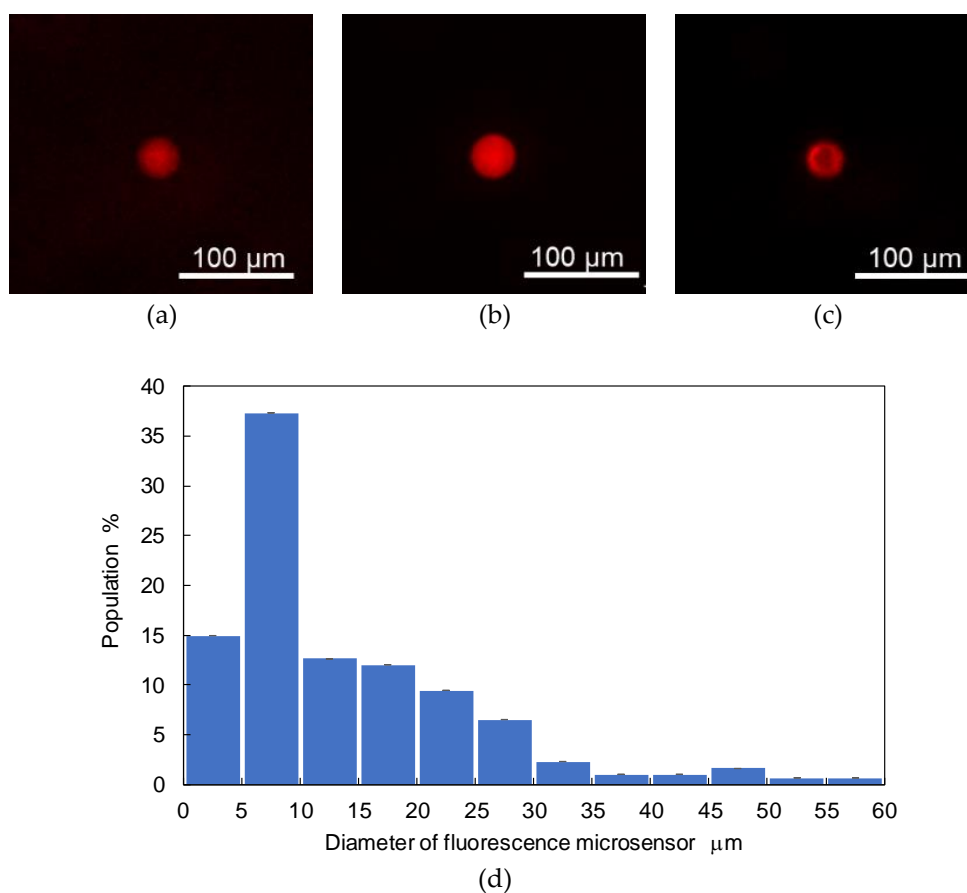


Figure 4.4 : Fluorescence images of fabricated microsensors. (a) Hydrogel fluorescence microsensor (low-concentration; 9% PEGDA 575), (b) Hydrogel fluorescence microsensor (high-concentration; 99% PEGDA 575) (c) Polystyrene fluorescence microsensor, (d) Diameter distribution of the hydrogel fluorescence microsensors (9% PEGDA575). (The concentration of Omnirad 1173 was 3.0%).

4.3 Results

4.3.1 Comparison of photobleaching compensation for different sensor materials

Figure 4.5 shows the comparison of the fluorescence intensity recovery for the different microsensor materials. To compare the diffusivity of the fluorescent dye in the microsensors, the concentrations of hydrogel material (PEGDA 575) used to form the hydrogel fluorescence microsensors were set at 9% and 99%. The concentration of Omnirad 1173 was 3.0%. The size of both hydrogel fluorescence microsensors was 20 μm . The exposure and interval times for excitation were 1 s and 10 min, respectively. The power of the excitation laser was 20 mW. The temperature was maintained at 25°C. The hydrogel fluorescence microsensor with 9% PEGDA 575 showed sufficient recovery of fluorescence intensity for stable fluorescence measurement. The standard deviation of the difference from the initial fluorescence intensity was within 1%. In contrast, the hydrogel fluorescence microsensors with 99% PEGDA 575 and the fluorescent polystyrene exhibited a continuous decrease in fluorescence intensity (99% PEGDA: approximately 10%, polystyrene: approximately 20%). The reason both the 99% PEGDA 575 and polystyrene fluorescence microsensors did not show recovery of their fluorescence intensity is thought to be that the unbleached fluorescent dye was not able to diffuse effectively into the depleted region within the interval time. These results indicate that the diffusivity of the fluorescent dye inside the microsensor was one of the critical parameters for photobleaching compensation.

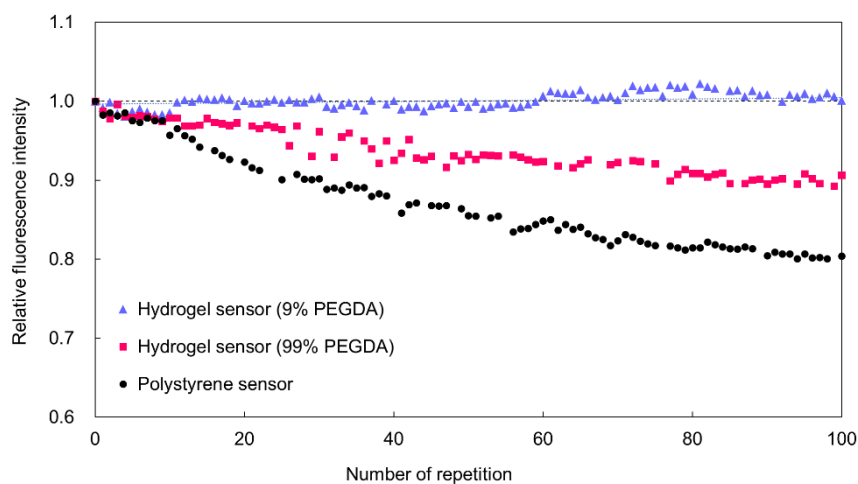


Figure 4.5 : Comparison of the fluorescence intensity recovery for the different sensor materials.

4.3.2 Effect of measurement interval time on photobleaching compensation

The fluorescence intensity of 20 μm hydrogel fluorescence sensors (9% PEGDA 575, 3.0% Omnirad 1173) was repeatedly measured at various time intervals to investigate the required interval time for the recovery of fluorescence intensity at each measurement. The exposure time was set at 1 s. The interval time was changed to 0, 1, 2, 4, 6, and 8 s. An excitation laser with wavelength of 561 nm was set at 20 mW. The temperature was maintained at 25°C throughout the experiments. Experiments with each of the interval periods were repeated 100 times. Figure 4.6 shows the relationship between the variation of fluorescence intensity of hydrogel fluorescence microsensors with different interval times. The relative fluorescence intensity of the hydrogel fluorescence microsensors decreased by more than 1% for interval times shorter than 4 s. However, for interval times of 6 or 8 s, the fluorescence intensity decreased slightly less than 1% after 100 excitations. These results showed that photobleaching compensation depends on the interval time between exposures.

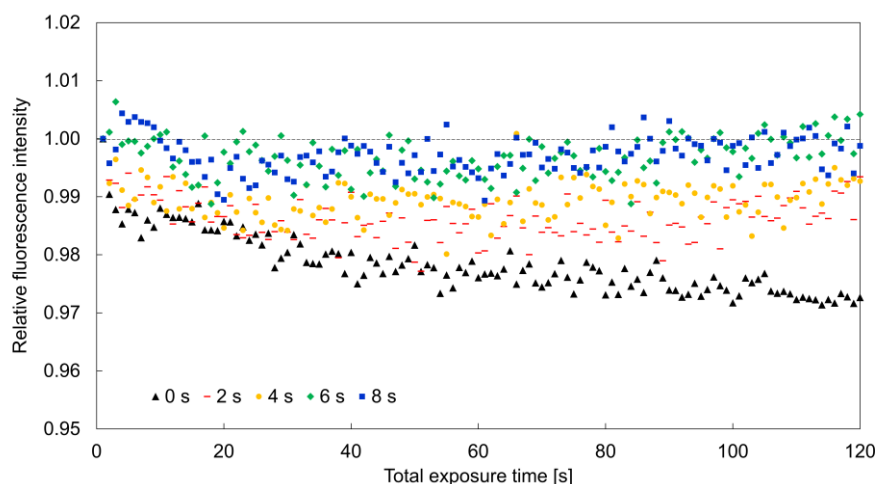
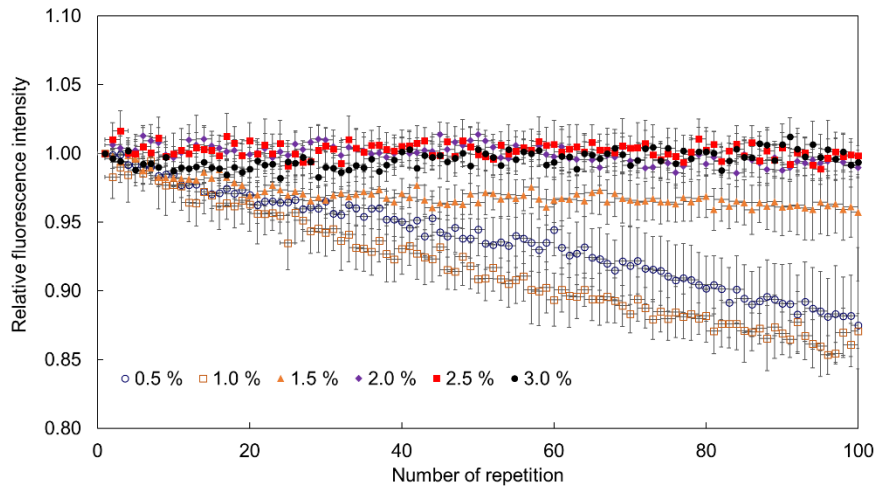


Figure 4.6 : Relationship between the variation of fluorescence intensity of the hydrogel fluorescence microsensors (9% PEGDA 575) and the interval time between exposures.

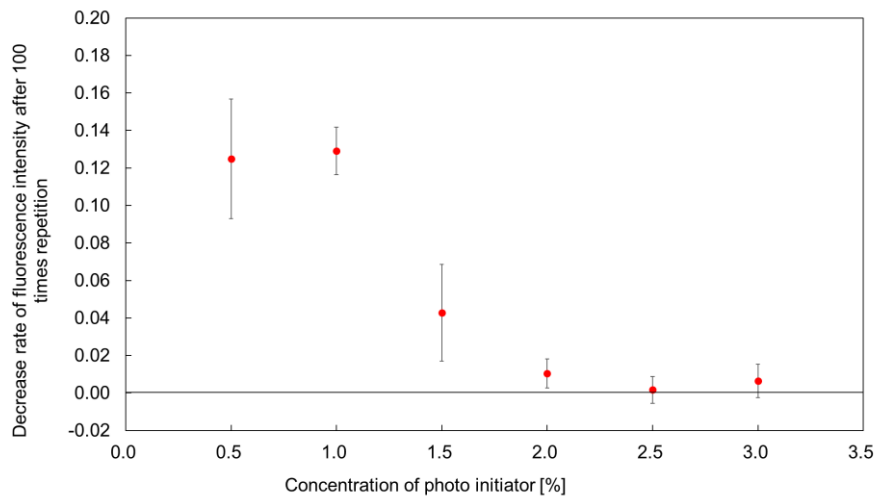
4.3.3 Effect of photo initiator concentration on photobleaching compensation

Figure 4.7(a) shows the relationship between the variation of fluorescence intensity and the concentration of photo initiator. For this investigation the excitation and interval times were set at 1 s and 6 s, respectively. The temperature was maintained at 25°C throughout the experiments. Each point in the figure shows the average value for 10 hydrogel fluorescence microsensors with different concentrations of photo initiator. Hydrogel fluorescence microsensors with less than 1.5 % photo initiator did not recover well. In contrast, hydrogel fluorescence microsensors with more than 2% photo initiator exhibited clear recovery from photobleaching (Figure 4.7(b)). The effect of the concentration of photo initiator on the diffusion coefficient of Rhodamine B in PEGDA 575 hydrogel has been reported previously [226]. The findings of the study indicated that the higher the concentration of photo initiator, the higher the diffusion coefficient of Rhodamine B in the PEGDA 575 hydrogel. Based on reference [226], a

concentration of photo initiator is considered influential for the recovery of fluorescence in the fluorescence microsensor.



(a)



(b)

Figure 4.7 : Evaluation of the effect of photo initiator concentration on photobleaching compensation.

(a) Comparison of the relative fluorescence intensity variation of hydrogel fluorescence microsensors with various concentrations of photo initiator. (b) Relationship between the photo initiator concentration and the fluorescence intensity decrease rate after 100 measurements.

4.3.4 Effect of sensor size on fluorescence intensity recovery

Figure 4.8 shows the relationship between the relative fluorescence intensity recovery and the size of the hydrogel fluorescence microsensor with 9% PEGDA 575. The concentration of Omnirad 1173 was 3.0%. The diameter

of the hydrogel fluorescence microsensors investigated was 5, 10, 20, 30, 40, and 50 μm . The exposure time and interval time were set at 1 s and 9 s, respectively. The temperature was maintained at 25°C throughout the experiments. Each measurement was repeated 900 times. Each point shows the averaged value and standard deviation of the relative fluorescence intensity of 5 points before and after every 100 repetitions. The decrease of fluorescence intensity after 900 repetitions for the 5 μm sensors was approximately 5%. While, the decreases in fluorescence intensity after 900 repetitions for the 10, 20, 30, 40, and 50 μm sensors were less than 3%.

The excitation area D for this experimental setup was calculated to be 4.7 μm using Equation 3.2. The fluorescent dye in the excitation area becomes non-fluorescent on irradiation. It is thought that in the proposed method the unbleached dye in the unexcited area diffuses into the excitation area, and the concentration of fluorescent dye recovers. Therefore, fluorescence microsensors larger than D (10, 20, 30, 40, and 50 μm in diameter) showed better recovery properties than the 5 μm fluorescence microsensor (similar size to D). Fluorescence microsensors larger than D exhibited a decrease in fluorescence intensity within 1% until 400 repetitions.

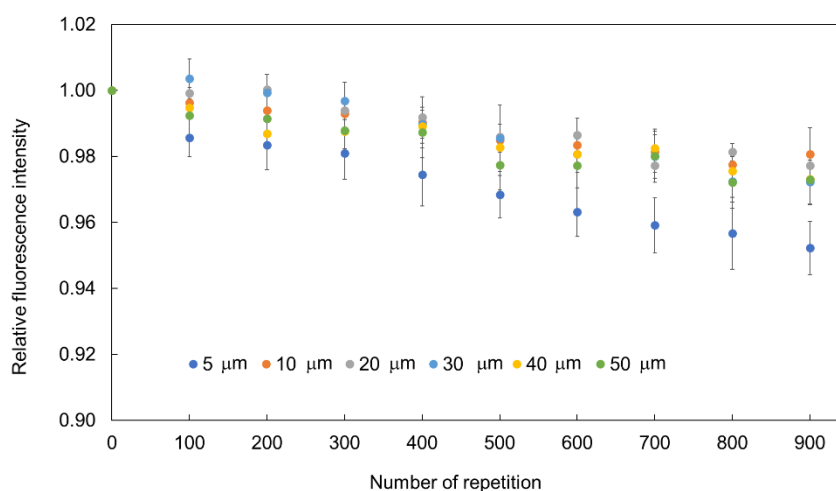


Figure 4.8 : Relationship between the recovery of relative fluorescence intensity and microsensor size.

4.3.5 Temperature measurement using hydrogel fluorescence microsensors

To demonstrate prolonged stable temperature measurement with photobleaching compensation, calibration of the hydrogel fluorescence microsensor was performed in the incubator at controlled temperatures from 36°C to 40°C in 0.5°C steps. The hydrogel fluorescence microsensors were attached to the bottom of a glass bottom dish. The fluorescence intensities of the microsensors were then measured at each temperature in the glass bottom dish filled with 2 mL of deionized water. The temperature of the deionized water was monitored by thermopile and controlled automatically. Figure 4.9 shows the calibration result of the relative fluorescence intensity based on the fluorescence intensity at 36°C. The horizontal axis shows the temperature measured by the thermopile and the vertical axis shows the relative fluorescence intensity based on the fluorescence intensity at 36°C. The relative fluorescence intensity of the hydrogel fluorescence microsensor showed a continual decrease with increasing temperature. The temperature sensitivity of the hydrogel fluorescence microsensor was calculated using the least-squares method. From these calibration results and linear fitting, the temperature sensitivity and standard deviation of temperature measurement were calculated to be $-1.4 \text{ %/}^\circ\text{C}$ and $\pm 0.5^\circ\text{C}$, respectively, as shown in Equation 4.3 [74].

$$\frac{I}{I_0} = -0.014 \cdot \text{Temp.} + 1.5 \quad (4.3)$$

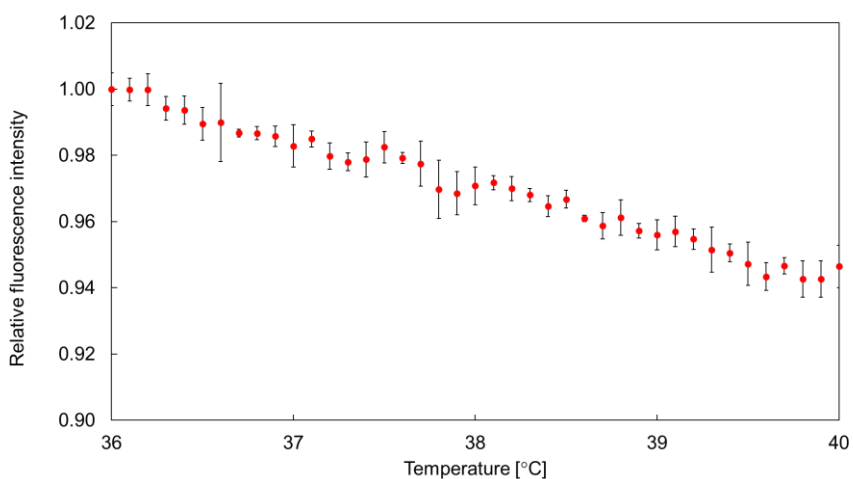


Figure 4.9 : Calibration of the relative fluorescence intensity with temperature.

Figure 4.10 shows the experimental result for temperature measurement in the deionized water in the glass bottom dish during temperature variation. The horizontal axis shows the elapsed time, while the vertical axis shows the temperature measured using the hydrogel fluorescence microsensor and the thermopile. The exposure and interval times were set to 1 s and 19 s, respectively. The total number of measurement repetitions using the hydrogel fluorescence measurement was 270, and the duration of the measurements was 5,400 s. The temperature of the water in the glass bottom dish was varied from 36°C to 40°C using the temperature controller. In Figure 8, the black points represent the temperature measured by the thermopile. The red points represent the temperature measured using the hydrogel fluorescence microsensor. The results show that the measured temperature values of the hydrogel fluorescence microsensor and thermopile exhibited good agreement. The maximum difference and standard deviation of the difference of the measured temperature between the sensors were 0.8°C and 0.3°C, respectively. These findings confirmed the effectiveness of photobleaching compensation for stable long-term fluorescence measurement.

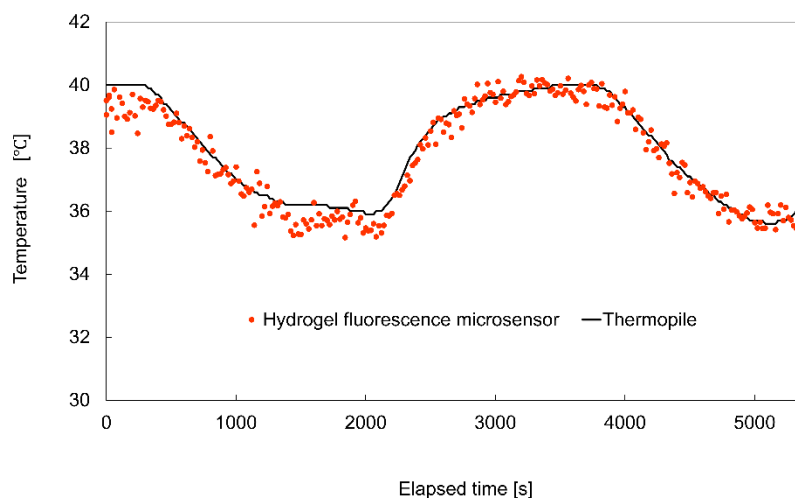


Figure 4.10 : Comparison of the temperatures measured by the hydrogel fluorescence microsensor with photobleaching compensation and a thermopile.

4.4 Discussion

In photobleaching compensation of hydrogel fluorescence microsensors, the diffusivity of the fluorescent dye inside the hydrogel, the time for diffusion of the fluorescent dye, and the stability of the fluorescence intensity are critical parameters. The diffusivity of fluorescent dyes is affected by the materials and composition of the microsensors. Rhodamine B was unable to diffuse inside the polystyrene microbeads in deionized water since the density of the crosslinks in the microbeads is high. As a result, no fluorescence recovery was observed for the polystyrene microbeads. For the hydrogel fluorescence microsensors, the difference in the concentration of the hydrogel affects the diffusion of the fluorescent dye. For the high hydrogel concentration (99% PEGDA 575), the crosslinking density of the hydrogel is high, and the mobility of the fluorescent dye is low. As a result, fluorescence recovery was not observed. In contrast, at low hydrogel concentration (9% PEGDA 575), the main component of the interior of the hydrogel microsensor is deionized water, and the mobility of the fluorescent dye is high. As a result,

fluorescence recovery was clearly observed. In addition to PEGDA 575, other hydrogel materials should be investigated and the longevity of the fluorescence microsensors in solutions such as culture medium should be evaluated as part of its future work.

The hydrogel fluorescence sensor with 9% PEGDA 575 was found not to be effective for fluorescence recovery with an interval time of 6 s when the concentration of the photo initiator was 1.5% or less. In contrast, the effectiveness of the fluorescence recovery with a 6 s interval time was confirmed at concentrations of 2.0% to 3.0%. The effect of photo initiator concentration on the diffusion properties of fluorescent dyes—other than Rhodamine B—in hydrogel materials will be considered in future work.

The time required for the diffusion of the fluorescent dye inside the hydrogel fluorescence microsensor depends on both the amount of photobleached fluorescent dye and the diffusion rate of the fluorescent dye determined by Fick's law. Photobleaching occurs as a result of the molecular structure change of the fluorescent dye from a fluorescent molecule to a non-fluorescent molecule due to the transfer of additional excitation energy to the unstable fluorescent dye during excitation. Therefore, the longer the excitation time in a single exposure is, the greater the photobleaching that occurs. To reduce photobleaching, it is useful to shorten the exposure time and reduce the fluorescence intensity. Increasing the concentration of the fluorescent dye increases the fluorescence intensity that can be achieved with short exposure times, based on the relationship in Equation 4.1. Evaluation of the influence of the exposure time, fluorescence intensity, and initial concentration of fluorescent dye will form part of the future work.

The sensitivity of fluorescence measurements of environmental parameters depends on the environmental sensitivity of the quantum yield in

each fluorescence indicator. In the case of Rhodamine B, the relationship between the relative fluorescence intensity and the temperature was calibrated as $-1.5 \text{ \%}/^{\circ}\text{C}$, as shown in Figure 4.9. If the fluorescence intensity decreases at 1% at a constant temperature, the 0.67°C temperature increase is measured by the fluorescence microsensor. This error value is similar to the precision of temperature measurement (0.5°C). The measurement error due to the variation of fluorescence intensity is therefore considered a severe limitation for detailed biological investigations.

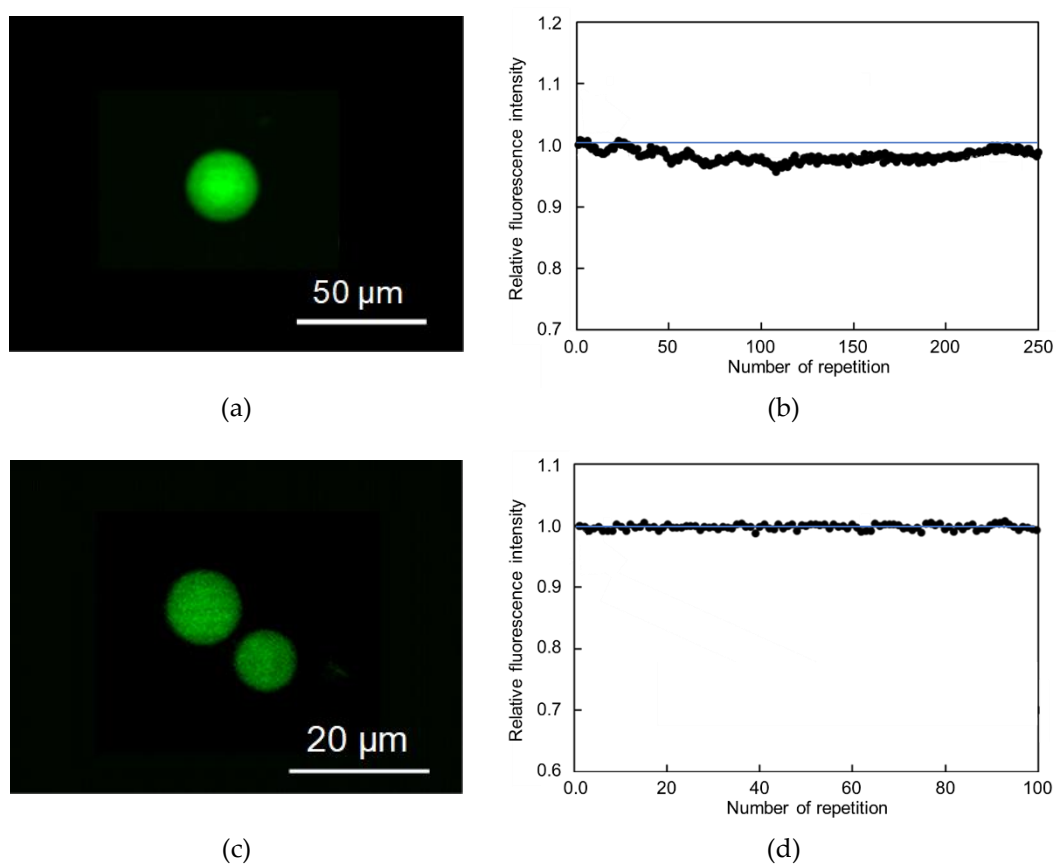


Figure 4.11 : Photobleaching compensation of hydrogel fluorescence microsensors containing FITC and $(\text{Ru}(\text{bpy})_2\text{Cl}_2)$.

(a) Fluorescence image of hydrogel fluorescence microsensor containing FITC, (b) Photobleaching compensation of hydrogel fluorescence microsensor containing FITC, (c) Fluorescence image of hydrogel fluorescence microsensor containing $(\text{Ru}(\text{bpy})_2\text{Cl}_2)$, (d) Photobleaching compensation of hydrogel fluorescence microsensor containing $(\text{Ru}(\text{bpy})_2\text{Cl}_2)$.

In addition, evaluation of photobleaching compensation using fluorescent dyes other than Rhodamine B is needed to validate the generality of the proposed method. Figure 4.11(a–b) and (c–d) show the relative fluorescence intensity of hydrogel fluorescence microsensors with an incorporated pH-sensitive fluorochrome, FITC, and an oxygen concentration sensitive fluorochrome, Tris(2,2'-bipyridyl)dichlororuthenium(II) hexahydrate ($\text{Ru}(\text{bpy})_2\text{Cl}_2$) [43,56]. The hydrogel fluorescence microsensors containing FITC and ($\text{Ru}(\text{bpy})_2\text{Cl}_2$) both showed fluorescence recovery from photobleaching. These results indicate that photobleaching compensation using a low-concentration hydrogel microsensor can be applied to various fluorescent dyes for measurements in microscale environments. Long-term stable measurement of various environment properties of cells and tissues using hydrogel fluorescence microsensors will be part of the future work.

4.5 Summary

In this work, a hydrogel fluorescence microsensor for prolonged stable temperature measurement was proposed, and the conditions for the recovery of the fluorescence intensity were evaluated. The experiments confirmed photobleaching compensation at 9% PEGDA 575. The required interval time for compensation of the hydrogel fluorescence microsensor assembled from 9% PEGDA 575 was 6 s. In addition, the degree of polymerization of the hydrogel affected the diffusivity of the fluorescent dye inside the hydrogel fluorescence microsensor. A photo initiator concentration of 2.0% or more was effective for photobleaching compensation. The stability of the fluorescence intensity depends on the size of the microsensor was confirmed.

Based on these results, temperature measurement of deionized water in a glass bottom dish in a stage-top incubator was performed using a thermocouple and hydrogel fluorescence microsensor. In repetitive measurements (total repetition: 270 times, total duration: 5,400 s), the maximum and standard deviation of measurement error between the thermocouple and hydrogel fluorescence microsensor were 0.8 °C and 0.3 °C, respectively, which confirmed the effectiveness of the hydrogel fluorescence microsensors for long-term measurement of environment parameter.

Arbitrary patterns of hydrogel fluorescence microsensors can be made on glass or polymer surfaces using photolithography. Physiological measurements of cells, tissues, and the culture environment will form part of the future work. The proposed method will make a significant contribution to the analysis of cellular responses during culture and differentiation using non-contact measurement of the cellular environment.

Chapter 5

Conclusions and Future Works

5.1 Conclusions

In this thesis, a novel fluorescent microsensor that is able to respond to temperature changes was synthesized. The microsensor was proposed to be used in (1) manipulation and injection into cell cytoplasm with short injection time and low invasive, and (2) measurements of temperature changes in hydrogel fluorescence microsensor. Based on experimental results and discussions, the main findings of this work can be summarized as follows:

In Chapter 2, a single microsensor was successfully manipulated by a micromanipulator and adhered selectively to the cell membrane via optical control of zeta potential. The success rate of pick-up and cell immobilization of the microsensor were 75% and 64%, respectively. Rapid microsensor

injection was achieved with an irradiation time approximately 1 second by applying local laser heating at 1064 nm wavelength. Cell injection and cell survival rates were 80% and 100%, respectively.

In Chapter 3, the author succeeded in the manipulation and cell injection of the fluorescence microsensor using multiple wavelength lights. The sensor made of 1 μm polystyrene particle-containing Rhodamine B and infrared (IR: 808 nm) absorbing dye. The polystyrene particle can be manipulated by 1064 nm in water since the refractive index of the polystyrene is 1.6 (refractive index of water: 1.3). Rhodamine B is a temperature-sensitive fluorescence dye (emission wavelength: 560 nm). IR absorbing dye absorbs 808 nm light but doesn't absorb 1064 nm laser. Transport of the fluorescence microsensor with optical tweezers by 1064 nm laser to the target cell. After transport to the cell membrane, the fluorescence microsensor is heated by 808 nm and injected into the cell by melting the cell membrane. The temperature increase at 808 nm (40 mW) illumination was approximately 15 $^{\circ}\text{C}$ for 10 seconds. The manipulation and injection of the microsensor to the MDCK cell by 1064 nm and 808 nm laser were demonstrated. From these results, the effectiveness of the proposed cell injection of fluorescence microsensor using multiple wavelength lights was confirmed.

In Chapter 4, a photobleaching compensation method based on the diffusion of fluorescent dye inside a hydrogel microsensor was proposed. The factors that influence compensation in the hydrogel microsensor system are the interval time between measurements, material, the concentration of photo initiator, and the composition of the fluorescence microsensor. These factors were evaluated by comparing a polystyrene fluorescence microsensor and a hydrogel fluorescence microsensor, both with diameters of 20 μm . The hydrogel fluorescence microsensor made from 9% PEGDA 575 and 2% photo

initiator showed excellent fluorescence intensity stability after exposure (standard deviation of difference from initial fluorescence after 100 measurement repetitions: within 1%). The effect of microsensor size on the stability of the fluorescence intensity was also evaluated. The hydrogel fluorescence microsensors showed a small decrease in fluorescence intensity, within 3%, after 900 measurement repetitions. The temperature of deionized water in a microchamber was measured for 5,400 s using both a thermopile and the hydrogel fluorescence microsensor. The results showed that the maximum error and standard deviation of error between these two sensors were 0.5 °C and 0.3 °C, respectively, confirming the effectiveness of the proposed method.

Overall, the fabrication of microsensor was realized by introducing several indicators to micro-nanoparticles and hence manipulation of microsensor was enhanced by optically control of zeta potential. Rapid injection of a single microsensor without damage to the cell also realized by applying optical heating. Fabrication of hydrogel fluorescence microsensor with fluorescence recovery was also evaluated for prolonged temperature measurements. In conclusion, the proposed methods allow the manipulation and cell injection of a single microsensor to be used as a carrier for intracellular and extracellular measurement, especially in biological and biomedical applications such as drug delivery and cancer diagnosis.

5.2 Future Works

The future works are briefly described in the following paragraph.

5.2.1 Microsensor manipulation in the cell cytoplasm

The author succeeded in the injection of a single microsensor in the cell cytoplasm. Therefore, the manipulation of the injected nanoparticle in the cell cytoplasm is expected can be done by optical control such as optical tweezers. Optical tweezers can be used to trap and transfer specific nanoparticles to the target location inside the cell such as the cell organelles including a nucleus, mitochondria, and others. Therefore, intracellular measurement is possible to be explored. For example, the manipulated microsensor can be used to investigate the temperature and pH values between different organelles on a cell membrane, inside the cell cytoplasm and nucleus. It was suggested that the difference in temperature among organs was influenced by intracellular cell activities. The research will benefit in the development of new medicine and drug delivery therapy in cancer and viral diseases.

5.2.2 Microsensor application in intracellular measurement

Liu *et al.* achieved a pH measurement of an influenza virus-infected cell on the cell membrane using a fluorescence microsensor [190]. However, the intracellular measurement was not achieved since the rapid injection of the selected microsensor into a specific cell was still too difficult. The currently proposed method allowing injection of a fluorescence microsensor will be a breakthrough for single-cell analyses, such as pH and temperature measurements, inside virus-infected cells.

5.2.3 Multi-fluorescence microsensor for intracellular measurement

In living cells, the environmental conditions such as ionic strength [227], pH [228,229], protein concentration, and viscosity [230,231] are not constant in space and time. In particular, temperature plays an important role in many

cellular events and thus has interactions between cell state and cellular functions [27]. The intracellular pH modulates the function of many organelles and has a relationship in physiological and pathological processes [40,232]. For example, Liu *et al.* designed a novel multi-fluorescent microsensor that can respond to both pH and temperature variations in micro-environments [43]. Therefore, measurement such critical multi-information can provide useful knowledge on cell activities which beneficial in biological and biomedical applications.

BIBLIOGRAPHY

1. de Souza, N. Supplement on single-cell analysis. *Nat. Methods Suppl.* **2011**, *8*.
2. Sweedler, J. V.; Arriaga, E.A. Single cell analysis. *Anal. Bioanal. Chem.* **2007**, *387*, 1–2.
3. Wong, F.K.; Haffner, C.; Huttner, W.B.; Taverna, E. Microinjection of membrane-impermeable molecules into single neural stem cells in brain tissue. *Nat. Protoc.* **2014**, *9*, 1170–1182.
4. Ertl, P.; Sticker, D.; Charwat, V.; Kasper, C.; Lepperdinger, G. Lab-on-a-chip technologies for stem cell analysis. *Trends Biotechnol.* **2014**, *32*, 245–253.
5. Yu, M.; Stott, S.; Toner, M.; Maheswaran, S.; Haber, D. a Circulating tumor cells: approaches to isolation and characterization. *J. Cell Biol.* **2011**, *192*, 373–382.
6. Ning, L.; Liu, G.; Li, G.; Hou, Y.; Tong, Y.; He, J. Current challenges in the bioinformatics of single cell genomics. *Front. Oncol.* **2014**, *4*, 1–7.
7. Macaulay, I.C.; Voet, T. Single cell genomics: Advances and future perspectives. *PLoS Genet.* **2014**, *10*, e1004126.
8. Saadatpour, A.; Lai, S.; Guo, G.; Yuan, G.-C. Single-cell analysis in cancer genomics. *Trends Genet.* **2015**, *31*, 576–586.
9. Wang, D.; Bodovitz, S. Single cell analysis: The new frontier in “omics.” *Trends Biotechnol.* **2010**, *28*, 281–290.
10. Polonsky, M.; Zaretsky, I.; Friedman, N. Dynamic single-cell measurements of gene expression in primary lymphocytes:

- Challenges, tools and prospects. *Brief. Funct. Genomics* **2013**, *12*, 99–108.
11. Lindstrom, S.; Andersson-Svahn, H. Single-cell analysis - Method and protocols. In *Methods in Molecular Biology*; Humana Press - Springer Verlag, 2012; Vol. 853, p. 248 ISBN 9781617795664.
 12. Takei, Y.; Arai, S.; Murata, A.; Takabayashi, M.; Oyama, K.; Ishiwata, S.; Takeoka, S.; Suzuki, M. A nanoparticle-based ratiometric and self-calibrated fluorescent thermometer for single living cells. *ACS Nano* **2014**, *8*, 198–206.
 13. Carlo, D. Di; Lee, L.P. Dynamic single-cell analysis for quantitative biology. *Anal. Chem.* **2006**, *78*, 7918–7925.
 14. Ishii, S.; Tago, K.; Senoo, K. Single-cell analysis and isolation for microbiology and biotechnology: Methods and applications. *Appl. Microbiol. Biotechnol.* **2010**, *86*, 1281–1292.
 15. Ishøy, T.; Kvist, T.; Westermann, P.; Ahring, B.K. An improved method for single cell isolation of prokaryotes from meso-, thermo- and hyperthermophilic environments using micromanipulation. *Appl. Microbiol. Biotechnol.* **2006**, *69*, 510–514.
 16. Kubo, K.; Ichikawa, M.; Yoshikawa, K.; Koyama, Y.; Niidome, T.; Yamaoka, T.; Nomura, S.I.M. Optically driven transport into a living cell. *Appl. Phys. Lett.* **2003**, *83*, 2468–2470.
 17. Kutsch, O.; Benveniste, E.N.; Shaw, G.M.; Levy, D.N. Direct and quantitative single-cell analysis of human immunodeficiency virus type 1 reactivation from latency. *J. Virol.* **2002**, *76*, 8776–8786.
 18. Ramsköld, D.; Luo, S.; Wang, Y.-C.; Li, R.; Deng, Q.; Faridani, O.R.; Daniels, G.A.; Khrebtukova, I.; Loring, J.F.; Laurent, L.C.; et al. Full-length mRNA-Seq from single cell levels of RNA and individual circulating tumor cells. *Nat. Biotechnol.* **2012**, *30*, 777–782.

19. Zare, R.N.; Kim, S. Microfluidic platforms for single-cell analysis. *Annu. Rev. Biomed. Eng.* **2010**, *12*, 187–201.
20. Yin, H.; Marshall, D. Microfluidics for single cell analysis. *Curr. Opin. Biotechnol.* **2012**, *23*, 110–119.
21. Zhu, J.; Paul, W.E. Heterogeneity and plasticity of T helper cells. *Cell Res.* **2010**, *20*, 4–12.
22. Torchilin, V.P. Multifunctional, stimuli-sensitive nanoparticulate systems for drug delivery. *Nat. Rev. Drug Discov.* **2014**, *13*, 813–827.
23. Ciampor, F.; Thompson, C.A.; Grambas, S.; Hay, A.J. Regulation of pH by the M2 protein of influenza A viruses. *Virus Res.* **1992**, *22*, 247–258.
24. Leonardi, A.; Doan, S.; Fauquert, J.L.; Bozkurt, B.; Allegri, P.; Marmouz, F.; Rondon, C.; Jedrzejczak, M.; Hellings, P.; Delgado, L.; et al. Diagnostic tools in ocular allergy. *Allergy Eur. J. Allergy Clin. Immunol.* **2017**, *72*, 1485–1498.
25. Choe, J.Y.; Kim, J.; Han, H. Simple molecular diagnostic tools in clinical medicine. *J. Clin. Diagnosis Res.* **2017**, *5*, 5–7.
26. Zitvogel, L.; Ma, Y.; Raoult, D.; Kroemer, G.; Gajewski, T.F. The microbiome in cancer immunotherapy: Diagnostic tools and therapeutic strategies. *Science (80-.).* **2018**, *359*, 1366–1370.
27. Okabe, K.; Inada, N.; Gota, C.; Harada, Y.; Funatsu, T.; Uchiyama, S. Intracellular temperature mapping with a fluorescent polymeric thermometer and fluorescence lifetime imaging microscopy. *Nat. Commun.* **2012**, *3*, 1–9.
28. Staudinger, C.; Borisov, S.M. Long-wavelength analyte-sensitive luminescent probes and optical (bio)sensors. *Methods Appl. Fluoresc.* **2015**, *3*.
29. Howard, R.; Scheiner, A.; Cunningham, J.; Gatenby, R. Cytoplasmic

- convection currents and intracellular temperature gradients. *PLoS Comput. Biol.* **2019**, *15*, e1007372.
30. Macairan, J.R.; Jaunky, D.B.; Piekny, A.; Naccache, R. Intracellular ratiometric temperature sensing using fluorescent carbon dots. *Nanoscale Adv.* **2019**, *1*, 105–113.
 31. Stasic, A.J.; Chasen, N.M.; Dykes, E.J.; Vella, S.A.; Asady, B.; Starai, V.J.; Moreno, S.N.J. The toxoplasma vacuolar H⁺-ATPase regulates intracellular pH and impacts the maturation of essential secretory proteins. *Cell Rep.* **2019**, *27*, 2132-2146.e7.
 32. Fan, Y.T.; Zhou, T.J.; Cui, P.F.; He, Y.J.; Chang, X.; Xing, L.; Jiang, H.L. Modulation of intracellular oxygen pressure by dual-drug nanoparticles to enhance photodynamic therapy. *Adv. Funct. Mater.* **2019**, *29*, 1–12.
 33. Harrison, R.P.; Chauhan, V.M.; Onion, D.; Aylott, J.W.; Sottile, V. Intracellular processing of silica-coated superparamagnetic iron nanoparticles in human mesenchymal stem cells. *RSC Adv.* **2019**, *9*, 3176–3184.
 34. Lian, Y.; Zhang, W.; Ding, L.; Zhang, X.; Zhang, Y.; Wang, X. Nanomaterials for intracellular pH sensing and imaging. *Nov. Nanomater. Biomed. Environ. Energy Appl.* **2019**, 241–273.
 35. Kucerova, P.; Cervinkova, M. Spontaneous regression of tumour and the role of microbial infection - possibilities for cancer treatment. *Anticancer. Drugs* **2016**, *27*, 269–277.
 36. Bai, T.; Gu, N. Micro/nanoscale thermometry for cellular thermal sensing. *Small* **2016**, *12*, 4590–4610.
 37. Shen, Y.; Liang, L.; Zhang, J.; Li, Z.; Yue, J.; Wang, J.; Xu, W.; Shi, W.; Xu, S. Interference-free surface-enhanced Raman scattering

- nanosensor for imaging and dynamic monitoring of reactive oxygen species in mitochondria during photothermal therapy. *Sensors Actuators, B Chem.* **2019**, *285*, 84–91.
38. Derieppe, M.; Bos, C.; De Greef, M.; Moonen, C.; Denis De Senneville, B. Correction for photobleaching in dynamic fluorescence microscopy: application in the assessment of pharmacokinetic parameters in ultrasound-mediated drug delivery. *Phys. Med. Biol.* **2015**, *61*, 588–600.
 39. Himms-Hagen, J. Cellular thermogenesis. *Annu. Rev. Physiol.* **1976**, *38*, 315–351.
 40. Moore, L.L.; Bostick, D.A.; Garry, R.F. Sindbis virus infection decreases intracellular pH: Alkaline medium inhibits processing of sindbis virus polyproteins. *Virology* **1988**, *166*, 1–9.
 41. Donner, J.S.; Thompson, S.A.; Kreuzer, M.P.; Baffou, G.; Quidant, R. Mapping intracellular temperature using green fluorescent protein. *Nano Lett.* **2012**, *12*, 2107–2111.
 42. Yang, J.M.; Yang, H.; Lin, L. Quantum dot nano thermometers reveal heterogeneous local thermogenesis in living cells. *ACS Nano* **2011**, *5*, 5067–5071.
 43. Liu, H.; Maruyama, H.; Masuda, T.; Honda, A.; Arai, F. Multi-fluorescent micro-sensor for accurate measurement of pH and temperature variations in micro-environments. *Sensors Actuators B Chem.* **2014**, *203*, 54–62.
 44. LaVan, D.A.; McGuire, T.; Langer, R. Small-scale systems for in vivo drug delivery. *Nat. Biotechnol.* **2003**, *21*, 1184–1191.
 45. Orellana, G. Luminescent optical sensors. *Anal. Bioanal. Chem.* **2004**, *379*, 344–346.
 46. Wolfbeis, O.S. Materials for fluorescence-based optical chemical

- sensors. *J. Mater. Chem.* **2005**, *15*, 2657–2669.
47. Boomer, J.A.; Inerowicz, H.D.; Zhang, Z.Y.; Bergstrand, N.; Edwards, K.; Kim, J.M.; Thompson, D.H. Acid-triggered release from sterically stabilized fusogenic liposomes via a hydrolytic DePEGylation strategy. *Langmuir* **2003**, *19*, 6408–6415.
 48. Caracciolo, G.; Pozzi, D.; Amenitsch, H.; Caminiti, R. Interaction of lipoplexes with anionic lipids resulting in DNA release is a two-stage process. *Langmuir* **2007**, *23*, 8713–8717.
 49. Chithrani, B.; Ghazani, A.; Chan, W. Determining the size and shape dependence of gold nanoparticles uptake into mammalian cells. *Nano Lett.* **2006**, *6*, 662–668.
 50. Wang, X.; Wolfbeis, O.S.; Meier, R.J. Luminescent probes and sensors for temperature. *Chem. Soc. Rev.* **2013**, *42*, 7834–7869.
 51. Wang, S.; Westcott, S.; Chen, W. Nanoparticle luminescence thermometry. *J. Phys. Chem. B* **2002**, *106*, 11203–11209.
 52. Susa, A.S.; Javier, A.M.; Parak, W.J.; Rogach, A.L. Luminescent CdTe nanocrystals as ion probes and pH sensors in aqueous solutions. *Colloids Surfaces A Physicochem. Eng. Asp.* **2006**, *281*, 40–43.
 53. Al Salman, A.; Tortschanoff, A.; Mohamed, M.B.; Tonti, D.; Van Mourik, F.; Chergui, M. Temperature effects on the spectral properties of colloidal CdSe nanodots, nanorods, and tetrapods. *Appl. Phys. Lett.* **2007**, *90*, 1–4.
 54. Borisov, S.M.; Krause, C.; Arain, S.; Wolfbeis, O.S. Composite material for simultaneous and contactless luminescent sensing and imaging of oxygen and carbon dioxide. *Adv. Mater.* **2006**, *18*, 1511–1516.
 55. Nagl, S.; Wolfbeis, O.S. Optical multiple chemical sensing: status and current challenges. *Analyst* **2007**, *132*, 507–511.

56. Maruyama, H.; Otake, T.; Arai, F. Photoprocessible hydrogel microsensor for local environment measurement on a microfluidic chip. In Proceedings of the IEEE/ASME Transactions on Mechatronics; 2011; Vol. 16, pp. 845–852.
57. Han, J.; Burgess, K. Fluorescent indicators for intracellular pH. *Am. Chem. Soc.* **2010**, *110*, 2709–2728.
58. Borisov, S.M.; Klimant, I. Optical nanosensors-smart tools in bioanalytics. *Analyst* **2008**, *133*, 1302–1307.
59. Baù, L.; Tecilla, P.; Mancin, F. Sensing with fluorescent nanoparticles. *Nanoscale* **2011**, *3*, 121–133.
60. Cao, J.; Deng, X.; Su, T.; He, B. Fabrication of polymeric nanoparticles for cancer therapy and intracellular tracing. *Nanomedicine Nanotechnology, Biol. Med.* **2016**, *12*, 449–575.
61. Bradley, M.; Alexander, L.; Duncan, K.; Chennaoui, M.; Jones, A.C.; Sánchez-Martín, R.M. pH sensing in living cells using fluorescent microspheres. *Bioorg. Med. Chem. Lett.* **2008**, *18*, 313–317.
62. Oyama, K.; Takabayashi, M.; Takei, Y.; Arai, S.; Takeoka, S.; Ishiwata, S.; Suzuki, M. Walking nanothermometers: spatiotemporal temperature measurement of transported acidic organelles in single living cells. *Lab Chip* **2012**, *12*, 1591–1593.
63. Troutman, T.S.; Leung, S.J.; Romanowski, M. Light-induced content release from plasmon resonant liposomes. *Adv. Mater.* **2009**, *21*, 2334–2338.
64. Al-Jamal, W.T.; Kostarelos, K. Liposomes: From a clinically established drug delivery system to a nanoparticle platform for theranostic nanomedicine. *Acc. Chem. Res.* **2011**, *44*, 1094–1104.
65. Mc Namara, K.P.; Nguyen, T.; Dumitrascu, G.; Ji, J.; Rosenzweig, N.;

- Rosenzweig, Z. Synthesis, characterization, and application of fluorescence sensing lipobeads for intracellular pH measurements. *Anal. Chem.* **2001**, *73*, 3240–3246.
66. Masuda, T.; Maruyama, H.; Honda, A.; Arai, F. Optical-controlled selective injection of liposome containing nanosensor into a specific cell. In Proceedings of the IEEE International Conference on Nanotechnology; 2012.
67. Maruyama, H.; Masuda, T.; Liu, H.J.; Arai, F. Selective and rapid cell injection of fluorescence sensor encapsulated in liposome using optical control of zeta potential and local mechanical stimulus by optical tweezers. In Proceedings of the IEEE/RSJ International Conference on Intelligent Robots and Systems; 2014; pp. 816–821.
68. Liu, H.; Maruyama, H.; Masuda, T.; Arai, F. Vibration-assisted optical injection of a single fluorescent sensor into a target cell. *Sensors Actuators B Chem.* **2015**, *220*, 40–49.
69. Zhang, L.; Gu, F.X.; Chan, J.M.; Wang, A.Z.; Langer, R.S.; Farokhzad, O.C. Teacher quality and student achievement: A review of state policy evidence. *Clin. Pharmacol. Ther.* **2008**, *83*, 761–769.
70. Oh, J.K.; Lee, D.I.; Park, J.M. Biopolymer-based microgels/nanogels for drug delivery applications. *Prog. Polym. Sci.* **2009**, *34*, 1261–1282.
71. Mao, S.; Sun, W.; Kissel, T. Chitosan-based formulations for delivery of DNA and siRNA. *Adv. Drug Deliv. Rev.* **2010**, *62*, 12–27.
72. Bhattarai, N.; Gunn, J.; Zhang, M. Chitosan-based hydrogels for controlled, localized drug delivery. *Adv. Drug Deliv. Rev.* **2010**, *62*, 83–99.
73. Maruyama, H.; Arai, F.; Fukuda, T. On-chip pH measurement using functionalized gel-microbeads positioned by optical tweezers. *Lab Chip*

- 2008, 8, 346–351.
74. Maruyama, H.; Fukuda, T.; Arai, F. Functional gel-microbead manipulated by optical tweezers for local environment measurement in microchip. *Microfluid. Nanofluidics* **2009**, 6, 383–390.
 75. Wu, W.; Zhou, S. Hybrid micro-/nanogels for optical sensing and intracellular imaging. *Nano Rev.* **2010**, 1, 1–17.
 76. Wu, W.; Shen, J.; Banerjee, P.; Zhou, S. Chitosan-based responsive hybrid nanogels for integration of optical pH-sensing, tumor cell imaging and controlled drug delivery. *Biomaterials* **2010**, 31, 8371–8381.
 77. Shen, J. Intelligent nano/microgels for cell scaffold and drug delivery system, 2014.
 78. Burns, A.; Ow, H.; Wiesner, U. Fluorescent core-shell silica nanoparticles: towards “Lab on a Particle” architectures for nanobiotechnology. *Chem. Soc. Rev.* **2006**, 35, 1028–1042.
 79. Burns, A.; Sengupta, P.; Zedayko, T.; Baird, B.; Wiesner, U. Core/shell fluorescent silica nanoparticles for chemical sensing: Towards single-particle laboratories. *Small* **2006**, 2, 723–726.
 80. Schulz, A.; McDonagh, C. Intracellular sensing and cell diagnostics using fluorescent silica nanoparticles. *Soft Matter* **2012**, 8, 2579–2585.
 81. Gallo, J.; Long, N.J.; Aboagye, E.O. Magnetic nanoparticles as contrast agents in the diagnosis and treatment of cancer. *Chem. Soc. Rev.* **2013**, 42, 7816–7833.
 82. Sarella, A.; Torti, A.; Donolato, M.; Pancaldi, M.; Vavassori, P. Two-dimensional programmable manipulation of magnetic nanoparticles on-chip. *Adv. Mater.* **2014**, 26, 2384–2390.
 83. Castro, C.M.; Ghazani, A. a; Chung, J.; Shao, H.; Issadore, D.; Yoon, T.-J.; Weissleder, R.; Lee, H. Miniaturized nuclear magnetic resonance

- platform for detection and profiling of circulating tumor cells. *Lab Chip* **2014**, *14*, 14–23.
84. Carrey, J.; Mehdaoui, B.; Respaud, M. Simple models for dynamic hysteresis loop calculations of magnetic single-domain nanoparticles : Application to magnetic hyperthermia optimization. **2011**, *083921*, 1–17.
 85. Kainz, Q.M.; Linhardt, R.; Grass, R.N.; Vilé, G.; Pérez-Ramírez, J.; Stark, W.J.; Reiser, O. Palladium nanoparticles supported on magnetic carbon-coated cobalt nanobeads: Highly active and recyclable catalysts for alkene hydrogenation. *Adv. Funct. Mater.* **2014**, *24*, 2020–2027.
 86. Tromsdorf, U.I.; Bruns, O.T.; Salmen, S.C.; Beisiegel, U.; Weller, H. A highly effective, nontoxic T1 MR contrast agent based on ultrasmall PEGylated iron oxide nanoparticles. *Nano Lett.* **2009**, *9*, 4434–4440.
 87. Giouroudi, I.; Keplinger, F. Microfluidic biosensing systems using magnetic nanoparticles. *Int. J. Mol. Sci.* **2013**, *14*, 18535–18556.
 88. Publico-Lansigan, M.H.; Hickling, W.J.; Japp, E.A.; Rodriguez, O.C.; Ghosh, A.; Albanese, C.; Nishida, M.; Van Keuren, E.; Fricke, S.; Dollahon, N.; et al. Magnetic nanobeads as potential contrast agents for magnetic resonance imaging. *ACS Nano* **2013**, *7*, 9040–9048.
 89. Zhang, Y.; Zeng, G.-M.; Tang, L.; Huang, D.-L.; Jiang, X.-Y.; Chen, Y.-N. A hydroquinone biosensor using modified core-shell magnetic nanoparticles supported on carbon paste electrode. *Biosens. Bioelectron.* **2007**, *22*, 2121–2126.
 90. Zhang, Y.; Zeng, G.-M.; Tang, L.; Li, Y.-P.; Chen, L.-J.; Pang, Y.; Li, Z.; Feng, C.-L.; Huang, G.-H. An electrochemical DNA sensor based on a layers-film construction modified electrode. *Analyst* **2011**, *136*, 4204–

4210.

91. Pankhurst, Q.A.; Connolly, J.; Jones, S.K.; Dobson, J. Applications of magnetic nanoparticles in biomedicine. *J. Phys. D. Appl. Phys.* **2003**, *36*, R167–R181.
92. Gao, J.; Gu, H.; Xu, B. Multifunctional magnetic nanoparticles: Design, synthesis, and biomedical applications. *Acc. Chem. Res.* **2009**, *42*, 1097–1107.
93. Plouffe, B.D.; Murthy, S.K.; Lewis, L.H. Fundamentals and application of magnetic particles in cell isolation and enrichment. *Rep Prog Phys.* **2015**, *78*, 1–76.
94. Xu, P.; Zeng, G.M.; Huang, D.L.; Feng, C.L.; Hu, S.; Zhao, M.H.; Lai, C.; Wei, Z.; Huang, C.; Xie, G.X.; et al. Use of iron oxide nanomaterials in wastewater treatment: A review. *Sci. Total Environ.* **2012**, *424*, 1–10.
95. Gertz, F.; Khitun, A. Biological cell manipulation by magnetic nanoparticles. *AIP Adv.* **2016**, *6*, 025308.
96. Zhong, J.; Liu, H.; Maruyama, H.; Arai, F. Optical heating of metallic nanoparticles for fast injection of nanoscale sensor into living cells. In Proceedings of the IEEE International Conference on Nanotechnology; 2015; pp. 721–723.
97. Zhong, J.; Liu, H.; Maruyama, H.; Masuda, T.; Arai, F. Continuous-wave laser-assisted injection of single magnetic nanobeads into living cells. *Sensors Actuators, B Chem.* **2016**, *230*, 298–305.
98. Shankar, P.D.; Shobana, S.; Karuppusamy, I.; Pugazhendhi, A.; Ramkumar, V.S.; Arvindnarayan, S.; Kumar, G. A review on the biosynthesis of metallic nanoparticles (gold and silver) using bio-components of microalgae: Formation mechanism and applications. *Enzyme Microb. Technol.* **2016**, *95*, 28–44.

99. Manojkumar, K.; Sivaramakrishna, A.; Vijayakrishna, K. A short review on stable metal nanoparticles using ionic liquids, supported ionic liquids, and poly(ionic liquids). *J. Nanoparticle Res.* **2016**, *18*, 1–22.
100. Zhang, H.; Liu, L.; Fu, X.; Zhu, Z. Microfluidic beads-based immunosensor for sensitive detection of cancer biomarker proteins using multienzyme-nanoparticle amplification and quantum dots labels. *Biosens. Bioelectron.* **2013**, *42*, 23–30.
101. Yue, G.; Su, S.; Li, N.; Shuai, M.; Lai, X.; Astruc, D.; Zhao, P. Gold nanoparticles as sensors in the colorimetric and fluorescence detection of chemical warfare agents. *Coord. Chem. Rev.* **2016**, *311*, 75–84.
102. Haume, K.; Rosa, S.; Grellet, S.; Śmiałek, M.A.; Butterworth, K.T.; Solov'yov, A. V.; Prise, K.M.; Golding, J.; Mason, N.J. Gold nanoparticles for cancer radiotherapy: A review. *Cancer Nanotechnol.* **2016**, *7*, 1–20.
103. Priyadarshini, E.; Pradhan, N. Gold nanoparticles as efficient sensors in colorimetric detection of toxic metal ions: A Review. *Sensors Actuators B Chem.* **2017**, *238*, 888–902.
104. Ajnai, G.; Chiu, A.; Kan, T.; Cheng, C.C.; Tsai, T.H.; Chang, J. Trends of gold nanoparticle-based drug delivery system in cancer therapy. *J. Exp. Clin. Med.* **2014**, *6*, 172–178.
105. Orsinger, G. V.; Williams, J.D.; Romanowski, M. Focal activation of cells by plasmon resonance assisted optical injection of signaling molecules. *ACS Nano* **2014**, *8*, 6151–6162.
106. Li, M.; Lohmuller, T.; Feldmann, J.; Lohmüller, T.; Feldmann, J. Optical injection of gold nanoparticles into living cells. *Nano Lett.* **2015**, *15*, 770–775.
107. Waleed, M.; Hwang, S.; Kim, J.; Shabbir, I.; Shin, S.; Lee, Y. Single-cell

- optoporation and transfection using femtosecond laser and optical tweezers. *Biomed. Opt. Express* **2013**, *4*, 2213–2217.
108. Boulais, É.; Lachaine, R.; Meunier, M. Plasma mediated off-resonance plasmonic enhanced ultrafast laser-induced nanocavitation. *Nano Lett.* **2012**, *12*, 4763–4769.
109. Hilderbrand, S.A.; Weissleder, R. Near-infrared fluorescence: application to in vivo molecular imaging. *Curr. Opin. Chem. Biol.* **2010**, *14*, 71–79.
110. Yan, L.; Zhang, J.; Lee, C.S.; Chen, X. Micro- and nanotechnologies for intracellular delivery. *Small* **2014**, *10*, 4487–4504.
111. Oh, N.; Park, J.H. Endocytosis and exocytosis of nanoparticles in mammalian cells. *Int. J. Nanomedicine* **2014**, *9*, 51–63.
112. Delgado, D.; Del Pozo-Rodríguez, A.; Solinís, M.Á.; Rodríguez-Gascón, A. Understanding the mechanism of protamine in solid lipid nanoparticle-based lipofection: The importance of the entry pathway. *Eur. J. Pharm. Biopharm.* **2011**, *79*, 495–502.
113. Shekaramiz, E.; Varadarajalu, G.; Day, P.J.; Wickramasinghe, H.K. Integrated electrowetting nanoinjector for single cell transfection. *Sci. Rep.* **2016**, *6*, 29051.
114. Ainla, A.; Xu, S.; Sanchez, N.; Jeffries, G.D.M.; Jesorka, A. Single-cell electroporation using a multifunctional pipette. *Lab Chip* **2012**, *12*, 4605–1609.
115. Kang, W.; Yavari, F.; Minary-Jolandan, M.; Giraldo-Vela, J.P.; Safi, A.; McNaughton, R.L.; Parpoil, V.; Espinosa, H.D. Nanofountain probe electroporation of single cells. *Nano Lett.* **2013**, *13*, 2448–2457.
116. Yang, F.; Zhang, M.; He, W.; Chen, P.; Cai, X.; Yang, L.; Gu, N.; Wu, J. Controlled release of Fe₃O₄ nanoparticles in encapsulated

- microbubbles to tumor cells via sonoporation and associated cellular bioeffects. *Small* **2011**, *7*, 902–910.
117. Villangca, M.; Casey, D.; Gluckstad, J. Optically-controlled platforms for transfection and single- and sub-cellular surgery. *Biophys. Rev.* **2015**, *7*, 379–390.
 118. Truschel, S.T.; Wang, E.; Ruiz, W.G.; Leung, S.-M.; Rojas, R.; Lavelle, J.; Zeidal, M.; Stoffer, D.; Apodaca, G. Stretch-regulated exocytosis/endocytosis in bladder umbrella cells. *Mol. Biol. Cell* **2002**, *13*, 830–846.
 119. Kurtz-Chalot, A.; Klein, J.P.; Pourchez, J.; Boudard, D.; Bin, V.; Sabido, O.; Marmuse, L.; Cottier, M.; Forest, V. Quantification of nanoparticle endocytosis based on double fluorescent pH-sensitive nanoparticles. *Biomed. Microdevices* **2015**, *17*, 1–12.
 120. Boulant, S.; Stanifer, M.; Lozach, P.-Y. Dynamics of virus-receptor interactions in virus binding, signaling, and endocytosis. *Viruses* **2015**, *7*, 2794–2815.
 121. Tiwari, G.; Tiwari, R.; Sriwastawa, B.; Bhati, L.; Pandey, S.; Pandey, P.; Bannerjee, S.K. Drug delivery systems: An updated review. *Int. J. Pharm. Investig.* **2012**, *2*, 2–11.
 122. Maruyama, H.; Masuda, T.; Honda, A.; Arai, F. Selective cell injection of fluorescence particle sensor encapsulated in fusogenic liposome using optical manipulation and control of surface potential using photochromic chemical. In Proceedings of the IEEE International Conference on Robotics and Automation; 2013; pp. 4421–4426.
 123. Hashim, H.; Lei, W.; Maruyama, H.; Masuda, T.; Arai, F. Optical control of adhesion property of magnetic nanosensor using photochromism for effective manipulation and cell injection. In

- Proceedings of the 16th International Conference on Nanotechnology; IEEE, 2016; pp. 683–686.
124. Maruyama, H.; Inoue, N.; Masuda, T.; Arai, F. Selective injection and laser manipulation of nanotool inside a specific cell using optical pH regulation and optical tweezers. In Proceedings of the IEEE International Conference on Robotics and Automation; 2011; pp. 2674–2679.
 125. Maruyama, H.; Masuda, T.; Arai, F. Optical control of surface potential using nanocapsule for selective injection into cell. In Proceedings of the Transducers; 2013; pp. 1127–1130.
 126. Sun, Y.; Nelson, B.J. Biological cell injection using an autonomous microrobotic system. *Int. J. Rob. Res.* **2002**, *21*, 861–868.
 127. Matsuoka, H.; Komazaki, T.; Mukai, Y.; Shibusawa, M.; Akane, H.; Chaki, A.; Uetake, N.; Saito, M. High throughput easy microinjection with a single-cell manipulation supporting robot. *J. Biotechnol.* **2005**, *116*, 185–194.
 128. Zhang, Y.; Yu, L.C. Single-cell microinjection technology in cell biology. *BioEssays* **2008**, *30*, 606–610.
 129. Shen, Y.; Fukuda, T. State of the art: micro-nanorobotic manipulation in single cell analysis. *Robot. Biomimetics* **2014**, *1*, 1–13.
 130. Malboubi, M.; Gu, Y.; Jiang, K. Surface properties of glass micropipettes and their effect on biological studies. *Nanoscale Res. Lett.* **2011**, *6*, 1–10.
 131. Xie, Y.; Sun, D.; Liu, C.; Tse, H.Y.; Cheng, S.H. A force control approach to a robot-assisted cell microinjection system. *Int. J. Rob. Res.* **2010**, *29*, 1222–1232.
 132. Huang, H.B.; Sun, D.; Mills, J.K.; Cheng, S.H. Robotic cell injection

- system with position and force control: Toward automatic batch biomanipulation. In Proceedings of the IEEE Transaction on Robotics; 2009; Vol. 25, pp. 727–737.
133. Olsson, S.B.; Getahun, M.N.; Wicher, D.; Hansson, B.S. Piezo controlled microinjection: An in vivo complement for in vitro sensory studies in insects. *J. Neurosci. Methods* **2011**, *201*, 385–389.
 134. Huang, H.; Mills, J.K.; Lu, C.; Sun, D. A universal piezo-driven ultrasonic cell microinjection system. *Biomed. Microdevices* **2011**, *13*, 743–752.
 135. Hayakawa, T.; Fukada, S.; Arai, F. Fabrication of an on-chip nanorobot integrating functional nanomaterials for single-cell punctures. *IEEE Trans. Robot.* **2014**, *30*, 59–67.
 136. Kotnik, T.; Frey, W.; Sack, M.; Haberl Meglič, S.; Peterka, M.; Miklavčič, D. Electroporation-based applications in biotechnology. *Trends Biotechnol.* **2015**, *33*, 480–488.
 137. Shintaku, H.; Hakamada, K.; Fujimoto, H.; Nagata, T.; Miyake, J.; Kawano, S. Measurement of local electric field in microdevices for low-voltage electroporation of adherent cells. *Microsyst. Technol.* **2013**, *20*, 303–313.
 138. Zheng, Y.; John, N.; Wei, Y.; Sun, Y. Recent advances in microfluidic techniques for single-cell biophysical characterization. *Lab Chip* **2013**, *13*, 2464–2483.
 139. Lin, C.Y.; Liu, T.M.; Chen, C.Y.; Huang, Y.L.; Huang, W.K.; Sun, C.K.; Chang, F.H.; Lin, W.L. Quantitative and qualitative investigation into the impact of focused ultrasound with microbubbles on the triggered release of nanoparticles from vasculature in mouse tumors. *J. Control. Release* **2010**, *146*, 291–298.

140. Theek, B.; Baues, M.; Ojha, T.; Möckel, D.; Veettil, S.K.; Steitz, J.; van Bloois, L.; Storm, G.; Kiessling, F.; Lammers, T. Sonoporation enhances liposome accumulation and penetration in tumors with low EPR. *J. Control. Release* **2015**, *231*, 77–85.
141. Mcdougall, C.; Stevenson, D.J.; Brown, C.T.A.; Gunn-moore, F.; Dholakia, K. Targeted optical injection of gold nanoparticles into single mammalian cells. *J. Biophotonics* **2009**, *743*, 736–743.
142. Stevenson, D.J.; Gunn-Moore, F.J.; Campbell, P.; Dholakia, K. Single cell optical transfection. *J. R. Soc. Interface* **2010**, *7*, 863–71.
143. Mitchell, C.A.; Kalies, S.; Cizmár, T.; Heisterkamp, A.; Torrance, L.; Roberts, A.G.; Gunn-Moore, F.J.; Dholakia, K. Femtosecond optoinjection of intact tobacco BY-2 cells using a reconfigurable photoporation platform. *PLoS One* **2013**, *8*, e79235.
144. Lee, J.; Sul, J.Y.; Eberwine, J.H. Single cell/cellular subregion-targeted phototransfection. *Cold Spring Harb. Protoc.* **2014**, 935–939.
145. Xiong, R.; Samal, S.K.; Demeester, J.; Skirtach, A.G.; De Smedt, S.C.; Braeckmans, K. Laser-assisted photoporation: fundamentals, technological advances and applications. *Adv. Phys. X* **2016**, *1*, 596–620.
146. Lyu, Z.; Zhou, F.; Liu, Q.; Xue, H.; Yu, Q.; Chen, H. Photoporation: A universal platform for macromolecular delivery into cells using gold nanoparticle layers via the photoporation effect. *Adv. Funct. Mater.* **2016**, *26*, 5787–5795.
147. Qin, Z.; Bischof, J.C. Thermophysical and biological responses of gold nanoparticle laser heating. *Chem Soc Rev* **2012**, *41*, 1191–1217.
148. Baffou, G.; Rigneault, H. Femtosecond-pulsed optical heating of gold nanoparticles. *Phys. Rev. B - Condens. Matter Mater. Phys.* **2011**, *84*, 1–13.
149. Soman, P.; Zhang, W.; Umeda, A.; Zhang, Z.J.; Chen, S. Femtosecond

- laser-assisted optoporation for drug and gene delivery into single mammalian cells. *J. Biomed. Nanotechnol.* **2011**, *7*, 334–341.
150. Tsukakoshi, M.; Kurata, S.; Nomiya, Y.; Ikawa, Y.; Kasuya, T. A novel method of DNA transfection by laser microbeam cell surgery. *Appl. Phys. B Photophysics Laser Chem.* **1984**, *35*, 135–140.
 151. Baumgart, J.; Humbert, L.; Boulais, É.; Lachaine, R.; Lebrun, J.J.; Meunier, M. Off-resonance plasmonic enhanced femtosecond laser optoporation and transfection of cancer cells. *Biomaterials* **2012**, *33*, 2345–2350.
 152. Dhakal, K.; Black, B.; Mohanty, S. Introduction of impermeable actin-staining molecules to mammalian cells by optoporation. *Sci. Rep.* **2014**, *4*, 6553.
 153. Hatano, S.; Horino, T.; Tokita, A.; Oshima, T.; Abe, J. Unusual negative photochromism via a short-lived imidazolyl radical of 1,1'-binaphthyl-bridged imidazole dimer. *J. Am. Chem. Soc.* **2013**, *135*, 3164–3172.
 154. Irie, M.; Fukaminato, T.; Matsuda, K.; Kobatake, S. Photochromism of diarylethene molecules and crystals: Memories, switches, and actuators. *Chem. Rev.* **2014**, *114*, 12174–12277.
 155. Honary, S.; Zahir, F. Effect of zeta potential on the properties of nano-drug delivery systems - A review (Part 2). *Trop. J. Pharm. Res.* **2013**, *12*, 265–273.
 156. Blundell, E.L.C.J.; Vogel, R.; Platt, M. Particle-by-particle charge analysis of DNA-modified nanoparticles using tunable resistive pulse sensing. *Langmuir* **2016**, *32*, 1082–1090.
 157. Liu, H.J.; Maruyama, H.; Masuda, T.; Honda, A.; Member, F.A. Rapid injection of fluorescence sensor into a target cell by local mechanical stimulus of optical tweezers. In Proceedings of the IEEE International

- Conference on Nanotechnology; 2014; pp. 160–163.
158. Ashkin, A. History of optical trapping and manipulation of small-neutral particle, atoms, and molecules. *IEEE J. Sel. Top. Quantum Electron.* **2000**, *6*, 841–856.
 159. Ashkin, A. Acceleration and trapping of particles by radiation pressure. *Phys. Rev. Lett.* **1970**, *24*, 156–159.
 160. Ashkin, A.; Dziedzic, J.M.; Bjorkholm, J.E.; Chu, S. Observation of a single-beam gradient force optical trap for dielectric particles. *Opt. Lett.* **1986**, *11*, 288.
 161. Neuman, K.C.; Nagy, A. Single-molecule force spectroscopy: optical tweezers, magnetic tweezers and atomic force microscopy. *Nat. Methods* **2008**, *5*, 491–505.
 162. Dholakia, K.; MacDonald, M.P.; Zemánek, P.; Cizmár, T. Cellular and colloidal separation using optical forces. In *Methods in Cell Biology*; 2007; Vol. 82, pp. 467–495 ISBN 9780123706485.
 163. Smith, R.L.; Spalding, G.C.; Dholakia, K.; MacDonald, M.P. Colloidal sorting in dynamic optical lattices. *J. Opt. A Pure Appl. Opt.* **2007**, *9*, S134–S138.
 164. Ashkin, A.; Dziedzic, J.M. Internal cell manipulation using infrared laser traps. In *Proceedings of the Proceedings of the National Academy of Sciences*; 1989; Vol. 86, pp. 7914–7918.
 165. Ashkin, A.; Dziedzic, J.M. Optical trapping and manipulation of viruses and bacteria. *Science (80-.)*. **1987**, *235*, 1517–1520.
 166. Sparkes, I.A.; Ketelaar, T.; de Ruijter, N.C.A.; Hawes, C. Grab a golgi: Laser trapping of golgi bodies reveals in vivo interactions with the endoplasmic reticulum. *Traffic* **2009**, *10*, 567–571.
 167. Grier, D.G. A revolution in optical manipulation. *Nature* **2003**, *424*,

810–816.

168. Zhong, M.-C.; Wei, X.-B.; Zhou, J.-H.; Wang, Z.-Q.; Li, Y.-M. Trapping red blood cells in living animals using optical tweezers. *Nat. Commun.* **2013**, *4*, 1–7.
169. Li, X.; Cheah, C.C.; Hu, S.; Sun, D. Dynamic trapping and manipulation of biological cells with optical tweezers. *Automatica* **2013**, *49*, 1614–1625.
170. Heller, I.; Hoekstra, T.P.; King, G.A.; Peterman, E.J.G.; Wuite, G.J.L. Optical tweezers analysis of DNA – protein complexes. *Chem. Rev.* **2014**, *114*, 3087–3119.
171. Gao, H.; Metz, J.; Teanby, N.A.; Ward, A.D.; Botchway, S.W.; Coles, B.; Pollard, M.; Sparkes, I. In vivo quantification of peroxisome tethering to chloroplasts in tobacco epidermal cells using optical tweezers. *Plant Physiol.* **2016**, *170*, 263–272.
172. Chung, Y.C.; Chen, P.W.; Fu, C.M.; Jheng, J.H. Particles sorting in micro-channel using magnetic tweezers and optical tweezers. *J. Magn. Magn. Mater.* **2013**, *333*, 87–92.
173. Wu, Y.; Sun, D.; Huang, W.; Xi, N. Dynamics analysis and motion planning for automated cell transportation with optical tweezers. In Proceedings of the IEEE/ASME Transactions on Mechatronics; 2013; Vol. 18, pp. 706–713.
174. Sugiura, T.; Miyoshi, H.; Nishio, T.; Honda, A. Cell palpation with an optically trapped particle. *J. Micro-Nano Mechatronics* **2012**, *7*, 131–136.
175. Ashkin, A.; Dziedzic, J.M.; Yamane, T. Optical trapping and manipulation of single cells using infrared laser beams. *Nature* **1987**, *330*, 769–771.
176. Arai, F.; Yoshikawa, K.; Sakami, T.; Fukuda, T. Synchronized laser

- micromanipulation of multiple targets along each trajectory by single laser. *Appl. Phys. Lett.* **2004**, *85*, 4301–4303.
177. Onda, K.; Arai, F. Multi-beam bilateral teleoperation of holographic optical tweezers. *Opt. Express* **2012**, *20*, 3633–3641.
 178. Godley, B.F.; Shamsi, F.A.; Liang, F.-Q.; Jarrett, S.G.; Davies, S.; Boulton, M. Blue light induces mitochondrial DNA damage and free radical production in epithelial cells. *J. Biol. Chem.* **2005**, *280*, 21061–21066.
 179. Urban, A.S.; Pfeiffer, T.; Fedoruk, M.; Lutich, A.A.; Feldmann, J. Single-step injection of gold nanoparticles through phospholipid membranes. *ACS Nano* **2011**, *5*, 3585–3590.
 180. Chen, X.; Kis, A.; Zettl, A.; Bertozzi, C.R. A cell nanoinjector based on carbon nanotubes. *Proc. Natl. Acad. Sci. U. S. A.* **2007**, *104*, 8218–8222.
 181. Arai, F.; Ng, C.; Maruyama, H.; Ichikawa, A.; El-Shimy, H.; Fukuda, T. On chip single-cell separation and immobilization using optical tweezers and thermosensitive hydrogel. *Lab Chip* **2005**, *5*, 1399–1403.
 182. De Vlaminck, I.; Dekker, C. Recent advances in magnetic tweezers. *Annu. Rev. Biophys.* **2012**, *41*, 453–472.
 183. de Vries, A.H.B.; Krenn, B.E.; van Driel, R.; Kanger, J.S. Micro magnetic tweezers for nanomanipulation inside live cells. *Biophys. J.* **2005**, *88*, 2137–2144.
 184. Blonder, R.; Katz, E.; Willner, I.; Wray, V.; Bückmann, A.F. Application of a nitrospiropyran-FAD-reconstituted glucose oxidase and charged electron mediators as optobioelectronic assemblies for the amperometric transduction of recorded optical signals: Control of the “on’-’off” direction of the photoswitch. *J. Am. Chem. Soc.* **1997**, *119*, 11747–11757.

185. Vasiliadou, I.A.; Chrysikopoulos, C. V. Cotransport of *Pseudomonas putida* and kaolinite particles through water-saturated columns packed with glass beads. *Water Resour. Res.* **2011**, *47*, 1–14.
186. Paulmichl, M.; Friedrich, F.; Wöll, E.; Weiss, H.; Lang, F. Effects of serotonin on electrical properties of Madin-Darby canine kidney cells. *Pflügers Arch. Eur. J. Physiol.* **1988**, *411*, 394–400.
187. Edahiro, J.I.; Sumaru, K.; Tada, Y.; Ohi, K.; Takagi, T.; Kameda, M.; Shinbo, T.; Kanamori, T.; Yoshimi, Y. In situ control of cell adhesion using photoresponsive culture surface. *Biomacromolecules* **2005**, *6*, 970–974.
188. Yamada, A.; Yamanaka, T.; Hamada, T.; Hase, M.; Yoshikawa, K.; Baigl, D. Spontaneous transfer of phospholipid-coated oil-in-oil and water-in-oil micro-droplets through an oil/water interface. *Langmuir* **2006**, *22*, 9824–9828.
189. Peterman, E.J.G.; Gittes, F.; Schmidt, C.F. Laser-induced heating in optical traps. *Biophys. J.* **2003**, *84*, 1308–1316.
190. Liu, H.; Maruyama, H.; Masuda, T.; Honda, A.; Arai, F. The influence of virus infection on the extracellular pH of the host cell detected on cell membrane. *Front. Microbiol.* **2016**, *7*, 1–8.
191. Stewart, M.P.; Langer, R.; Jensen, K.F. Intracellular delivery by membrane disruption: Mechanisms, strategies, and concepts. *Chem. Rev.* **2018**, *118*, 7409–7531.
192. Maruyama, H.; Kimura, T.; Liu, H.; Ohtsuki, S.; Miyake, Y.; Isogai, M.; Arai, F.; Honda, A. Influenza virus replication raises the temperature of cells. *Virus Res.* **2018**, *257*, 94–101.
193. Mandal, K.; Asnacios, A.; Goud, B.; Manneville, J.B. Erratum: Mapping intracellular mechanics on micropatterned substrates. *Proc. Natl. Acad.*

- Sci. U. S. A.* **2018**, *115*, E6384.
194. Onal, C.D.; Ozcan, O.; Sitti, M. Automated 2-D nanoparticle manipulation using atomic force microscopy. In Proceedings of the IEEE Transactions on Nanotechnology; 2011; Vol. 10, pp. 472–481.
 195. Liu, H.; Wen, J.; Xiao, Y.; Liu, J.; Hopyan, S.; Radisic, M.; Simmons, C.A.; Sun, Y. In situ mechanical characterization of the cell nucleus by atomic force microscopy. *ACS Nano* **2014**, *8*, 3821–3828.
 196. Langan, L.M.; Dodd, N.J.F.; Owen, S.F.; Purcell, W.M.; Jackson, S.K.; Jha, A.N. Correction: Direct measurements of oxygen gradients in spheroid culture system using electron paramagnetic resonance oximetry. *PLoS One* **2016**, *11*, 1–13.
 197. Mizutani, Y.; Otani, Y.; Umeda, N. Micromanipulators comprising optical fiber cantilevers. *Int. J. Optomechatronics* **2009**, *3*, 18–29.
 198. Hochmuth, R.M. Micropipette aspiration of living cells. *J. Biomech.* **2000**, *33*, 15–22.
 199. Zhang, X.; Leung, C.; Lu, Z.; Esfandiari, N.; Casper, R.F.; Sun, Y. Controlled aspiration and positioning of biological cells in a micropipette. In Proceedings of the IEEE Transaction on Biomedical Engineering; 2012; Vol. 59, pp. 1032–1040.
 200. Hunt, T.P.; Westervelt, R.M. Dielectrophoresis tweezers for single cell manipulation. *Biomed. Microdevices* **2006**, *8*, 227–230.
 201. Kilinc, D.; Lee, G.U. Advances in magnetic tweezers for single molecule and cell biophysics. *Integr. Biol.* **2014**, *6*, 27–34.
 202. Wang, X.; Ho, C.; Tsatskis, Y.; Law, J.; Zhang, Z.; Zhu, M.; Dai, C.; Wang, F.; Tan, M.; Hopyan, S.; et al. Intracellular manipulation and measurement with multipole magnetic tweezers. *Sci. Robot.* **2019**, *4*, eaav6180.

203. Du, X.; Wang, J.; Zhou, Q.; Zhang, L.; Wang, S.; Zhang, Z.; Yao, C. Advanced physical techniques for gene delivery based on membrane perforation. *Drug Deliv.* **2018**, *25*, 1516–1525.
204. Hashim, H.; Maruyama, H.; Masuda, T.; Arai, F. Manipulation and immobilization of a single fluorescence nanosensor for selective injection into cells. *Sensors* **2016**, *16*, 1–10.
205. Sakakibara, J.; Hishida, K.; Maeda, M. Measurements of thermally stratified pipe flow using image-processing techniques. *Exp. Fluids* **1993**, *16*, 82–96.
206. Masuda, T.; Maruyama, H.; Arai, F.; Anada, T.; Tsuchiya, K.; Fukuda, T.; Suzuki, O. Application of an indicator-immobilized-gel-sheet for measuring the pH surrounding a calcium phosphate-based biomaterial. *J. Biomater. Appl.* **2017**, *31*, 1296–1304.
207. Aoki, H.; Mogi, C.; Hisada, T.; Nakakura, T.; Kamide, Y.; Ichimonji, I.; Tomura, H.; Tobo, M.; Sato, K.; Tsurumaki, H.; et al. Proton-sensing ovarian cancer G protein-coupled receptor 1 on dendritic cells is required for airway responses in a murine asthma model. *PLoS One* **2013**, *8*, 1–14.
208. Bennet, M.A.; Richardson, P.R.; Arlt, J.; McCarthy, A.; Buller, G.S.; Jones, A.C. Optically trapped microsensors for microfluidic temperature measurement by fluorescence lifetime imaging microscopy. *Lab Chip* **2011**, *11*, 3821–3828.
209. Paviolo, C.; Clayton, A.H.A.; Mcarthur, S.L.; Stoddart, P.R. Temperature measurement in the microscopic regime: A comparison between fluorescence lifetime- and intensity-based methods. *J. Microsc.* **2013**, *250*, 179–188.
210. Amao, Y. Probes and polymers for optical sensing of oxygen.

- Microchim. Acta* **2003**, *143*, 1–12.
211. Maruyama, H.; Kito, M.; Arai, F. Fluorescence sensor array for non-contact measurement of oxygen consumption rate of single oocyte on a microfluidic chip. *IEEE Int. Conf. Robot. Autom.* **2015**, 3495–3500.
 212. Wang, X.D.; Wolfbeis, O.S. Optical methods for sensing and imaging oxygen: Materials, spectroscopies and applications. *Chem. Soc. Rev.* **2014**, *43*, 3666–3761.
 213. Quaranta, M.; Borisov, S.M.; Klimant, I. Indicators for optical oxygen sensors. *Bioanal. Rev.* **2012**, *4*, 115–157.
 214. Arppe, R.; Näreoja, T.; Nylund, S.; Mattsson, L.; Koho, S.; Rosenholm, J.M.; Soukka, T.; Schäferling, M. Photon upconversion sensitized nanoprobe for sensing and imaging of pH. *Nanoscale* **2014**, *6*, 6837–6843.
 215. Sasaki, K.; Shi, Z.-Y.; Kopelman, R.; Masuhara, H. Three-dimensional pH microprobing with an optically-manipulated fluorescent particle. *Chem. Lett.* **1996**, *25*, 141–142.
 216. Carullo, P.; Chino, M.; Paolo, G.; Terreri, S.; Lombardi, A.; Manco, G.; Cimmino, A.; Febbraio, F. Direct detection of organophosphate compounds in water by a fluorescence-based biosensing device. *Sensors Actuators B Chem.* **2018**, *255*, 3257–3266.
 217. Zhao, Y.; Pang, C.; Wen, Z.; Liu, Y.; Qiao, X.; Yang, Z.; Raghavan, N.; Zhao, Y.; Yang, Q. A microfiber temperature sensor based on fluorescence lifetime. *Opt. Commun.* **2018**, *426*, 231–236.
 218. Berezin, M.Y.; Achilefu, S. Fluorescence lifetime measurements and biological imaging. *Chem. Rev.* **2010**, *110*, 2641–2684.
 219. Waters, J.C. Accuracy and precision in quantitative fluorescence microscopy. *J. Cell Biol.* **2009**, *185*, 1135–1148.

220. Song, L.; Hennink, E.J.; Young, I.T.; Tanke, H.J. Photobleaching kinetics of fluorescein in quantitative fluorescence microscopy. *Biophys. J.* **1995**, *68*, 2588–2600.
221. Tsai, H.M.; Souris, J.S.; Kim, H.J.; Cheng, S.H.; Chen, C.T.; Lo, L.W.; Chen, L.; Kao, C.M. Rapid measurement of fluorescence lifetimes using SiPM detection and waveform sampling. *2016 IEEE Nucl. Sci. Symp. Med. Imaging Conf. Room-Temperature Semicond. Detect. Work. NSS/MIC/RTSD 2016* **2017**, *2017-Janua*, 9–11.
222. Chary, S.R.; Jain, R.K. Direct measurement of interstitial convection and diffusion of albumin in normal and neoplastic tissues by fluorescence photobleaching. *Proc. Natl. Acad. Sci. U. S. A.* **1989**, *86*, 5385–5389.
223. Kino, G.S.; Corle, T.R. *Confocal scanning optical microscopy and related imaging systems*; Academic Press, 1996;
224. Maruyama, H.; Masuda, T.; Arai, F. Fluorescent-based temperature measurement with simple compensation of photo-degradation using hydrogel-tool and color space conversion. *J. Robot. Mechatronics* **2013**, *25*, 596–602.
225. Bopp, M.A.; Jia, Y.; Li, L.; Cogdell, R.J.; Hochstrasser, R.M. Fluorescence and photobleaching dynamics of single light-harvesting complexes. *Proc. Natl. Acad. Sci. U. S. A.* **1997**, *94*, 10630–10635.
226. O'Donnell, K.; Boyd, A.; Meenan, B.J. Controlling fluid diffusion and release through mixed-molecular-weight Poly(ethylene) Glycol Diacrylate (PEGDA) hydrogels. *Materials (Basel)*. **2019**, *12*.
227. Ohtsuka, K.; Sato, S.; Sato, Y.; Sota, K.; Ohzawa, S.; Matsuda, T.; Takemoto, K.; Takamune, N.; Juskowiak, B.; Nagai, T.; et al. Fluorescence imaging of potassium ions in living cells using a

- fluorescent probe based on a thrombin binding aptamer-peptide conjugate. *Chem. Commun.* **2012**, *48*, 4740–4742.
228. Bright, G.R.; Fisher, G.W.; Rogowska, J.; Taylor, D.L. Fluorescence ratio imaging microscopy: Temporal and spatical measurements of cytoplasmic pH. *J. Cell Biol.* **1987**, *104*, 1019–1033.
229. Llopis, J.; McCaffery, J.M.; Miyawaki, A.; Farquhar, M.G.; Tsien, R.Y. Measurement of cytosolic, mitochondrial, and Golgi pH in single living cells with green fluorescent proteins. *Proc. Natl. Acad. Sci.* **1998**, *95*, 6803–6808.
230. Wang, L.; Xiao, Y.; Tian, W.; Deng, L. Activatable rotor for quantifying lysosomal viscosity in living cells. *J. Am. Chem. Soc.* **2013**, *135*, 2903–2906.
231. Kuimova, M.K.; Botchway, S.W.; Parker, A.W.; Balaz, M.; Collins, H. a; Anderson, H.L.; Suhling, K.; Ogilby, P.R. Imaging intracellular viscosity of a single cell during photoinduced cell death. *Nat. Chem.* **2009**, *1*, 69–73.
232. Lv, H.-S.; Liu, J.; Zhao, J.; Zhao, B.-X.; Miao, J.-Y. Highly selective and sensitive pH-responsive fluorescent probe in living Hela and HUVEC cells. *Sensors Actuators B Chem.* **2013**, *177*, 956–963.

ACCOMPLISHMENTS

I. Journal Articles

1. H. Hashim, H. Maruyama, T. Masuda, and F. Arai, "Manipulation and immobilization of a single fluorescence nanosensor for selective injection into cells," *Sensors*, vol. 16, no. 2041, pp. 1–10, **2016**.
2. H. Hashim, H. Maruyama, Y. Akita, and F. Arai, "Hydrogel fluorescence microsensor with fluorescence recovery for prolonged stable temperature measurements," *Sensors*, vol. 19, no. 5247, pp. 1-13, **2019**.

II. International Conferences

1. H. Hashim, W. Lei, H. Maruyama, T. Masuda, and F. Arai, "Optical control of adhesion property of magnetic nanosensor using photochromism for effective manipulation and cell injection," in *16th International Conference on Nanotechnology*, Sendai, Japan, August 22-25, **2016**, pp. 683–686.
2. H. Hashim, H. Maruyama, T. Masuda, and F. Arai, "Manipulation and injection of a specific magnetic nanosensor using optical zeta potential control and local laser heating," in *27th 2016 International Symposium on Micro-NanoMechatronics and Human Science*, Nagoya, Japan, November 28-30, **2016**, pp. 221–222.

III. Domestic Conferences

1. 丸山央峰, Hairulazwan Hashim, 益田泰輔, 新井史人, “蛍光ナノセンサの細胞への選択的導入のための光ゼータ電位制御によるナノセンサの選択的操作,” *34th Annual Conference of Robotics Society of Japan (RSJ2016)*, Yamagata, Japan, September 7-9, **2016**.
2. 丸山央峰, Hairulazwan Hashim, 益田泰輔, 新井史人, “蛍光ナノセンサへの光照射による選択的細胞導入,” *17th SICE System Integration Division Annual Conference (SI2016)*, Sapporo, Japan, December 15-17, **2016**, pp. 1750-1751.

IV. Awards

1. **2016**, 27th 2016 International Symposium on Micro-Nano Mechatronics and Human Science, *Best Poster Award*, “Manipulation and injection of a specific magnetic nanosensor using optical zeta potential control and local laser heating,” H. Hashim, H. Maruyama, T. Masuda, and F. Arai.